DESIGN AND DEVELOPMENT OF THULIUM LASER SYSTEM FOR MEDICAL APPLICATIONS

by

TEMEL BİLİCİ

B.S., in Electronics and Electrical Engineering, Boğaziçi University, 2000

M.S., in Electronics and Electrical Engineering, Boğaziçi University, 2003

Submitted to the Institute of Biomedical Engineering

in partial fulfillment of the requirements

for the degree of

Doctor

of

Philosophy

Boğaziçi University

January 2012

Annem, Meryem Bilici, için

For my mother, Meryem Bilici

—

Babam, Rıfat Bilici, için

For my father, Rıfat Bilici

—

To my love, Eray Sevingil

ACKNOWLEDGMENTS

I would like to offer my sincerest gratitude to my thesis advisor Assoc. Prof. Murat Gülsoy for his continuous support and guidance. He inspired me not only for this thesis but also in every aspects of my academic and professional life. I am grateful to Assoc. Prof. Ata Akın for his valuable insight, contributions and suggestions as a member of my thesis committee. I would like to thank Prof. Ahmet Ademoğlu as well as his encouragement and his existence my thesis committee. I would like to acknowledge Assoc. Prof. Can Yücesoy for being in my thesis committee. I would like to thank Prof. İnci Çilesiz for her previous studies that enlighten my thesis topic and for her valuable contributions since my qualification exam during my Ph.D. study.

I would like to thank Prof. Hale Saybaşılı for her suggestions as a member of my thesis progress committee. I would like to thank Prof. Alphan Sennaroğlu, Dr. Hamit Kalaycıoğlu, and Adnan Kurt for their cooperation and guidance throughout my study. I would like to thank Prof. Reşit Canbeyli for his contributions that made this study possible in Psychobiology Laboratory of Boğaziçi University. I would like to thank Assist. Prof. Özgür Tabakoğlu, Nermin Topaloğlu, Ayşe Sena Sarp, Sevinç Mutlu, and Burcu Tunç for their friendship and partnership in Biophotonics Laboratories of Boğaziçi University. I would like to thank Institute of Biomedical Engineering of Boğaziçi University and Electrical and Computer Engineering Department of Boston University for being my "sweet home" in my Ph.D. study.

And my mother, Meryem Bilici, and my father, Rıfat Bilici, this thesis is for you. Finally, my heartfelt appreciation goes to my love, Eray Sevingil, for her unflagging love and support throughout my life.

This study is supported by TUBITAK (Project No: 107E119, Design and Development of Tm:YAP Surgical Laser System, 218.000 USD).

ABSTRACT

DESIGN AND DEVELOPMENT OF THULIUM LASER SYSTEM FOR MEDICAL APPLICATIONS

The Thulium (Tm:YAP) laser is suitable for medical applications due to strong absorption in water. In this thesis, a computer controlled Tm:YAP laser system with a power output up to 1 W and emission wavelength of 1980 nm were established. Once the laser system was stabilized, its output power, spot size, and light intensity measurements were performed. The thermal effects of the laser system on brain, liver, heart, and kidney tissues were macroscopically analyzed. The ablation efficiency of the laser system was experimentally tested on ex-vivo brain tissue. The maximum ablation efficiency was obtained at a power level of 200 mW with a duration of 10 seconds (69 W/cm^2). The fluence effect for skin ablation was analyzed by histology on Wistar rat skin tissues during a 4-day healing period. Temperature measurements by thermal camera and thermocouples were investigated to see the temperature effect of CW and modulated mode of the Tm:YAP laser under skin and on skin surface. The temperature increase was faster and the temperature decrease was found slower in CW mode. The main aim of the study is to explore the welding capabilities of Tm:YAP laser in modulated and CW modes of operation on Wistar rat skin during 21-day healing period. Full-thickness incisions were welded at 100 mW and 5 s (34.6 W/cm^2). The results were compared to conventional suture techniques by both histology and tensile strength measurements. After day 4, full closure was obtained for both laser modes, whereas, full closure was not observed till day 4 in suture group. In tensile strength analysis, tensile forces found for both modulated and CW modes of operation were significantly higher than the tensile force values found for conventional suture technique. Tm:YAP laser tissue welding possessed significantly stronger closure than conventional suture technique.

Keywords: Thulium (Tm:YAP) laser, laser tissue welding, wound healing, skin, brain, ablation, temperature measurement, histology, suturing, tensile strength test

ÖZET

MEDİKAL UYGULAMALAR İÇİN TULYUM LASER SİSTEMİ TASARIMI VE GELİŞTİRİLMESİ

Tulyum (Tm:YAP) laseri su tarafından iyi soğrulduğundan dolayı medikal uygulamalar için uygundur. Bu tezde, bilgisayar kontrollü 1 W güçlerinde ve 1980 nm dalgaboyunda ışıyan Tm:YAP laser sistemi geliştirilmiştir. Laser sistemi kararlı hale getirildikten sonra, çıkış gücü, spot büyüklüğü ve ışık yoğunluğu ölçümleri yapılmıştır. Laser sisteminin beyin, karaciğer, kalp, ve böbrek dokuları üzerindeki ısısal etkileri canlı doku üzerinde yapılacak gelecek çalışmalar öncesinde fotoğraflar ile analiz edilmiştir. Laser sisteminin ablasyon verimi canlı beyin dokusu üzerinde deneysel olarak test edilmiştir. En yüksek ablasyon verimi 200 mW gücünde ve 10 saniye süresi (69 W/cm^2) için elde edilmiştir. Deri dokusu üzerinde ablasyon uygulamaları için laser sisteminin ışınım etkisi Wistar sıçanlarının deri dokusu üzerinde 4 günlük iyileşme süresi boyunca histoloji çalışması ile analiz edilmiştir. Termal kamera ve ısılçiftler ile deri üstünden ve altından sıcaklık ölçümleri yapılarak, Tm:YAP laser sisteminin sürekli dalga ve darbeli operasyon modlarındaki ısıl etkisi incelenmiştir. Sürekli operasyon modunda sıcaklık artışı daha hızlı, sıcaklık düşüşü ise daha yavaştır. Çalışmanın ana amacı sürekli dalga ve darbeli operasyon modlarındaki Tm:YAP laserinin Wistar sıçan derisi üzerinde 21 günlük iyileşme süresi boyunca doku kaynağı özelliklerin ortaya çıkarılmasıdır. Tam-kalınlıklı kesilere 100 mW ve 5 saniye süresince (34.6 W/cm^2) doku kaynağı yapılmıştır. Sonuçlar histoloji ve çekme testi ölçümleri yapılarak göreneksel dikiş yöntemi ile karşılaştırılmıştır. Laser modlarında 4. günden sonra tam kapanma sağlanmıştır, oysaki dikiş yapılan grupta 4. güne kadar tam kapanma gözlemlenmemiştir. Çekme testi analizlerinde, darbeli ve sürekli operasyon modlarındaki çekme güçleri, dikiş tekniği ile elde edilen güçlere göre yüksek bulunmuştur. Tm:YAP laseri ile doku kaynağı geleneksel dikiş yöntemine göre güçlü kapamalar sağlamıştır.

Anahtar sözcükler: Tulyum (Tm:YAP) laseri, laser doku kaynağı, yara iyileşmesi, deri, beyin, ablasyon, sıcaklık ölçümleri, histoloji, dikiş, çekme testleri

TABLE OF CONTENTS

LIST OF FIGURES

LIST OF TABLES

LIST OF SYMBOLS

%	percentage
a	albedo
g	anisotropy factor
h	height
I	intensity
P	power
Pav	average light intensity
t	time
T	temperature
Ta	temperature of ambient surroundings
z	optical axis
ϵ	emissivity
μa	absorption coefficient
μm	micrometer
μs	scattering coefficient
μs	microsecond
μt	total attenuation coefficient
π	pi
σ	Stefan's constant
ω	$1/e^2$ radius of the laser beam

LIST OF ABBREVIATIONS

A	Ampere
AD	Ablation Diameter, also Ablation Depth
AE	Ablation Efficiency
AgBrCl	Silver Bromide Chloride
Alb	Albumin
AlGaAs	Aluminium Gallium Arsenide
BSA	Bovine Solder Albumin
CAPPS	Concentrated Autologous Plasma Protein Solder
CD	Coagulation Diameter
CI	Closure Index
cm	centimeter
CO_2	Carbon Dioxide
CPT	Pooled cryoprecipitate
Cr;Tm:YAG	Chromium, Thulium-doped Yttrium Aluminum Garnet
CSA	Canine Solder Albumin
CW	Continuous-Wave
DSC	Differential Scanning Calorimetry
E	Energy
e-PTFE	Polytetrafluoroethilene
Er:YAG	Erbium-doped Yttrium Aluminium Garnet
ET	Epidermal Thickness
F	Fluorine
FAC	Fatty Acid Containing
FAF	Fatty Acid Free
GA	Granulation Area
H	Hydrogen
HIV	Human Immunodeficiency Virus
Ho:YAG	Holmium-doped Yttrium Aluminium Garnet

Ho:YSGG	Holmium-doped Yttrium Scandian Gallium Garnet
HSA	Human Solder Albumin
Hz	Hertz
ICG	IndoCyanine Green
InGaAs	Indium Gallium Arsenide
J	Joule
K	Kelvin
kg	kilogram
KTP	potassium-titanyl-phosphate
Laser	Light amplification by the stimulated emission of radiation
LASIK	Laser-Assisted in Situ Keratomileusis
LiYF4:Ho, Er, Tm	Thulium,Holmium,Erbium-doped Yttrium Lithium Fluoride
m	meter
MB	Methylene Blue
MIAM	Multispectral Imaging Autofluorescence Microscopy
mK	milliKelvin
ml	milliliter
mm	millimeter
MRI	Magnetic resonance imaging
mW	milliWatt
N	Newton
Nd:YAG	Neodymium-doped Yttrium Aluminium Garnet
nm	nanometer
no.	number
°C	degree Celcius
O-H	Hydroxyl
OPD	Optical Penetration Depth
p	probability
PC	Personal Computer
PDT	Photodynamic Therapy
PIR	Polycrystalline Infra-Red

PLGA	Poly Lactic-co-Glycolic Acid
PSA	Porcine Solder Albumin
r	radius
RS 232	Recommended Standard 232
s	second
T	Temperature
TAA	Thermally Altered Area
TAL	Thermally Altered Length
TEM_{00}	lowest order Transverse Electromagnetic Mode
TF	Tensile Force
THC	Thulmium-Holmium-Chromium
Tm,Ho:YLF	Thulium/Holmium co-doped Yttrium Lithium Fluoride
Tm:LuAG	Thulium-doped Lutetium Aluminium Garnet
Tm:YAG	Thulium-doped Yttrium Aluminium Garnet
Tm:YALO	Thulium-doped Yttrium Aluminate
Tm:YAP	Thulium-doped Yttrium Aluminium Perovskite
Tm^{3+}	Thulium ion
TmLRP-TT	Thulium Laser Resection of Prostate-Tangerine Technique
W	Watt
YAG	Yttrium Aluminium Garnet
$YAlO_3$:Er	Erbium-doped Yttrium Aluminate
$YAlO_3$:Ho, Er, Tm	Thulium,Holmium,Erbium-doped Yttrium Aluminate
Yb,Er:glass	Ytterbium/Erbium co-doped glass
YLF	Yttrium Lithium Fluoride

1. INTRODUCTION

1.1 Aim of the Study

Thulium lasers emitting around 2-μm have been used in applications of distance measurements, atmospheric imaging, telecommunication. It has been reported in the literature that the lasers at these wavelengths are used in tissue ablation and laser evoked potential applications due to their high absorption by water, which constitutes the main element of biological tissues. Furthermore, diode and crystal lasers around 1.9 - 2.0 μm have been experimented for laser tissue welding.

The aim of the thesis is to develop a diode-pumped Thulium (Tm:YAP) laser system at 1.98 μm for medical applications. Having higher absorption characteristics by water, Tm:YAP laser is selected as the source of the laser system design in this thesis due to its suitable properties such as easy pumping by 800 nm diode lasers, crystal durability at high powers, high efficiency, ability of coupling to conventional fibers, and being harmless to human eye retina. The laser system can be considered as a first step towards a multi-functional medical instrument both ablation and welding capabilities in the same device.

The thermal effects of the laser system on biological tissues are experimentally studied. Optical fiber coupled Tm:YAP laser beam is experimented on target tissues in different energy densities by optimization of parameters such as power, spot size, and duration. The thermal properties of the proposed laser system on soft tissues are investigated and dosimetry studies are performed. The thermal effects, coagulation and ablation zones are investigated in vivo. The success of the interactions is analyzed by histologically under light microscopy.

For instant temperature detection, several temperature measurement systems such as thermal camera and thermocouple systems are investigated to compare the

thermal effects between modulated and continuous wave (CW) mode of operation of Tm:YAP laser on skin tissue. The laser tissue welding by Tm:YAP laser system is compared to conventional suture techniques by both histology and tensile strength measurements.

Previous skin welding studies have mostly used CW delivery of radiation. The CW laser would probably cause heat damage to surrounding healthy tissue in the processes of welding by thermal diffusion. This damage may prevent normal wound healing. Strong welds and minimal thermal damage can be achieved by the radiation in a modulated mode. By using modulated lasers, the laser radiation energy will neither be diffused to the surrounding healthy tissue, nor contribute to the temperature rising as a result of thermal energy transform. Therefore, the modulated mode of the laser system is also emphasized in this thesis. This versatility makes the thulium laser especially attractive for the wide medical field.

In the literature, the zone of thermal damage was found inversely proportional to absorption coefficient. Therefore, the laser systems with higher absorption characteristics can produce less thermal damage to the surrounding tissues. The spectral region above 3 μm has the highest absorption in tissue since it overlaps with the fundamental 0-H vibrational stretch mode of water. However, silica fibers are not transparent above 3 μm region. The Tm:YAP laser in this study can be coupled by the conventional silica fibers contrary to longer wavelengths lasers such as CO_2 lasers operating at 10.6 μm.

The lasers having wavelengths longer than 1.4 μm are mentioned as in the "eyesafe" band. Because the laser radiation in this range is strongly absorbed by liquid water and the fluid in the human eye consists primarily of water, laser radiation in this range does not damage the retina because it is absorbed before reaching the retina. Therefore, the use of the laser system in clinics will be safer.

In tissue welding experiments in the literature, most of the applications are about skin welding. However, in most of the applications, solder materials like albumin protein are used to increase the absorption effect by the laser wavelength used. In this

thesis, no solder are used because the absorption coefficient by water at 1.98 μm is highly desirable. The laser welding operation time is decreased and adverse effects due the solders are eliminated. Furthermore, due to the same reason, the laser powers used are less than the powers at smaller wavelengths.

As the main study in this thesis, laser tissue welding by the Tm:YAP laser system are analyzed in CW and modulated modes of operation. After dosimetry experiments and temperature measurements in vivo, the effect of laser parameters is determined. The welding success is shown by histology and tensile tests during the healing period up to 21 days.

1.2 Overview of the Thesis

Chapter 2 includes a detailed description and literature survey of laser-tissue interactions by 2-μm lasers. First of all, laser mechanism and characteristics of lasers at 2-μm are given. The detailed Thulium laser mechanism is also presented. Laser-tissue interaction mechanism is given by discussing its main parameters such as absorption coefficient and wavelength. Modeling studies on laser-tissue interaction and its limitations are summarized. Some applications of 2-μm lasers in the literature are presented. The second part of Chapter 2 gives the detailed definition, advantages, and mechanism of laser tissue welding. The literature is presented by comparing laser tissue welding, laser tissue soldering, and suturing. Effect of laser modulation in laser tissue welding is also given in this chapter. The chapter ends with a summary of laser tissue welding applications in the literature.

Chapter 3 includes the laser system development in this thesis. The components of the laser system are given and its power and intensity studies are explained.

Chapter 4 starts with the dosimetry studies by Tm:YAP laser in vitro. Then, the in vivo experiments on brain and skin tissue ablation are given. The skin optics and ablation studies in the literature are also given. The histology method applied

during the study is presented in this part. The skin ablation parameters are analyzed during 4-day healing period in both CW and modulated modes of the Tm:YAP laser. In the last part of the chapter, the background on temperature measurements and its limitations are given before the temperature measurements of in vivo skin tissue during the Tm:YAP laser application are presented.

Chapter 5 includes the laser tissue welding experiments. A summary of background, methods, histology and tensile strength analysis are given for in vivo skin tissue incisions. The discussion is concluded with the clinical and future applications of the laser system by presenting several clinical limitations.

Chapter 6 is the conclusion chapter. The summary of the results are given.

2. BACKGROUND

2.1 Laser-Tissue Interactions by 2-μm Lasers

Lasers are frequently being used in specialized clinical centers and medical centers, as well as in local hospitals for many surgical applications. The laser systems with wavelengths above 1.4 μm are finding widespread use in medicine. 2-μm lasers are set to replace a number of medical lasers and open up a range of new medical applications with many advantages such as smaller size, higher efficiency, better beam quality, and the ability to operate in either modulated or continuous-wave mode.

Comprehension of the phenomena of heat transfer and related photothermal interactions in tissues is of great importance and contributes to a variety of medical applications. Design and characterization of strategies for delivering thermal therapy provide optimization of a thermal treatment by maximizing the therapeutic effect while minimizing unwanted side effects. Comparison of various treatment parameters and new treatment strategies has widely been investigated.

In this part of the thesis, an overview of laser mechanism with 2-μm lasers, background of laser-tissue interactions, and applications of 2-μm lasers will be given by a detailed literature survey.

2.1.1 Laser Mechanism

Laser is an acronym of Light Amplification by the Stimulated Emission of Radiation. Laser is produced by the stimulated emission mechanism. It consists of a laser medium, an excitation source (pumping energy), and mirrors (resonator) [1]. The laser medium can be solid, liquid, or gas. The specific components of a laser vary depending specifically on the laser medium. The pump source can be an electrical discharge, a

flash lamp, or another laser. The pumping energy injects light into the laser medium, where there are electrons exciting at the outermost layer of the atoms. At this moment, some electrons will return to a lower energy level by emitting photons. The emitted photons will be reflected by the mirrors inside the resonator to stimulate more electrons to undergo stimulated emissions. One of the mirrors in the resonator will not reflect small portion of photons that passes through the mirror. This mechanism constitutes the laser light.

The laser produced from stimulated emission has the following three major characteristics: (1) It is monochromatic. Only a single wavelength is produced in the laser process. All light waves are of the same wavelength. (2) It is coherent. All photons have the same phase and the same polarization; hence they produce a very high intensity. (3) It is collimated. The waves are all parallel to one another. It goes through in a direction with a minimal degree of divergence.

Electrons surrounding an atom or molecule can exist at more than one energy level. Normally, they are found at their lowest energy state (resting state). If an electron absorbs the energy of a photon of light, it makes a rapid transition from an inner to an outer energy level. It rises to a higher energy level, which is called "excited" state. This electron can give up its energy by emitting one photon of light identical to the photon that was initially absorbed. This is called spontaneous emission. If another photon of the appropriate wavelength collides with the excited electron, the electron will return to its resting state by emitting two photons which are synchronized in time and space. This is called stimulated emission of radiation.

To increase the stimulated emission, a higher proportion of excited electrons must be present. This state is called "population inversion". When a population inversion occurs, the photons have a higher probability of encountering excited electrons and stimulating further emission of photons with the same energy. An external source of energy (electrical, chemical, or light) is required to provide as a source of excitation process. This external source is called pumping in the laser mechanism.

Several important parameters of lasers can be defined as follows. Energy is the capacity to do work and is measured in Joules (J). Power is the rate at which energy is expended and is measured in watts (W or J/s). Fluence or energy density is defined as the amount of energy per amount of surface area and is expressed in J/cm^2. The energy density is inversely proportional to the radius (r) of the spot size of the area of the tissue over which the laser beam is spread (πr^2). Irradiance or power density or average light intensity is defined as the rate of energy delivery per amount of tissue surface derived from a continuous wave source (W/cm^2). It describes the intensity of energy delivery. Some lasers have a uniform distribution of their energy across the whole area of the beam, while others have more energy centrally called as Gaussian beams. Other important laser parameters are duration (called pulse width or pulse duration for pulsed lasers) and profile of a laser beam. The laser exposure duration sets the time over which the energy is delivered.

Laser light in its time domain can be divided into three main categories: (1) continuous wave (CW), (2) quasi-continuous (modulated) wave, and (3) pulsed wave. The continuous wave lasers emit a beam continuously at a constant power. Quasi-continuous lasers deliver a beam with a train of pulses from microseconds to millisecond widths. Pulsed lasers achieve the short emissions of high peak power. As a type of pulsed lasers, Q-switched lasers contain a photo-optical switch or shutter within the laser cavity that creates a sudden population inversion in the lasing medium and allows the release of extremely short powerful bursts of high-energy light within the nanosecond domain. Q-switched lasers modulate the resonator losses so that all the energy stored in laser media is released in a few roundtrip times, producing pulses of nanosecond lengths and peak powers in the megawatt range.

A considerable number of lasers in several wavelengths are available for medical applications in pulsed or modulated mode. Some example of these lasers are dye lasers, excimer lasers, semiconductor lasers, Nd:YAG, Er:YAG, Ho:YAG, Tm:YAG, and CO_2 lasers. Continuous (CW) laser radiation is also used in medical application to cut, shape, treat and remove soft tissues of the body. The modulated or pulsed lasers have found applications in localized laser surgery, tissue welding and soldering, detection

of tumors in human bodies, computed tomography, micromachining, remote sensing, particle size detection, and non-invasive detection of inhomogeneties in turbid media.

2.1.2 Characteristics of Lasers at 2-μm

Diode-pumped solid-state lasers are generally considered the most practical source of laser radiation for applications requiring high efficiency, compact, and low-weight. Laser diode pump sources have high electrical-to-optical conversion efficiency. For efficient conversion of the pump radiation into laser output, a significant fraction of the pump radiation should be absorbed by the solid-state laser medium. The narrow-band spectral output of laser diodes is chosen to closely match the absorption bands of solid-state laser materials. Some examples of diode-pumped solid state lasers include the 1.53-μm ytterbium/erbium co-doped glass (Yb,Er:glass) laser, the 2.05-μm thulium/holmium co-doped yttrium lithium fluoride (Tm,Ho:YLF) laser, the 2.01-μm thulium-doped yttrium aluminum garnet (Tm:YAG) laser, the upper-state-pumped 2.10-μm Ho:YAG laser, and the upper-state-pumped 1.6-μm erbium-doped bulk crystal Er:YAG laser [2].

The 1.53-micron Yb,Er:glass laser does not perform well at high average power owing to the poor thermo-mechanical properties of the glass host material. This limits operation of the laser to low pulse repetition frequencies. Thulium is co-doped with holmium, leading to lasing at 2.1 μm in YAG or 2.06 μm in YLF. Thulium-doped YAG lases at 2.02 μm room temperature. These lasers at first had to be operated at liquid nitrogen temperatures in 1960s. In 1982, a thulium vapor column was irradiated with the fourth harmonic of a Nd:YAG laser at 266 nm where many of the emissions were due to inversions to the ground state of both neutral and singly ionized Tm atoms [3].

The 2.05-μm Tm,Ho:YLF laser suffers from upconversion loss from the upper laser state between pairs of Tm and Ho ions, which reduces the efficiency and energy storage capacity of the laser medium. In typical Tm,Ho:YLF lasers, the energy storage time is reduced from an intrinsic lifetime of 10 ms by upconversion to a lifetime of

approximately 1 ms. The 2.01-μm Tm:YAG laser similarly suffers from upconversion loss [4].

The detrimental effects of upconversion loss can be eliminated by pumping the Ho:YAG laser directly into its upper laser state. In this case a low concentration of Ho can be utilized, which suppresses the concentration-dependent upconversion process. The Ho:YAG laser can not be operated efficiently when pumped directly into the upper state by laser diodes [4].

The upper-state-pumped 1.6-μm Er-doped bulk crystal laser operates in a similar fashion to the upper-state-pumped Ho:YAG laser. In particular, the upper-state pumped 1.6-μm Er-doped bulk crystal laser has been considered to be impractical because of the lack of a suitable pump source. The 1.6-μm Er-doped laser is known to operate with two pump sources of flashlamp-pumped Yb,Er:glass lasers, and 1.5-μm InGaAs laser diodes. Neither of these pump devices provides output radiation suitable for efficient operation of the 1.6-μm Er-doped laser. The laser emission of YAlO3:Er at 1.663 μm, LiYF4:Ho, Er, Tm at 2.065 μm, and YAlO3:Ho, Er, Tm at 2.12 μm has been investigated in order to find the best conditions with respect to crystal orientation, doping concentration, and output coupling [5].

Pulsed room-temperature lasers based on the thulium 2.3 μm 3H4-3H5 transition have been achieved in 1.5% Tm:YAG, 2% Tm:LuAG, and 1.5% Tm:YLF crystals using a pulsed alexandrite laser at 785 nm as the pump source in a collinear geometry [6]. The experimental results indicate 1.5% Thulium to be the most optimum concentration for 2.3 μm laser action. The energy level diagram of Thulium 2.3 μm laser is given in Figure 2.1.

2.1.3 Thulium (Tm:YAP) Laser

Diode-pumped solid-state lasers based on Tm-doped crystals have gained significant interest in recent years. Tm:YAP or so-called Tm:YALO is one of the most

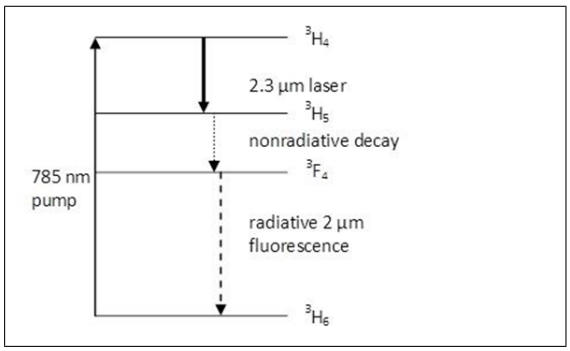

Figure 2.1 Energy level diagram of Thulium 2.3 μm laser [6].

interesting crystals as a material of choice for development of a solid-state laser source with emission wavelength in 1.9 - 2.0 μm region, which has excellent tissue absorption characteristics for medical applications [7]. First of all, the absorption band between 3H6 and 3H4 levels with a peak at 795 nm is easily accessible with high power AlGaAs lasers diodes, compared to Tm:YAG, which is pumped at 785 nm. Furthermore, Tm^{3+} is well-known as active ion to achieve population inversion for the 3F4-3H6 transition between 1.9 and 2 μm by pumping the 3H4 manifold by means of diode laser operating around 800 nm via the cross-relaxation process (3H4,3H6)-(3F4,3F4) [8]. Secondly, the 4-nm wide absorption peak of Tm:YALO is broader compared to Tm:YAG resulting in better tolerance to pump diode wavelength variations. Thirdly, it has a self-quenching mechanism between 3H4 and 3F4 levels that produces two excitation photons in the upper laser level for one absorbed pump photon, which makes the laser potentially well efficient [9]. Most of these features are observed also in Tm:YLF. However, Tm:YLF laser includes upconversion and low fracture limit, which limits the laser efficiency [10].

Laser emission from Tm:YAP is observed over the range 1.93-2.00 μm [11]. Thulium pumped between 780 and 785 nm, which is in the range of available high-power diode lasers, has a surprising effect called the "two-for-one" effect. This effect makes energy transfer from the pumped to the lasing level more efficient. If thulium doping is high enough, the initial pumped atom creates two excited atoms. One pump photon lifts two thulium atoms to identical excited states. The best possible efficiency is the ratio of the lasing photon energy to the pump photon energy. In thulium pumping, there exists two excited atoms, and hence two identical photons for each pump photon

are observed. Therefore the thulium material turns out to have the same efficiency as Nd:YAG, although the 2-μm photon has half the energy of the 1-μm photon.

The pumping diagram for the 2-μm Tm:YAP laser is shown in Figure 2.2. The 795-nm pump populates the 3H4 state, and the self-quenching process then populates the 3F4 state. This produces two excitations in the 3F4 upper laser state for every pump photon.

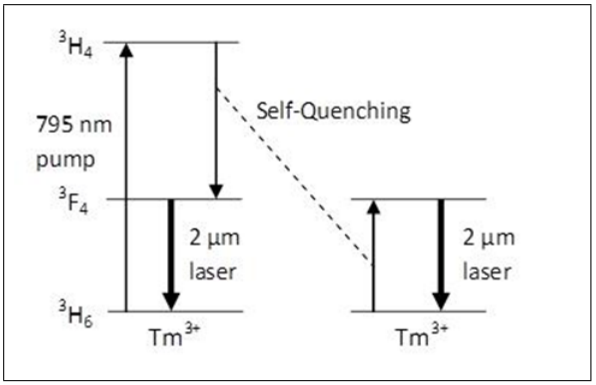

Figure 2.2 Pumping diagram for the 2-μm Tm:YAP laser [11].

A Tm:YAP laser end-pumped by a 794 nm laser diode array is reported as the output power is 1.2 W. The Tm:YAP laser operates at 1940 nm with an output coupling of 2.5%, and at 1945 nm and 1990 nm simultaneously with an output coupling of 2.0% [12]. Another room-temperature operation of a continuous-wave Tm:YAP laser is pumped with a 3 W laser diode and the output is obtained as 730 mW. The laser operates on a number of lines in the wavelength range 1965 to 2020 nm [13].

2.1.4 Laser-Tissue Interactions

Laser light can only impose a tissue effect when it is absorbed and converted to energy, and mostly heat. The induced biological effect is determined by the temperature reached within the tissue. When light is absorbed by a target, heat loss occurs immediately by conduction to all adjacent tissues. The speed of thermal relaxation varies depending on the thermal relaxation time of the tissue. Thermal relaxation time is defined as the time necessary for the targeted tissue to cool down to half the tem-

perature to which it was heated. The tissue effect of lasers is primarily affected by the heating of chromophores and the secondary spread of heat to the adjacent tissues.

Conduction is the major heat transfer mechanism responsible in transferring heat energy from the topmost layer into inner layers of the tissue. Heat transfer depends on the following items; geometry of the organism, heat capacity of the organism (thermal inertia), thermophysical and physiological properties of various organs and tissues (thermal conductivity, specific heat, density, blood perfusion rate, and their dependence upon temperature and location, heat production due to radiative absorption, conduction of heat due to thermal gradients, the role of blood flow in heat transfer (transport of thermal energy by circulating blood and countercurrent heat exchange between large blood vessels), heat exchange with environment, and heat production due to metabolic processes [1].

The degree of thermal damage is dependent on the temperature reached within the target relating to the energy density, and the length of time that the target remains at that temperature depending on the pulse duration. As a result, the tissue damage is dependent of the energy density, the pulse duration, and the heat conduction.

Photothermal laser-tissue interactions occur when laser energy is absorbed by the target tissue and converted into heat. The photothermal reactions are initiated by the heat generated from absorption of laser light by tissue chromophores. A temperature rise is induced, and subsequent thermal gradients promote heat diffusion into areas not directly irradiated by the laser [14]. The temperature effect on the tissue depends on both the magnitude and rate of temperature elevation. Temperature elevations less than 10°C in minutes generally cause cell damage or death without causing structural alterations to the tissue. This kind of temperature elevation on tissue is called photoheating. Greater temperature elevations around 20-30°C occurring over shorter time intervals around 1 second cause thermal coagulation of tissue with cellular death and irreversible structural damage to the tissue due to denaturation (loss of the three-dimensional molecular structure) of tissue proteins. This kind of temperature elevation causes photocoagulation. Laser energy depositions that rapidly (much

less than 1 s) heat the tissue above its boiling point cause thermally-mediated tissue removal by explosive vaporization called photovaporization.

The photothermal effects are summarized in Table 2.1 with respect to the temperature of the tissue [15]. Depending on the duration and peak value of the temperature achieved, different thermal effects like coagulation, vaporization, melting or carbonization may be distinguished. When the tissue is being heated to temperatures between 60 and 80°C, the proteins in the tissue undergo structural changes. In this case the tissue usually becomes more opaque and whiter [16].

Temperature	**Molecular and tissue reactions**
42-45°C	Hyperthermia leading to protein structural changes
45-50°C	Drastical conformational changes, enzyme inactivation, oedema
50-60°C	Coagulation, protein denaturation
80°C	Collagen denaturation, permeabilization of membranes
80-100°C	Dehydration, formation of extracellular vacuoles, vaporization
>100°C	Boiling, streaming, breaking of the vacuoles
100-300°C	Vaporization, tissue ablation
>300°C	Carbonization

Table 2.1
Photothermal effects due to the temperature of the tissue [16].

The wavelength of laser radiation, the absorption coefficient of the tissue, the power density (average light intensity), and the duration of laser radiation also determine the photothermal effects on the tissue. The interaction of a laser light with tissue depends also on the optical properties of the tissue which is determined by the structure, water content, and blood circulation, heat conductivity, heat capacity, heat flow and density of tissue. Thermal effects can be caused by either continuous wave (CW) or pulsed laser radiation.

2.1.5 Parameters in Laser-Tissue Interactions

Despite the structural complexities, tissues are regarded as homogeneous and isotropic mediums in which the propagation of the light radiation is described via basic optical phenomena like reflection, absorption, transmission and diffusion. The most important problem in laser applications is to estimate the right dose specific to the target tissue. Choosing the wavelength, pulse width, pulse shape, beam profile, power density depend on the predosimetry estimations.

Wavelength of the laser, power setting, continuous/pulsed mode, pulse duration, pulse frequency, and exposure time are important laser parameters governing the extent of thermal effects to the tissues [17]. When one parameter is adjusted, the other parameters can also change [18].

The wavelength selected affects the depth of penetration and therefore the heating profile at different depths in the tissue. The penetration of the wavelength should accurately match the tissue characteristics including the degree of pigmentation, water content, and depth and thickness of the tissue. The penetration of the wavelength should approximately match tissue thickness to provide even heating. If the penetration depth is low, all energy will be absorbed near the surface of the tissue. If the optical penetration depth is much greater than the tissue thickness, absorption in the tissue is low. A large amount of energy will be transmitted to underlying structures, with potential for unwanted tissue injury. In addition, the power required will be higher and total energy delivered greater without additional benefit. Even with properly selected wavelengths, different depths will receive different amounts of energy, reaching different peak temperatures.

The preferred power densities and spot sizes vary with the clinical application selected. A large laser spot diameter is used to reduce attenuation of the laser beam due to light scattering in the subsurface layers of the tissue, and thus provides a more uniform and deeper heating of the weld site [19].

Tissue optical properties are usually described in terms of three parameters; (1) the scattering coefficient μs, (2) absorption coefficient μa, and (3) anisotropy factor g. They depend on tissue structure, geometry, and chromophores [16]. Optical measurements on tissue, such as reflectance, transmittance, and scattering, are the result of the combined effect of these properties making it necessary to understand light transport [20]. The effect of the absorption coefficient in tissue damage is more significant than that of the scattering coefficient at higher wavelengths [21]. The parameters in laser-tissue interactions are summarized in Figure 2.3.

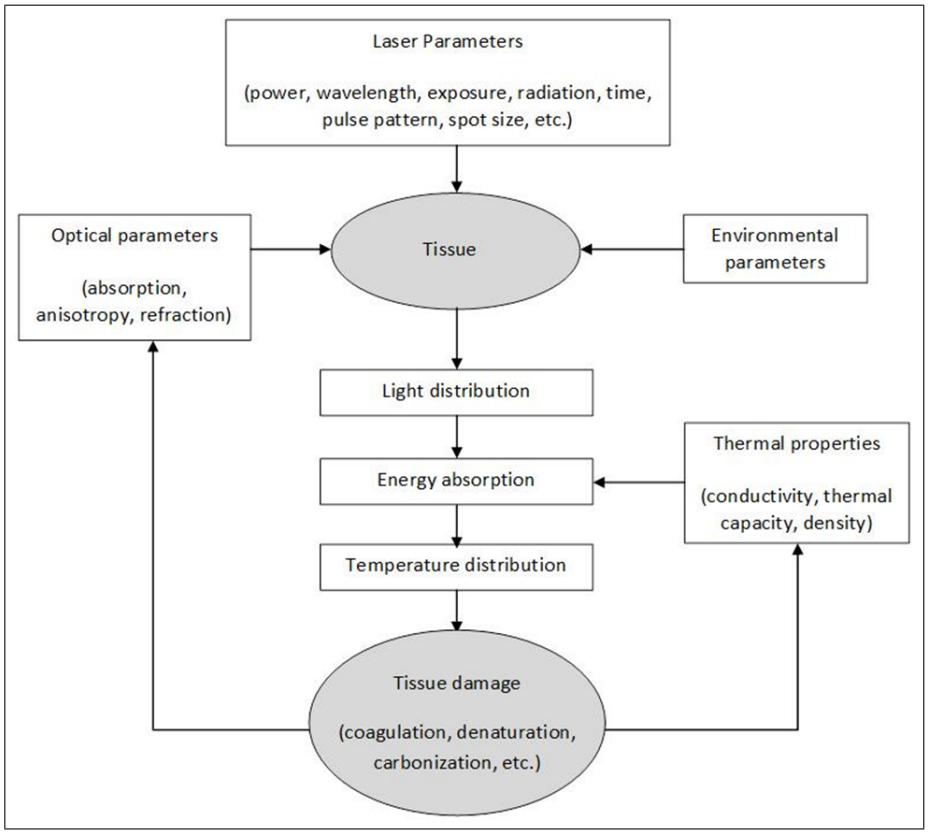

Figure 2.3 Photothermal interaction parameters [21].

In biological tissue, absorption is mainly due to the presence of free water molecules, proteins, pigments, and other macromolecules. The absorption coefficient strongly depends on the wavelength of the incident laser radiation. The intensity of incident electromagnetic radiation is attenuated when light goes through the medium. Due to the energy conservation rule, the radiant energy is converted into the heat motion or molecular vibrations of the absorbing medium. Absorption is dependent on several factors such as the electronic and nuclear constitution of the atoms and

molecules of a medium, the wavelength of the light, the thickness of the irradiated medium, and the variables which determine the state of the medium like temperature and the concentration of the absorbing agent. When light radiation is incident on matter composed of discrete electrical charges, the charges are forced to oscillate at the frequency of the incident electric field. The range of frequencies covered by radiation in the infrared region of the electromagnetic spectrum is comparable to the natural frequencies at which atoms or molecules will vibrate in the absence of an applied field. Thus when infrared radiation is incident on a matter, resonance will occur around the natural frequencies, whereby energy is transferred from the incident field to the system and its amplitude of vibration is greatly increased. The atoms or molecules will usually lose their energy by colliding with one another, thereby raising the kinetic energy of the other particles involved in the collisions. Hence, the energy associated with the incident field is most often dissipated as heat within the medium.

The absorption coefficient μa determines how far light can travel before losing its intensity while still in its original path. Biological tissues are optically inhomogeneous and absorbing media, whose refractive index is higher than that of air. Some part of light coming from the source is reflected backward, when the other part goes deep inside the tissue. Multiple scattering and absorption occurs during the penetration, and the light attenuates as it travels [22].

In turbid media, total attenuation coefficient can be expressed as $\mu t = \mu a + \mu s$, where μa is absorption coefficient and μs is scattering coefficient. The mean free optical paths (penetration depth) of incident photons are determined by $1 / \mu s' = \mu s (1 - g)$ where μs' is called reduced scattering coefficient and g is called anisotropy factor. The anisotropy factor can be explained by average cosine of the scattering angle. The anisotropy factor approaches -1, 0, +1 that corresponds highly backward, isotropic, and forward scattering, respectively. Anisotropy factor (g) of the tissue close to 1 shows that the scattering is forward and the light is mostly absorbed. As another definition, albedo (a) is a dimensionless parameter defined as the ratio of scattering to the sum of scattering and absorption ($a = \mu s / \mu t$). If $a = 0$, attenuation is exclusively due to absorption but if $a = 1$, only scattering occurs.

2.1.6 Absorption Coefficients and Wavelengths

Water is the main constituent (60-80%) of all biological tissues. The absorption capability of water becomes an important parameter for the laser wavelength choice. Water is the primary absorbing component in tissue at wavelengths above around 1.4 μm, with absorption increasing through the mid-infrared to a maximum at approximately 3 μm [23].

The primary chromophore for absorption of the Ho:YAG wavelength of 2.09 μm is water, whereas the primary chromophore for the argon wavelengths is blood. In the absence of blood, the penetration depth of argon radiation is about the same as that of the Ho:YAG laser. The penetration depth in soft tissue for both 500 nm and 2.09 μm light is 300-400 mm. However, the penetration depth of the argon light is governed by absorption and scattering, whereas the penetration depth of the Ho:YAG light is determined solely by absorption. That is, the absorption coefficient of tissue at 500 nm is much smaller than that at 2.09 μm. For the same irradiance, the rate of heat generation at the surface for 2.09 μm is larger than the rate of heat generation at 500 nm. For similar rates of heat generation at the two wavelengths, the irradiance at 500 nm must be much larger than the irradiance at 2.09 μm [24].

The CO_2 wavelength at 10.6 μm is strongly absorbed by water. Because water is the major constituent of biological tissues, most of the CO_2 energy is absorbed in the topmost layer of the tissues. Due to its desirable properties of low tissue penetration and limited spread in tissue, the CO_2 lasers have been used for microsurgical tissue welding [25]. The optical penetration depth for CO_2 in water has been found around 13 μm [26], whereas in another study, it has been calculated as 30 μm [27]. In human tissue, the penetration depth of Nd:YAG at 1064 nm and a diode laser at 830 nm is between 1300 - 1400 μm [28].

The absorption coefficient of water for CO_2 laser wavelength is 794 cm^{-1}. Since water content in soft tissues is relatively high (60 - 80%), their absorption coefficient is close to that of water. There is negligible scattering at this wavelength [29]. Because

of the lower tissue penetration at 10.6 μm, the CO_2 laser is currently one of the lasers used also for laser-assisted nerve repair. As the CO_2 laser energy is absorbed mostly at the tissue surface, it is expected to cause minimal damage within the substance of the nerve at short pulse durations [25].

A wide variety of 2-μm lasers are currently used in medical applications such as ablation, coagulation and welding. 2-μm lasers are attractive because of high water absorption, flexible delivery via low hydroxyl silica optical fibers, and a wide selection of solid state and diode lasers that irradiate around that wavelength. At room temperature, absorption coefficient of water at 1.88 to 2.05 μm varies from 3.78 to 14.25 mm^{-1} and the penetration into tissue is approximately 500 μm [30]. There is no significant difference found between tissue absorption at 1.93 and 1.97 μm. The optical absorption coefficients of water at these two wavelengths have been found as 24 cm^{-1} and 65 cm^{-1} for a holmium laser operating at 2.12 μm and a thulium laser operating at 2.01 μm, respectively [31]. There are also several other values found theoretically for the absorption coefficient of water around 1980 nm, which are 91.20 cm^{-1} for 1984 nm [32], 86.32 cm^{-1} for 1979.80 nm [33], 88.89 cm^{-1} for 1982 nm [34], and 92.03 cm^{-1} for 1980 nm [35].

The optical penetration depth of the 1.9 μm laser wavelength in cornea was roughly reported as 150 μm [36]. At this wavelength water is the primary absorber of the laser radiation and the laser radiation is mainly deposited within a 300 μm depth in the dermis [37]. The absorption coefficient of human dermis closely tracks the absorption coefficient of water in the wavelength region between 1.9 and 2.4 μm. Around these wavelengths, scattering is also small relative to absorption [38].

Water absorption around 2 μm is strongly temperature dependent and tissue ablation is highly temperature dynamic process [39]. At both wavelengths of 2,090 and 2,014 nm, the absorption coefficient found decreasing substantially as temperature increases. To examine the effect of temperature on the absorption coefficient, the transmission of pulsed Ho:YAG, Ho:YAG, Ho:YSGG, and Tm:YAG laser radiation through water of 22, 49, and 70°C was measured as a function of the thickness of the water

layer. At all three wavelengths, the absorption coefficients decreased when increasing the temperature. In addition, the absorption spectrum of water was measured from 1,850 - 2,150 nm with a spectrophotometer. It was found that the absorption peak at 1.94 μm (at 22°C) shifts to shorter wavelengths with increasing temperatures, to 1.92 μm at 70°C [40].

The considerable reduction of absorption coefficient with rising temperature results that water will bleach if high fluence at 2-μm are applied. The absorption peaks are the result of absorption of radiation by the fundamental stretching and bending variations of OH bonds in the water molecule. Increase in temperature weakens the hydrogen-bond network structure. This leads to significantly lower peak temperatures and higher penetration depths in laser heating [41].

2.1.7 Applications of 2-μm Lasers

Lasers, emitting light at wavelengths centered in the wavelength region around 2 μm, are being developed to address a number of important applications. They employed in many medical applications, as the emitting wavelengths absorbed strongly by water [42].

Several applications by 2-μm lasers in tissue ablation and pain studies will be covered in this part. The detailed description and applications of the laser tissue welding will be given in the second part of this chapter.

2.1.7.1 Tissue Ablation by 2-μm Lasers.

Ablation-based laser surgery using visible or near infrared nanosecond laser pulses has gained significant recognition owing to the potential to achieve precise ablation and reduce collateral tissue damage. Ablation thermal laser ablation of tissue can be described as an explosive event and that a decrease of water content in the target alters

the penetration depth which control the ablation rate.

The Holmium laser at 2.1 μm wavelength is gaining wide acceptance among orthopedic surgeons as a useful arthroscopic surgical tool [43]. It has a minimal amount of thermal necrosis and is able to cut and ablate tissues with great ease [44]. The 2.1 μm laser produced effective destruction of human adipose tissue [45]. The nonablative application of Ho:YAG laser energy to the joint capsule of patients with glenohumeral instability was found to shrink capsular tissue and to help stabilize the joint in an in vivo rabbit model [46].

The ablation rates and tissue effects produced by a pulsed holmium laser with a wavelength of 2.12 μm and pulse duration of 250 μs and a pulsed Thulium laser with a wavelength of 2.01 μm and pulse duration of 250 μs have been compared in vitro. Ablation rates have been found to increase linearly with delivered radiant exposure. Because the absorption coefficient of water is almost three times greater at the shorter wavelength, the Thulium laser have a significantly lower threshold of ablation and produce significantly less residual thermal injury. The zone of thermal damage has been found 2.7 times greater with the holmium laser as compared to the Thulium laser [31].

Thulium laser has been found an effective energy source for enucleating the prostate and is comparable to current methods. The advantages of its use include better visualization of tissue ablation with no collateral damage to adjacent tissue. It is also particularly useful for ablation on superficial tumors in the lower and upper urinary tracts [47].

The efficacy and optimal settings of the CO_2, diode and Thulium laser systems have been found both efficient in superficial tissue ablation with minimal coagulation depth. The Thulium laser has a significantly lower threshold of ablation and produce significantly less residual thermal injury [48]. Furthermore, unlike the 10.6-μm radiation, radiation at 2.0 μm can be delivered over a flexible silica fiber [49]. Since the Thulium laser is fiber delivered, it shows to be a versatile laser system for a broad

range of applications both in air and water [50]. The ability of the thulium-fiber laser to operate near the 1.94 μm water absorption peak in tissue has provided improved precision in cutting tissues compared to the Holmium and KTP lasers [51].

The impact of Ho:YAG laser (2.12 μm) laser photothermal interactions on tissue damage and recovery was studied for rabbit skin with different operating parameters by measurement of laser-induced lesions and by tissue histology [52].

Ho: YLF 2.06 μm 100 μsec pulsed silica fiber was performed for plaque ablation in vascular surgery. The Ho:YSGG and the Ho:YAG lasers operate in a pulsed mode and hence offer the advantage of causing minimal collateral thermal damage. They are reported as effective ablative lasers for bony surgery, which may be used for nasal procedures. These characteristics, makes them of potential value for pediatric tracheobronchial surgery [53].

The Er:YAG laser at a wavelength of 2.94 μm shares many similarities with the Ho:YAG, however, like the CO_2 laser, the fiber delivery system is difficult to optimize. The absorption coefficient for water is approximately ten times greater than that of the CO_2 laser. The Er:YAG is able to obtain a high power density in biological tissue resulting in a more precise cut. The pulsed nature allows tissue cooling between interval pulses hence causing less adjacent tissue injury. Er:YAG laser has also been shown to be quite effective in cutting bone and cartilage [27].

Ho:YAG and Er:YAG laser interactions with hard and soft tissue have also been discussed. The differences in interaction can be directly related to the absorption coefficients at the two wavelengths, namely 7700 cm^{-1} for 2.9 μm (Er:YAG) and 40 cm^{-1} for 2.1 μm (Ho:YAG). The results suggests that the Holmium laser is suitable for producing lesions in highly vascular tissue, whereas the Erbium laser is better suited to a vascular tissue requiring large depths of incision [48].

The Cr;Tm:YAG laser compared to Cr;Tm;Ho:YAG laser at 2.1 μm has provided better specificity, shorter operation times, and reduced energy requirements as a

result of increased laser tissue interaction. Another important advantage of the 2 μm Cr;Tm:YAG laser has been reported as the reduction of acoustic transients generated during tissue ablation. Acoustic transients in the form of large pressure waves are created as a result of rapid localized heating and vaporization of biological tissue and blood [54].

Due to strong absorption of laser radiation, 2 μm lasers can be carried with minimal photothermal damage of the surrounding regions. The laser performances and temperature dependence of Erbium:YAG and Chromium:Thulium:Holmium:YAG laser crystals have been compared. The interaction with tissue shows that Erbium produces a deep incision with little damage. Holmium by contrast causes coagulation with a much shallower primary slot [55]. The ablation rates and tissue effects produced by a pulsed Ho:YAG laser (wavelength 2.12 μm, pulse duration 250 μs) and a pulsed thulium:chromium:YAG laser (wavelength 2.01 μm, pulse duration 250 μs) have been compared [31]. Because the absorption coefficient of water is almost three times greater at the shorter wavelength (65 versus 24 cm^{-1}), the thulium laser had a significantly lower threshold of ablation and produce significantly less residual thermal injury [31]. Higher absorption of the laser radiation at the Thulium wavelength results in more efficient and rapid tissue cutting. Several advantages of Thulium laser over the Holmium laser have been reported as including improved spatial beam quality, more precise tissue incision, and operation in continuous-wave/pulsed modes.

Laser-assisted autoaugmentation gastrocystoplasty has been performed using both a 1.9-μm diode and a 1.32-μm Nd:YAG laser with a 50% human albumin solution. A 1.9-μm diode laser were compared with a 1.32-μm Nd:YAG laser with and without thermal control. The 1.32-μm laser group had primarily severe tissue injury. Demucosalized gastrocystoplasty with autoaugmentation can be safely and successfully performed with a 1.9-μm diode laser without significant differences in tensile strength when compared with suture controls [26].

Thulium laser is capable of rapid vaporization and coagulation of prostate tissue. Therefore a thulium laser procedure called "thulium laser resection of prostate-

tangerine technique" (TmLRP-TT) has been designed to perform the treatment of benign prostatic hyperplasia (BPH). TmLRP-TT has defined an almost bloodless procedure with high efficacy and little perioperative morbidity [56].

In another study, Thulium laser (2 μm, 30 W) enucleation of the prostate has represented a safe and effective treatment [57]. Thulium:YAG (RevoLix system) vaporesection has been introduced for the treatment of benign prostatic enlargement [58].

2.1.7.2 2-μm Lasers in Pain Studies.

Solid-state lasers around 2 μm wavelength ensure a steeper slope of temperature rise, thus allowing the use of shorter pulses than CO_2 lasers, which enhances the amplitude of cortical responses [59].

The properties of a Thulium-YAG laser have been evaluated with a penetration depth in the skin that matches the intracutaneous depth of nociceptors. Temperature measurements and modeling shows that the Thulium laser generates painful intracutaneous temperatures with less surface heating than the carbon dioxide laser and with no side effects Therefore, the thulium-YAG laser is a useful tool for assessment of impaired pain sensitivity. Advantages of thulium lasers over carbon dioxide lasers include the lack of side effects, such as erythema and transient skin discoloration, and the possibility to use standard glass fibers for energy transmission. Thulium lasers thus currently seem to be the most effective laser stimulators for use in clinical neurophysiology [60].

A one-dimensional finite difference model has been used to investigate the temperature distribution within Thulium fiber laser-irradiated tissue. The effectiveness of the Thulium fiber laser for thermally stimulating cutaneous nerves has been confirmed. As a result, the Thulium laser generates painful intracutaneous temperatures with less surface heating and produces less associated tissue damage than the CO_2 lasers [61]. A Thulium:YAG laser stimulator at 2000 nm in wavelength has been used to produce

noxious stimuli to the dorsum of the right hand at an interval of between 15 and 20 s [62].

A CW Tm^{3+}-silica fibre laser was used for nerve activation and pain stimulation [63]. Evoked fields were measured by Thulium-laser stimuli that selectively activated nociceptive nerve fibers [64]. Lowerlimb thulium YAG laser evoked somatosensory potentials and cutaneous-sympathetic reflex were also studied [65].

2.2 Laser Tissue Welding

During the last decade, there has been increase in new technology within biophotonics and medical sciences. The technical aspects of new ideas have been challenging. Laser tissue welding is such an innovation that is about to transition itself from the theoretical or laboratory environment to the clinical practice.

2.2.1 Definition of Laser Tissue Welding

While many body tissues can heal themselves in the long term, this will occur if the tissue edges are held tight together. In addition, there is a need to ensure that the bond is fully bonded and leak-proof. A number of methods are used to bond tissues, such as suturing, stapling, and adhesive bonding. Laser tissue welding is gradually becoming popular as a means of surgically sealing certain tissues.

Laser tissue welding is undergoing a transition from laboratory experimentation to accepted clinical practice. The laboratory studies of the laser welding phenomenon has included exploring the types of tissues that could be welded, the wavelengths that may be of use, and the best laser parameters for each application. Research groups investigating these parameters have proceeded with different experimental models and conditions.

Laser tissue welding is an alternative technique for tissue repair over conventional suture techniques. Since laser tissue welding is firstly described in 1964 [66] and 1966 [67], researchers have attempted to perform sutureless surgery to decrease operative time, lessen the inflammatory response, maintain consistency, and increase the ease of use. The baseline to satisfy the surgical requirements is to get stronger welding strength and to minimize tissue thermal injury [68].

Laser tissue welding makes the two edges of the wound together by heating them gently with a laser beam. Laser tissue welding is accomplished by directing the laser beam of an appropriate wavelength at the opposed edges of tissue. It is a surgical technique for bonding of tissues by using a laser beam to activate photothermal bonds and/or photochemical bonds. Another distinct approach to laser tissue welding is called "laser soldering". Laser soldering is a type of bonding technique in which a solder material is applied to the surfaces to be joined followed by application of laser light to seal the solder to the tissue surfaces [26]. Laser tissue welding implies that the bond is produced by actually denaturing the bonded materials themselves without any applied bonding material, while laser tissue soldering implies the use of an adhesive which becomes effective when laser energy is applied [69]. Different biological substances, typically albumin [70], have been used as solders to increase the laser absorption in the welded site on top or between them and then to reduce the thermal damage [71]. As another type of thermal welding, in dye-assisted tissue welding, an external chromophore, in the form of a dye, is introduced to the weld site during dye-assisted tissue welding, to selectively absorb radiation and limit thermal damage to surrounding healthy tissue. One of the major drawbacks of laser tissue soldering and dye-assisted tissue welding was reported as the weak tensile strength of the solder welds when compared to sutures [72].

As another type of tissue welding, photochemical welding is performed without heat. Photochemical welding combines photoactive dyes with visible light to create fluid-tight seals between tissue surfaces without causing collateral thermal damage. In its mechanism, it is unclear but type I collagen can be chemically crosslinked using a photochemical process [72]. However, some questions that remain to be solved in this

technique still include the toxicity and tensile strength changes during healing [26]. /clearpage

In tissue, laser light can be reflected, absorbed, scattered or transmitted. Absorption of laser light results in heating of tissue and denaturation of proteins. At a specific wavelength, the absorption of laser energy varies within different tissues. In the visible wavelength range, light is predominantly absorbed in blood, whereas in the infrared wavelength range absorption predominantly occurs in water. Each tissue has its own wavelength specific absorption coefficient. Tissue absorption, scattering and the predominant direction of scattering determine the penetration depth of a laser. Tissue thickness is another important factor to consider in laser welding. The thicker tissues may require deeper penetration of laser light. Clinical progress in laser tissue welding has been slow due to the large number of parameters that need to be optimized. The intent of many studies has been to optimize the parameters of the entire laser welding process for clinical use. These parameters include wavelength, laser exposure or irradiance, pulse duration, repetition rate, irradiation time, spot diameter, and beam profile.

Laser tissue welding is achieved by directing a low-energy laser beam of an appropriate wavelength at the edges of the tissue welds. An effective tissue welding wavelength should have the following characteristics: efficient energy absorption with a minimum of scatter, a depth of penetration closely matching surface of the weld; and energy output suitable for heating of the tissue to avoid thermal injury. More uniform delivery of radiation results in less thermal denaturation to the epidermis and dermis, and thus less scarring during wound healing [73]. By delivering the radiation to the weld site in pulsed mode, an adequate cooling between the irradiations can be obtained and thermal denaturation can be achieved in the immediate area of the weld site. This kind of irradiation can avoid excessive denaturation in adjacent healthy tissue. In addition, parameters such as exposure duration and laser power need to be also optimally determined.

Laser welding can be performed more rapidly than surgical closure, it causes less

inflammation, and it is probably simpler to master [74], by providing reconstructive effects on tissues [75].

2.2.2 Advantages of Laser Tissue Welding

Laser welding of tissues is a method of closure of surgical incisions that have advantages over conventional closure methods. The special properties and precision of laser light offer a good alternative method to connect tissue without the use of foreign materials such as staples and suture to hold it together during healing [76]. Laser welding are inherently sterile and non-contact technique, which do not involve a foreign body (such as sutures, clips, staples, or synthetic glues), causing a delay in the wound healing process [26]. Laser tissue welding does not create tissue injury during passage of the needle and tying a knot [25]. These injuries may lead to scarring by impairing dermal capillary blood flow leading to ischemia or by providing a site for infection [77]. Laser tissue welding can also provide preserving the mechanical integrity of the weld site [24]. Tissue welding may be possible using the absorption bands of water region around 2-μm without additional proteins or dyes.

Laser welding procedure offer many other advantages, with respect to standard techniques: a watertight bond [78], a faster wound healing process [79], potentially little scar formation [80], a procedure that is both faster to apply and easier to master [81], achievement in long duration [82], reduction of trauma caused by excessive instrument manipulation during surgery, a biodegradable closure [83], and the prospect of simpler methods of minimally invasive and endoscopic wound closure [84]. Laser tissue welding was found four times faster to process than conventional suture technique [82].

Laser tissue welding in surgical specialties such as endoscopic [85], and micro-surgical techniques [86] are most useful for applications where suturing or stapling is difficult or impossible [87, 88]. The use of lasers in surgery introduces some desirable features over normal surgical methods such as increased precision, improved hemostasis, and less tissue manipulation [28]. Laser tissue welding of eye tissues also provides

the advantages of an instantaneous seal of the separated tissues and less tissue disruption [75]. Laser tissue welding could be carried out via optical fiber devices, making it suitable for endoscopic applications with easy handling. In addition, laser applications do not cause any electrical interference in the body [89].

Laser-assisted repair of peripheral nerves can offer several advantages over conventional suturing methods, such as less trauma to the tissue, less inflammatory reaction, and minimal foreign-body reaction. Because of less instrumental manipulation of the nerve segments and avoidance of an excessive number of sutures, better axonal alignment of the nerve ends is achieved, and the cellular and fibroblastic reaction can be restricted to a minimum [90]. Welding also has the potential to form complete closures enabling an immediate watertight anastomosis intraoperatively in the case of blood vessels [91]. Suggested benefits of laser welding also include improved anastomotic compliance and unrestricted enlargement of growing vessels [92].

Laser tissue welding in dermatology has also several advantages such as minimal tissue handling, maximal tissue alignment, maintenance of luminal continuity, early re-epithelialization, maximal tensile strength during early healing, no foreign body reaction, minimal scar formation [93], granulation tissue formation, and less wound contraction [71]. Laser tissue welding does not need to return for suture removal [26].

The laser radiation at 1980 nm would be considered eye-safe because the light would be absorbed by the water in the cornea before it could arrive at and damage the sensitive rods and cones found in the retina. However, surface tissues like the cornea and sclera could be adversely affected by prolonged exposure to this light [75].

2.2.3 Suturing and Laser Tissue Welding

Conventional methods for surgical wound closure involve the approximation of tissue segments with sutures, clips, or staples. There are a number of limitations such as scar formation and foreign body reaction that have prompted a search for alternative

methods of wound closure [94]. However, suturing is still the most commonly used tissue closure method. They can be applied as both absorbable and non-absorbable.

Sutures are a flexible that can be adapted to almost any tissue conditions. Furthermore, sutures are inexpensive, reliable, and readily available. However, sutures create tissue injury during passage of the needle and tying the knot. Therefore, sutures result in a foreign body being left in the tissue [95]. This tissue injury and foreign body reaction can result in inflammation, granuloma formation, scarring, and stenosis. In addition, the application of sutures involves a complex series of movements that may be difficult to execute in microsurgical or minimally invasive endoscopic applications [26].

A potential disadvantage of suturing is the injury caused by needle passage. Due to this injury, foreign body reaction can result in a prolonged inflammatory reaction, granuloma formation, excessive scarring and adhesion formation [26]. Sutures are known to cause mechanical damage to the tissue during their insertion, and more importantly, cause chronic foreign-body reactions which result uncomplicated wound healing [90].

Research comparing healing in sutured and laser soldered wounds with albumin solder showed that sutured wounds had a greater and longer duration inflammatory response than laser soldered wounds [96]. Foreign body reaction and poor tissue alignment were seen in the sutured groups in another study [97]. In suturing, initial tissue edema and inflammation were observed. Necrotic tissue was then replaced by the formation of scar [26]. Furthermore, while sutured tissue is initially held together only at the suture points, laser tissue welding creates an immediate, uniform, and fluid-tight bonding of tissue across the wound site [78]. Laser tissue soldered wounds showed tensile strength significantly stronger than sutured wounds [93].

In nerve repair, conventional microsurgical suture resulted in more pronounced foreign-body granulomas at the repair site, with more connective-tissue proliferation and axonal misalignment. Laser-assisted nerve repair by CO_2 laser performed with a

protein solder results in a good early peripheral nerve regeneration, with an optimal alignment of nerve fibers and minimal connective tissue proliferation at the repair site [90].

In vessel repair operations, surgical suturing depends upon the skills of the surgeon to achieve a tight adaptation of the vessel ends. In some cases suturing might even be impossible due to limited access [98]. In anastomosis, one of the drawbacks of the suture technique was reported as time consuming. The circulation in the artery has to be interrupted for a long duration during suturing [89]. Both operating time and foreign body reaction may be reduced by using a laser tissue welding [99].

Alternatives to the conventional suture technique are also being evaluated. Compared to sutures, mechanical methods of tissue closure, such as staples or clips, have the advantage of a more uniform result, since tissue tension and staple spacing are determined by the stapling device itself. However, these mechanical devices capable of exerting these large forces while maintaining precision of alignment are difficult to build in the small size range [26]. Staples were reported as fast and easy way of vascular wall adaptation. However, they remain in the vessel wall contains some risk for foreign body reactions similar to tissue response after suturing [98]. Furthermore, they were reported as more traumatic to the vessel than conventional sutures due to the considerable force necessary for bending clips or staples. Fibrin glues and cyanoacrylate glues were also reported as easy to apply and time saving. However, they need the use of additional sutures in order to prevent aneurysm formation [100]. Moreover, suturing and stapling do not provide a watertight seal, leading to inevitable blood leakage at the operative site, which may result in substantial blood loss, poor wound healing, and/or surgical complications in patients. Laser tissue welding can reduce operative time, surgical skill, foreign-body reaction, trauma to the vessel wall and blood leakage at the anastomosis site [101]. Furthermore, these traditional methods are hardly applicable to tissue closure not only in vascular anastomosis but also in closure of nerves, and uterine horn [102]. On the other hand, stapling requires subsequent removal of the material implying additional labor costs and discomfort for the patient [103].

The use of welding together with sutures may also be preferred, but this may negate many of the benefits of welding, which include ease of use, speed of use and reduced inflammation [104].

Clinicians and scientists have been exploring the use of lasers as an alternative method of conventional tissue closure such as sutures, staples, and tapes. While sutures have proven effective for most applications of tissue closure, they suffer from several limitations such as less fluid-tight closure of the wound, its difficulty, time-consuming, higher risks of infection, and a larger amount of scarring. Laser tissue welding is a minimally invasive method of surgery that has the ability to solve some of the problems of conventional tissue close techniques.

2.2.4 Laser Tissue Soldering

Laser tissue soldering is a bonding technique in which a protein solder is applied to the tissue surfaces to be joined, and laser energy is used to bond the solder to the tissue surfaces [1]. In laser soldering, a biological solder is applied and the solder and underlying tissues are heated by laser. Laser soldering method is based on the assumption that when the solder hardens, it provides a watertight seal and additional mechanical strength [105]. The solder absorbs laser energy to denature and coagulate protein components and bonds to the native tissue, thus acting as biological glue [106]. Solders will enlarge the bonding surface of the weld, and thus increase the strength of the weld. Solder also acts as a heat sink to reduce thermal damage. [100].

In the case of laser welding, the optical penetration depth (OPD) of the laser energy is determined by the laser wavelength and the absorption properties of the tissue at this wavelength. It is possible to change the OPD by adding soldering agents to the laser-welded tissues. In the laser soldering, it is desirable that the solder layer absorbs most of the laser energy in order to lessen the thermal damage [71]. The tissue solder absorbs the photons and reduces native tissue damage. The solder also undergoes thermal remodeling via denaturation and acts as a bonding agent as it

becomes incorporated into the weld. Applying the solder films alters both optically and thermally the solder surface boundary conditions [107].

The use of wavelength-specific solders makes a differential absorption possible between the welded region and the surrounding tissue. The advantage is primarily a selective absorption of laser radiation by the target without the need for a precise focusing of the laser beam. Moreover, lower laser irradiance can be used because of the increased absorption of welded tissue [108].

2.2.4.1 Solder Types.

To improve on the success of laser welding, albumin solders have been used to increase wound strength and increase the consistency of repairs. Human (HSA), bovine (BSA), porcine (PSA), and canine (CSA) albumin both fatty acid containing (FAC) and fatty acid free (FAF) were evaluated by using differential scanning calorimetry (DSC). FAF albumin solders were found to denature at significantly lower temperatures, while also having a 30% reduction in enthalpy when compared with their FAC counterparts [109]. Albumin solder were shown to decrease thermal damage and increase tensile strength of wounds [110].

Among bovine, human, porcine, and canine albumin when laser welding strengths are examined, BSA delivers the highest breaking strengths, whereas CSA has the lowest. Differences also were analyzed when albumin was examined both with long-chain fatty acids and without them. The presence of fatty acids seemed to decrease welding strengths for human, porcine, and canine albumin, whereas they increase breaking strength for BSA [83]. A serum albumin solder containing heparin designed to reduce microvascular thrombosis rates [111].

Endogenous and exogenous materials such as indocyanine green (ICG) are often added to solders to enhance light absorption. ICG dye has a maximum absorption coefficient at 805 nm. The depth of light absorption was predominantly determined by

the concentration of the ICG dye added to the solder [112]. On the other hand, the welding strength in laser tissue soldering is dependent on solder concentration [88].

Another development of solid albumin glues was to design and manufacture two-layer systems, in which the layer in contact with tissue absorbs the laser and bonds to tissue while the second layer provides cohesive strength and flexibility [72]. In the two-layer solder, a film solder consisted of a white layer (BSA and distilled water) and a black layer (BSA, carbon black, and distilled water). The two-layer solder was found to be more efficient by 810 nm laser at 200 $\pm$ 20 mW than the one-layer solder application [113].

The Methylene blue (MB) and porcine serum albumin (PSA) based solder was produced and used to form end-to-end anastomoses in porcine splenic arteries by a laser diode emitting at 670 nm. This solder is able to produce anastomoses capable of withstanding high pressures. MB displays photobleaching, giving the surgeon visual feedback, preventing overexposure of tissue [114].

Due to the disadvantages of solid solders and their short shelf life compared to liquid albumin solders, an alternative technique were used with a liquid albumin solder with a biodegradable polymer film patch composed of poly lactic-co-glycolic acid (PLGA) [96]. The PLGA thin film was chosen as the reinforcing material because films of various thicknesses were easily created by using the solvent casting technique. In addition, PLGA is readily available commercially and it is now a biodegradable material approved for medical use [84].

Pooled cryoprecipitate (CPT), 50% albumin (Alb), or polytetrafluoroethilene (e-PTFE) were used as solder medium to test in vitro the feasibility of welding amniotic membranes using Nd:YAG laser energy. Laser welding of amniotic membranes was successful in 82.6% of experiments with e-PTFE and in 10.7% of experiments with CPT ($P < 0.001$). Laser welding was unsuccessful in 100% of experiments with Alb [115].

A tissue sealant (SynthaSeal) was developed for tissue approximation. The sealant's hybrid polymerization mechanism rapidly formed short-chain, hard mechanical bonds at the tissue interface, and longchain, flexible polymerization within the bulk of the adhesive [116].

Gold nanoshells were produced as new class of nanoparticles that can be designed to strongly absorb light in the near infrared. Mechanical testing of the skin wounds showed sufficient strength for closure and strength increased over time. Histological examination showed good wound-healing response in the soldered skin [81].

A human albumin solder was used with transforming growth factor-β1. Tissue welding is obtained by the combination of a laser, a solder, and an exogenous growth factor, which stimulates the healing process [82].

A polysaccharide adhesive was designed for tissue repair that overcomes some of the shortcomings of traditional solders. It was chitosan-based adhesive, insoluble, flexible, and it adhered firmly to tissue upon infrared laser activation [117]. A chitosan adhesive effectively bonded to tissue causing only localized thermal damage in vivo [118].

2.2.4.2 Advantages of Laser Tissue Soldering.

The absorbed energy is uniformed in the solder region in the laser soldering [102]. Solder was incorporated within the dermis in all wounds at 21 days. Solder-tissue interaction initially, and extracellular matrix infiltration of solder later, provided the basis for improved wound strength in some studies [97].

The use of albumin solder was consistently observed to result in a lower rate of necrosis and higher mean wound strengths than in wounds closed without solder. Thus, the albumin solder appeared to have a protective effect against cellular injury [119].

Using the albumin stent increased the reliability of ureter end-to-end laser anastomosis. They could reinforce the strength of laser welding and provide a watertight seal to improve welding outcomes in the ureteral sutureless anastomoses [88]. The combination of 1.32-μm laser light and 50% human albumin solder were used to create a deep tissue weld resulting in higher acute repair tensile strength [120].

The solders used in peripheral nerve repair provided extra protein for the fusion process to hold the tissue together and result in stronger welds, and theoretically in less thermal damage to the tissue [25, 90]. Nerves in rats were repaired by utilizing a semiconductor diode-laser-activated protein solder applied longitudinally across the join. Welding was produced by selective laser denaturation of solid solder bands containing the dye indocyanine green [95]. In another study, the nerve was repaired by laser-solder technique and this technique, when used with optimal parameters, proved to be a reliable method to achieve satisfactory peripheral nerve anastomosis and nerve regeneration [121].

If a thin layer of concentrated autologous plasma protein solder (CAPPS) was used with a laser at 1.9 μm and deep thermal injury were avoided [122].

Effective and reproducible laser tissue soldering may be achieved primarily by power density control. Alterations in power density show the most direct and predictable effects on the healing properties of skin closed by laser tissue soldering [123].

In some studies on laser anastomosis, solders that absorb laser energy have been used to minimize the area of heat diffusion. This enables not only enhancement of the efficiency of welding but also reduction in the degree of thermal damage to surrounding tissue [124].

A diode laser (810-nm wavelength) and 50% albumin with 0.1% indocyanine green dye was used to show promise in middle ear reconstruction [69]. A microjet technique allows microdroplets of solder to be deposited at the tissue substrate. Each droplet can be totally coagulated by fixed laser parameters [125]. In another study,

laser-soldered incisions exhibited stronger closure and presented better wound healing behavior, compared with sutured incisions [71]. Addition of BSA-genipin solder with 170 mW at 808 nm, significantly increased the tensile strength of adhesive-tissue bonds [72].

2.2.4.3 Disadvantages of Laser Tissue Soldering.

Some technical, practical, and theoretical problems were reported in laser tissue soldering. First, the thickness of the solder layer is important. If it is too thick, lack of coagulation and adhesion of the solder to the underlying tissue produced a weak bond. If the layer is too thin, the coagulated solder will not have the volume required to have enough bonding process, resulting also in a relatively low bonding strength. Another important factor is the energy fluence rate. High energy fluence rates either will vaporize the solder or will create bubbles as vaporized water inside the solder, which do not contribute to the weld strength. A low energy fluence rate will not sufficiently coagulate the solder [126].

The additives used such as human albumin or dye are foreign bodies and remain expensive. Moreover, their applications could make the surgical procedure heavier because the application of additive is difficult to control.

In the soldering mechanism, a temperature gradient is established over the depth of the solder. Depending on the temperature gradient and the laser exposure, the upper portion of the solder can become over-coagulated but the solder/tissue interface does not get fully coagulated. Such under-coagulated solder has been shown to create unstable bonds with tissue [112]. Non-uniform denaturation across the solder thickness can result in the formation of an unstable solder tissue bond [127].

The solders have intrinsic limitations that impair their widespread use, such as limited tensile strength of repaired tissue, poor solder solubility, and brittleness prior to laser denaturation. Laser-activated solders for tissue repair are traditionally based on

three proteins: albumin, fibrinogen, and collagen. They are blood-derived and have risk of viral infection for the host organism. The use of albumin solders, especially in the solid form, is limited by their water solubility, lack of flexibility, and brittleness before being irradiated by lasers [128]. Furthermore, the required activation temperature of albumin solders can induce significant thermal damage to tissue [117]. Another major limitation of protein solder was reported as the mechanical weakness of their tissue bond, acutely and during the first week post-operation [113].

One of the disadvantages of fibrin glue as a combination of fibrinogen, thrombin, and calcium chloride was reported as hypotension if the agent enters the bloodstream, which has led to the death of two patients [129]. The use of fibrin glue complicate wound treatment and lead to impaired wound healing and hypertrophic scarring. Furthermore, fibrin glue can be hazardous with respect to transmittable diseases [103]. The glues were also reported to produce strong inflammatory responses [130]. Furthermore, evidence of strong fibrous reaction with intense inflammatory response was observed [131]. In addition, fibrin glues carry a potential for allergic reaction [132].

Albumin solders (fluid and solid) are soluble in physiological fluids before laser irradiation. The solder in blood dilution during operation weakens the repair tensile strength and change the mechanical characteristics of the solder. This is an impairment of the reliability and reproducibility of the laser solder technique with albumin solders [94]. In another study, adding albumin found no effect on tensile strength [133].

The addition of some dyes, such as indocyanine green can reduce laser energy to avoid surrounding tissue thermal damage. However, the use of proteins increases the possibility of contamination and viral infection. Dyes are possibly toxic and carcinogenic [134]. In another study, it is reported that the application of fluid glues may be technically difficult, and it is impossible to determine the protein surface area and thickness, as well as the optimum laser energy dose required to coagulate the protein solder [121]. On the other hand, solid solders become dried and rigid, making their use less desirable [76].

In order to limit the thermal damage, India ink as a strong absorber was applied to the apposing edges of the incision and scanned the laser beam (Nd:YAG, 1.06 μm) rapidly across the weld. The India ink was reported inefficient where cosmesis is an important result especially in skin welding [78].

Low welding strength, poor reproducibility, and extensive tissue thermal damage were reported among the disadvantages of protein solders [88]. ICG is known to be hydrolytically sensitive and susceptible to photobleaching in the presence of light [81].

Several studies preferred to use laser welding with no solder [24]. It was reported that it could be possible to accelerate wound healing without thermal damage and to improve cosmetic appearance of scars by assisting skin closure with a 815-nm laser alone [82]. The 1455-nm near-infrared laser welding system provided strong, full thickness welds in cornea and sclera tissue and it did not require the use of extrinsic dyes, chromophores, or solders [75].

2.2.5 Mechanism of Laser Tissue Welding

When laser energy hits a target tissue, it may be transmitted, reflected, absorbed, and scattered. The effect of laser radiation will depend on both the properties of the target, such as specific absorption, chemical structure, density, optical properties, and also on the properties of the laser radiation. The properties of laser radiation include wavelength, pulse duration, repetition rate, energy per pulse, and energy density [135]. Each tissue has specific absorption characteristics base on its composition and content. The principal chromophores present in mammalian tissues are water, hemoglobin, melanin, and protein. Infrared light is absorbed primarily by water, while visible and ultraviolet light are primarily absorbed by hemoglobin and melanin, respectively. With proper selection of the wavelength, exposure time, and intensity of the incident laser energy, the biologic effect on the target tissue can be optimized and undesirable collateral effect on adjacent tissue can be minimized.

The main effect of surgical near infrared laser systems on tissue is thermal. The absorbed photon energy in tissues is converted to heat, which induces thermal changes such as hyperthermia, coagulation, carbonization, ablation inside the tissue. The diffusion of heat to the cooler regions depends on the heat conductivity and diffusivity of the tissue. In laser-tissue mechanism of soft tissues with infrared laser, water is the prominent molecule. High absorption allows the ablation of target tissue better [136].

Laser welding is thought to take place by a photothermal mechanism. Photothermal interactions result from the transformation of absorbed light energy to heat. When laser light is absorbed in tissue and it is converted into thermal energy. Then, different thermal effects are obtained, depending on temperature range [137]. If the heating of the tissue reaches a temperature of 45°C, cells will die and at 65°C, the collagen will denature due to the breakage of interpeptide hydrogen bonds, resulting in a shortening of the collagen fibers in their long axis and the swelling of the tissue in the direction of the incident light beam. There is a main transition in the range between 63°C and 68°C, with a peak at 65°C that could be attributed to the maximum of the disordered phase due to the intramolecular H-bonds breakage, causing fiber contraction and swelling [108]. At temperatures reaching 85°C and above, there is hydrolysis of the collagen cross links that results in the destruction of the collagen fibrillar structure and a relaxation of the previous tissue shrinkage. The dead cells and modified tissues undergo apoptosis, necrosis fibroplasia, neovascularization, and fibrovascular scar formation [75].

Two distinct types of cell death are involved in tissue injury: necrosis and apoptosis (programmed cell death). Although many mechanical and traumatic injuries are characterized mostly by necrotic cell death, apoptosis can also constitute an important part of many pathologic and physiologic processes including heat induced injury, ischemia, organ development, and tissue remodeling. Therefore, both necrosis and apoptosis may play an important role in wound healing after closure by laser welding. Therefore, necrosis and apoptosis were studied together in the evaluation of the rate of cell death associated with laser welding. There was essentially no difference found in cell death in wounds repaired at 65°C or 75°C. Tissue temperatures of 85°C and 95°C

were generally associated with significantly increased apoptotic and necrotic cell death. In the wound edge close to the laser beam during the welding procedure, necrosis was the most prominent finding. As the distance increased from the wound edge, where the tissue was progressively more removed from the direct path of the laser energy, the predominantly necrotic area transitioned gradually to apoptosis [119].

As temperature increases, denaturation of vital mitochondrial enzyme proteins and rupture of the cellular membranes can lead to necrosis of tissues and cells. As temperatures reach up to 100°C, water-vaporization causes tissue desiccation, the formation and expansion of steam vacuoles and explosive fragmentation. Tissue carbonization and ablation occur when temperatures are higher than the pressure dependent boiling point of tissue water [37].

Tissue welding is achieved by laser induced heating of tissue to levels that can cause immediate irreversible damage of the structural proteins of the tissue through cell necrosis and denaturation. Denaturation is a rate process governed by the local temperature-time response, which can be approximated by a simple Arrhenius model. The extent of the reaction is linearly proportional to time and an exponential function of temperature [91].

While the exact mechanism of laser tissue welding is not fully understood, it is generally known that collagen synthesis is stimulated during the healing process after laser welding and welding may occur by fusion of collagen fibers [138]. Collagen fibers are altered and become fused, intertwined, swollen, and dissolved [22]. Laser energy provides for a photothermal process which involves an alteration of tissue collagen as well as the formation of an acellular coagulum, which acts as an adhesive. Most of the native tissue welding effect of laser light is attributed to collagen binding from the thermal dissipation of the energy in the tissue [139]. Since the biologic tissue is composed primarily of water [140], its water absorption characteristic becomes important in tissue welding [134]. The degree of correlation will depend on other factors such as amount of water, tissue characteristics, sample thickness, and fashioning of the tissue to be welded. During welding, water in the tissue absorbs the laser energy and subsequently

heats the collagen helix [131]. When the collagen tissue temperature rises above 60°C, bonding is disrupted and partial dissociation occurs, followed by covalent and/or non-covalent bonding of the tissue protein molecules as the tissue cools [75]. The fibers of the apposed collagen strands apparently unravel under sufficient heat and re-intertwine during the cooling phase [71]. Some proposed mechanisms of laser tissue welding also include denaturation of structural proteins, dehydration of the proteins, acceleration of natural fibrinogen polymerization, collagen-to-collagen fusion, crosslinking of proteins, formation of non-covalent bonding between collagen, and interdigitation of collagen fibers.

In the electron microscopy studies, collagen denaturation was observed by uncoiling the native triple helical structure. The thickening and shrinkage of collagen fibrils is a consequence of the unwinding of the triple helix [141]. The triple helical protein collagen is believed to play a major role in the tissue fusion mechanism. An unraveling of the collagen triple-helix follows by interdigitation between fibers upon cooling, with generation of new bonds. The noncovalent bonding was found the major mechanism in current laser tissue welding protocols. Whereas covalent bond cleavage or formation may take place during laser welding, it was not found necessary for weld strength [133]. The organization and cross-linking of collagen fibers is responsible for the strength of the wound. The amount of collagen does not correlate directly with wound strength [26].

In laser tissue soldering, conformational changes in albumin monomers, polymerization, and cross-linking to extracellular matrix proteins and collagen all may play important roles in the mechanism of wound healing [83]. In another study, laser tissue soldering was found providing scaffolding under which normal wound healing proceeds. A scaffold-like internal lattice is formed when the water content of the solder vaporizes and allows the albumin component to bubble and desiccate. This scaffolding is not limited to the surface, but undergoes incorporation into the healing dermal layers [97]. In laser tissue soldering, the coagulated solder acts as a dense homogeneous cast in which the collagen fibrils are embedded, acting both as an internal and an external glue. On the other hand, in tissue welding without solder, the bonding strength seems

to originate from the collagen- to-collagen connections and possibly from cellular debris acting as microsolder [126].

The success of laser tissue welding depends primarily on thermal denaturalization of tissue collagen and protein coagulation [142]. The fibrils of apposed collagen strands apparently unravel under sufficient heat and re-entwine during the cooling phase [124]. The localized heating causes denaturation of the protein component. The laser heating induces the fusion of collagen fibers on both sides of the incision [121]. When the laser irradiation is discontinued, the denatured protein cools and coagulates. By apposing two separate edges of tissue and applying laser irradiation at the interface, a heat-fused bond is formed by holding the two edges together [143]. Laser welds tissues by producing noncovalent bonds from denatured collagen [115]. The normal healing process is also regulated by growth factors. These proteins were induced in a longlasting manner, because they appeared after wounding and returned to baseline levels after 7-14 days [82].

2.2.6 Collagen in Laser Tissue Welding

Collagen is believed to play a major role in laser tissue welding. Collagen comprises about 6% of body weight in mammals, qualifies as the most widespread structural protein in higher vertebrates and the main means of their structural support. Its molecules consist of three amino acid chains convoluted in a rod-shaped, triple helix [144].

An understanding of the laser impact at the subcellular level is necessary to improve the strength of the bonding. The effect of laser irradiation was analyzed on covalent bonding in pure collagen using irradiance typically applied for tissue soldering. Laser irradiation of pure collagen at typical power settings and exposure times did not induce covalent bonding between collagen molecules. Therefore, forces other than the covalent bonding of collagen molecules were assumed to be responsible for successful laser tissue welding. Cell-rich tissues can additionally offer the assumed advantage of

additional intracellular proteins that could create non-covalent bonds with the solder and increase the post-irradiation tensile strength [133].

The increase in the emission intensity from the tissue after laser application is different for different temperatures. The changes in protein structure are correlated to emission intensity increase. It is known that when the temperature rises to 60°C, collagen denatures. Its helical structure becomes unfolded. Another possible reason for the increase in emission efficiency is the change in the tertiary and/or secondary protein structures under thermal treatment due to hydrogen bond breakage and crosslink changes between the proteins. The energy transfer channels in the protein are distorted by heat, which can induce a quantum efficiency of the fluorophores in the tissue. With additional fluophores being formed with temperature increase, this may cause emission intensity to increase in the two different temperature ranges with different rates of intensity increase. During these periods, tissue coagulation, vaporization, and carbonization occur. These kinds of changes in protein structure caused by laser application or heat are not reversible [145].

The fundamental welding mechanism includes thermal denaturation (unraveling) of the collagen triple helix and subsequent random intertwining of adjacent collagen fibers. The hydrogen bonds of water within triple helix stabilize the collagen structure and the temperature of pure collagen denaturation decrease with increasing water content. The denaturation temperature increase upon water loss may be due to decreased chain mobility and the elimination of secondary water molecules which interact with the primary stabilizing water molecules [146].

The morphologic electron microscopy study showed that some collagen fibers fuse with each other after laser welding. Therefore, the welding process was found as a result of the unraveling of collagen bundles at the cut ends, with partial interdigitation of the bundles across the cut. The crosslinking was not only occurring at the cut ends of collagen fibers, but also between their parallel faces. Two parallel collagen fibers can be "roped" after laser welding. It is still unknown the types of collagen, which are fused and roped, thus playing a role in the laser welding; and the types of collagen

fibers retain a normal structure after laser irradiation [147].

By optical methods, irreversible thermal conformational changes induced to collagen were studied and irreversible phase transition was found around 63 - 64°C. From 55 to 77°C, there was a notable increase found in the permanent destruction of collagen fluorophores which reaches a maximum at about 63°C and then drops again to a steady state of destruction of the residual collagen fluorophores after complete denaturation [144].

The tissue welding effect is accompanied by significant collagen shrinkage that occurs when collagen is exposed to temperatures around 60°C. Collagen has been shown to be reduced to two-thirds its original length (after CO_2 laser irradiation), leading to clinical skin tightening. Finally, new collagen formation and alteration of elastin in the dermis are most likely responsible for laser tissue welding [148].

The collagen in dermis is mainly type I collagen. Type I collagen has a domain within the triple helix that is completely devoid of hydroxyproline. Since hydroxyproline readily forms hydrogen bonds that stabilize the molecule, its absence makes this domain particularly susceptible to thermal damage. In the collagen molecule, three peptide chains are twisted around each other to form a helical, rod-shaped molecule. In the semi-crystalline fibril, the collagen molecules are assembled side-by-side in a staggered manner with the long axis of each molecule aligned with axial orientation of the fibril. When collagen is heated, the heat-labile intramolecular crosslinks are broken and the collagen undergoes a transition from a highly organized crystalline structure to a random, gel-like state, which is the denaturation process. Collagen shrinkage occurs through the cumulative effect of the unwinding of the triple helix, due to the destruction of the heat-labile intramolecular cross-links, and the residual tension of the heat-stable intermolecular cross-links [149]. This mechanism is shown in Figure 2.4 [149] and Figure 2.5 [146]. In Figure 2.5, (A) shows bonding pattern and triple helix of the native collagen molecules and (B) shows the interdigitation of collagen molecules after laser heating.

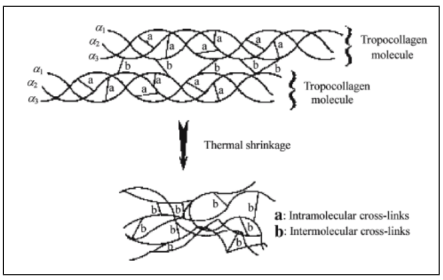

Figure 2.4 Schematic of thermal denaturation of collagen [149].

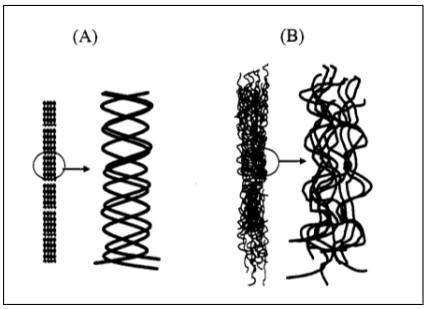

Figure 2.5 Schematic of the effect of laser irradiation on collagen [146].

Collagen molecules from a triple helix structure as the collagen are folded during formation; the effects of packing of the collagen triple helix structure are seen in the larger fibrils and fibers found in tissue and showing characteristic bonding effect. The inter-digitations of collagen after heating are found the most likely mechanism of tissue bonding [146].

By laser welding with 830 nm (0.5 W, 8 sec, 250 W/cm^2), histological modifications in collagen fibers were observed through optic, scanning electron, and electron microscopic examination. Under electron microscope, the different changes in collagen fibers were visualized being either (1) fused with each other which could be identified with two different directions of periodicity, (2) rope yarns, intertwined with each other and formed a "rope", (3) swollen and their diameters varied twice their normal diameter, and (4) dissolved and their periodicity was completely unrecognizable. Collagen fibers lost a proportion of birefringence [147].

Collagen is a linearly birefringent tissue constituent with its rodlike triple helix conformation resulting in both linear and circular anisotropic properties. The funda-

mental building block of collagen fibers is the tropocollagen molecule. Tropocollagen is comprised of three lefthanded a-helices that combine to form a single righthanded super helix. The collagen fiber is formed from a staggered array of the tropocollagen molecules. The refractive index along a fiber's length is greater than the crossectional refractive index. Since the denaturation of collagen results in a loss of tissue birefringence, birefringence was used to quantify the relative conformational state of heated tissues as a tool for the histologic identification of thermal-damage zones in tissue. In the loss of birefringence, tropocollagen loses some of its helical rodlike structure when thermally denatured [150].

By electron microscopy, heat-induced shrinkage associated with denaturation of collagen is found as the main mechanism of laser tissue welding. At shrinkage temperatures, thermal unwinding of the triple helices outweighs the constraints of natural crosslinks, causing the fibrils to denature and shrink. Fibroblastic morphology was found altered in the laser-treated sites with both pyknotic changes and loss of cytoplasmic and nuclear membrane integrity evident. These changes were found most likely caused by the thermal and/or mechanical effects of laser energy. The synthesis, accumulation, and degradation of collagen were found as dynamic processes that occur intracellularly and extracellularly during morphogenesis, growth, inflammation, and repair. At the interfaces of the treated regions and normal tissue, increased numbers of actively secreting fibroblasts were found present, which was established by an increase of cytoplasmic organelles, including rough endoplasmic reticulum, mitochondria, golgi, and secretory vesicles. Fine collagen fibrils adjacent to laser-altered fibrils were assumed to provide evidence of newly secreted collagen matrix and tissue repair. It appears that reactive fibroblasts migrate into the treated regions using the larger denatured collagen fibrils as a scaffold in order to initiate collagen repair. In laser-treated sites, over time, pyknotic nuclei fragmented and degraded to form acellular regions. No macrophages or phagocytic cells were evident within the treated region; however, active fibroblasts were significantly increased adjacent to and infiltrating these areas [46]. New collagen synthesis as well as collagen remodeling occurs in response to laser irradiation over the subsequent days to weeks in response to collagen coagulation [151].

2.2.7 Healing in Laser Tissue Welding

Recent investigations led to a better understanding of the acute wound healing processes. A better wound healing process should be monitored through the entire period. Such quantitative evaluation may yield the optimal conditions necessary for wound repair [152].

A typical curve pattern was suggested for the evaluation of wound healing processes. The normal average wound healing process is demonstrated by a curve made of dots that integrate the relevant wound healing information as a function of elapsed time intervals. The information includes physical features such as tensile strength, as well as qualitative and quantitative histological parameters, for each time interval. In the case where the plotted curve has a shift to the right, a delay in the wound healing pace is expected and the wound dehiscence rate will increase, as in cases of bacterial contamination or other pathological states [153]. In the case where the plotted curve shifts to the left, an advantageous wound healing process is expected, leading to a shorter healing-recovery time and a superior quality of the reparative tissue [154]. The healing mechanism is described in Figure 2.6 [155].

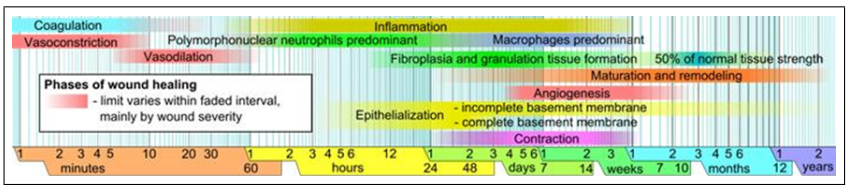

Figure 2.6 Approximate times of the different phases of wound healing [155].

Conventional wound healing proceeds as a continuum, beginning with an initial injury and inflammatory phase, progressing through a granulation or proliferative phase, and completed by a remodeling phase, resulting in a scar [25]. The dermis is the site of most abundant collagen and actively dividing connective tissue whereas the cornified epithelial layer is a dead cell layer with little or no collagen. Therefore, in wound healing, the dermal layer results in greater wound strength than the epithelial layer. The whitening changes in the end-point of wound healing represent a range of effects of thermal coagulation, including irreversible alterations of proteins, organelles,

and membranes. These include hyperchromasia, cell shrinkage, membrane rupture, hyalinization, and loss of birefringence in collagen [26].

Histologically, the wound healing process undergoes overlapping steps: (1) immediate events (0 to 5 days post wound injury), including homeostasis and inflammation; (2) the proliferation stage (3 to 28 days post wound injury), including granulation tissue formation, reepithelialization, fibroplasia and wound contraction; and (3) the remodeling stage (14 days to over 1 year), involving the re-assembling of the extracellular matrix and the collagen fibers to form a mature, strong and flexible compact scar [156]. During the final stage of wound healing, the remodeling stage, collagen matures and forms intermolecular crosslinks. There is no evidence to suggest that laser tissue welding provides additional strength over the long term like after 3 weeks [93]. The healing steps can be seen in Figure 2.7 [155].

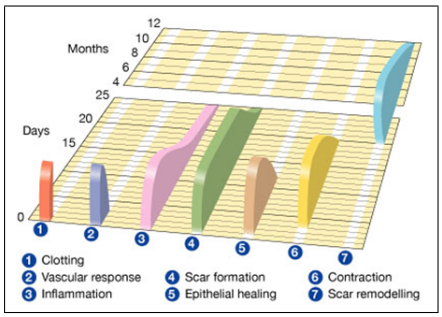

Figure 2.7 Healing steps [155].

In wound healing, early in the inflammatory process, fibroblasts and vascular endothelial cells start to proliferate. This begins as early as 24 hours after injury. By 3-5 days, a specialized type of tissue appears that is known as granulation tissue. This specialized tissue is composed largely of these proliferating fibroblasts and newly formed blood vessels. This tissue appears pink in color. This is so because there is proliferation of new blood vessels, production of extra cellular matrix, mostly in the form of a scar. The reason why there is an increase in blood vessel formation is because the growing cells and tissues need more amount of oxygen and nutrients. This blood also helps to drain away the waste products, like phagocytosed cells and other foreign cells [157].

Granulation tissue is the tissue that is rich in collagen and forms at an injury site. It initially consists of a network of type III collagen, which is a weak and is later replaced by the stronger and longer stranded type I collagen. Type I collagen is generally seen in scar tissue. Granulation tissue generally has considerable numbers of macrophages. These cells phagocytize old and damaged tissue and thus, protect the new forming cells, minimizing the chances of an infection. This aids in the healing process and speeds it up [158].

Collagen deposition in Nd:YAG treated samples was compared with thermally burned pig skin. There was found increased collagen synthesis in the first 7-14 days in both groups. However, there was decreased synthesis in the laser group with normal collagenolytic activity but increased synthesis with normal collagenolytic activity in the burned group. Low power Nd:YAG laser was shown to have a stimulatory effect on collagen synthesis by fibroblasts, whereas high power Nd:YAG exposures had an inhibitory effect [26].

As the body tries to heal, this tissue eventually fills up the injury site and may eventually lead to a scar as well. This scar may fade over time, as is often seen in cases where the wound is small. This is one of the most important wound healing stages. After scar formation, there is complete closure of the wound [158].

2.2.8 Laser Modulation in Tissue Welding

Photothermal interactions result from the transformation of absorbed light energy to heat. At this type of interaction a local temperature increase occur. Thermal effects can be caused by either CW or pulsed laser radiation. Photo thermal effects are intervened primarily by absorption of optical energy and secondly governed by fundamental principles of heat transport. Depending on the duration and peak value of the temperature achieved, different effects like coagulation, vaporization, melting or carbonization may be distinguished.

The CW exposure can produce unwanted collateral thermal injury. A series of pulsed laser parameters were studied in welding a rat skin model in vitro to determine if comparable weld strength could be obtained to CW welding parameters; if thermal injury could be spatially confined and what the appropriate pulse width and interval is to achieve successful welding. Exposure duration was found a more significant contributor to weld strength than power density.

In a study in the literature, the aim was to diminish the thermal diffusion and damage associated with conventional CW or relatively long-pulsed laser tissue welding and soldering. The possible advantages associated with the use of ultrafast lasers were found as the reduction of thermal damage and the improvement of heating uniformity. The use of short laser pulses for tissue welding was found to have reduced thermal damage to the healthy tissue and improves the uniformity of heating in the tissue closure region in both the depth and radial directions [102]. Modulated mode resulted in larger coagulated area with minimum carbonizations. Therefore, modulated mode was found to be a promising regime for safer laser surgery [136]. One of the advantages of CW lasers was reported in the literature as that the generation of potentially damaging stress waves in tissue is avoided by use of the CW mode compared to pulsed lasers [23]. Excessive thermal damage produced during CW welding may result in initially high weld strengths, which then decrease because of sloughing of the necrotic tissue during wound remodeling [78]. Pulsed lasers at high-powers are capable of producing significant mechanical damage in certain tissues in the form of fissures and fractures [159].

In the literature, The Tm^{3+} silica fibre laser (1.99 μm) in Q-switched and continuous-wave operation was investigated to determine its efficiency in the interaction with soft and hard tissues. Residual damage and affected zones using the Q-switched laser were found nearly six times smaller than using the CW mode, and they increased with pulse repetition rate. The energy required to ablate tissue with the Q-switched fiber laser was significantly smaller than that for the CW fiber laser. Under both high-resolution reflected optical microscopy and histological examination, tissue crater depths were observed as cleanly cut with smooth walls and minimal charring in

the case of Q-switched operation of the fiber laser. The Q-switched Tm^{3+}-doped silica fibre laser effectively ablates tissue with little secondary damage [48].

Continuous-wave with high-power applications may result in thermal damage. To minimize the irreversible thermal damage, the time interval between subsequent laser pulses must be greater than the thermal relaxation time. When the laser-pulse width is less than the tissue thermal relaxation time, which is a function of tissue thermodynamic properties and wavelength, thermal diffusion outside the optical zone is reduced and hence the collateral thermal damage can be greatly minimized [27]. In low-power applications, on the other hand, the aimed results may not be obtained due to insufficient temperature increase. Long exposure times might be needed to achieve tissue closure [160]. Modulated laser with suitable power exposures will be effective for successful results for the duration concerns of the applications.

The continuous-wave laser may cause heat damage to surrounding healthy tissue in the processes of welding or soldering by thermal diffusion because of the long time irradiation of CW laser beam. By using ultrashort lasers, the laser radiation energy does not be diffused extensively to the surrounding healthy tissue, and it does not contribute to the temperature rising as a result of thermal energy transform [102]. By delivering the radiation to the weld site in a series of sufficiently short times with adequate cooling between the radiations, thermal confinement of the absorbed energy to the immediate area of the weld site was achieved [78]. When the pulse is shorter than the thermal relaxation time of the tissue and the interval between pulses is long, relative spatial confinement of heat from that pulse occurs [102]. If the pulse is longer than the thermal relaxation time, or if the tissue experiences a CW radiation, then local thermal build-up occurs, resulting in larger zone of thermal injury [26].

An important concept in understanding the utility of modulated delivery is the thermal relaxation time of the tissue. This tissue-dependent factor is a measure of the rate at which heat can be diffused to surrounding tissue to prevent local thermal buildup. Ideally, in welding as in ablation, the laser pulse width (exposure time) must be shorter than the thermal relaxation time for the input energy to provide maximum

effect at the target site with minimal collateral thermal damage due to diffusion of that energy into areas not involved in the weld. The concepts of wavelength-dependent tissue absorption, optical penetration depth, and thermal relaxation time allow the rational selection of laser wavelengths and exposure parameters. Parameters can be selected to provide maximum weld strength with minimal tissue injury [26].

The cooling time in the literature was defined as the average time the laser beam took to return to a particular 5-mm spot at the weld site during scanning. The intermediate cooling times allow the weld site to cool below collagen denaturation temperatures between laser pulses. The long cooling times allow the weld site to cool to approximately its initial temperature between laser pulses [135]. This prevents a buildup in the baseline temperature above collagen denaturation temperatures with the application of successive pulses [18].

Modulated lasers have been used to reduce collateral thermal damage during laser tissue welding as an alternative to laser tissue soldering [70]. Modulated radiation was found to produce strong welds with limited thermal damage to surrounding healthy tissue [18]. The heat of ablation for the continuous-wave Tm^{3+}-doped silica fiber laser was reported as significantly higher than for Q-switched fiber laser [48].

During modulated radiation, it is necessary to allow the temperature at the weld site to cool approximately to initial prewelding temperatures between successive pulses. Therefore, the baseline temperature does not rise above the thermal damage threshold. Optimization of the cooling time will prevent unnecessary thermal damage in the tissue surrounding the weld site. It also eliminates unnecessary cooling time and then the total operation time may also be reduced, thus making welding more competitive with other tissue closure techniques [18].

On the other hand, controlled heating will be greatly facilitated by pulsing the laser light will greatly effect the controlled heating. The ability to vary pulse width is a significant issue in selecting a laser for welding. Pulse width, interval and spot size can be chosen to prevent thermal buildup and undesired collateral thermal injury. At

pulse widths shorter than the thermal relaxation time of the tissue, this will provide a narrow depth of adhesion, limiting weld strength. If CW delivery is used to provide full thickness heating, lateral spread will occur as well, increasing the zone of cell death.

2.2.9 Laser Tissue Welding Applications

Laser tissue welding applications has been performed in several other disciplines such as cardiovascular surgery [161], thoracic surgery [162], laparoscopic and endoscopic surgery [163], general (nonendoscopic) surgery [164], gynecology [165], neurosurgery [166], ophthalmology [167], orthopedics [168], pediatric surgery [169], urology [170].

The first report of laser welding was in 1966 when Yahr and Strully performed a side-to-side anastomosis without success [67]. Lasers have been used to repair arteries successfully since 1979 [171]. Laser welding for vascular anastomosis has been shown to produce good patency and faster anastomotic time in comparison with suturing [172]. An end-to-end microvascular laser soldering anastomosis has been performed by a 808 nm laser diode [98].

Lasers have gained popularity in cartilage welding and several wavelengths have been experimentally and clinically used such as Excimer (l.308 nm), Ho:YAG (2.12 μm) [173] or Er:YAG (2.94 μm) [174].

Laser tissue welding has been used to date in the repair of hollow or tubular structures, such as intestines, ureters, and trachea [105]. Laser tissue soldering by using liquid albumin has been performed for welding liver injuries [70]. The repair of esophageal injuries has been performed by CO_2 laser under tight temperature feedback control [105].

Laser soldering has been performed for the repair of the dura [175]. The application of the CO_2 laser combined with an infrared fiberoptic delivery system has been performed for welding grafts onto perforated eardrums in an animal model. Fiberop-

tic CO_2 laser myringoplasty has been found a potentially important technique for the treatment of tympanic membrane perforation [74].

Laser-assisted soldering has been found feasible for mesh fixation in hernia repair [131]. The closure of gingival flaps has been performed by CO_2 laser after periodontal surgery [176]. Oral tissue and mucosa incisions have been closed by laser welding [26, 17]. CO_2 laser-assisted nerve repair with soldering has been performed by CO_2 milliwatt laser at 100 mW, with pulses of 1.0 s and a spot size of 320 μm [90].

Laser tissue welding has also been popular and effectively performed in Ophthalmology. A near-infrared laser system at 1455 nm has effectively welded cornea and sclera tissue with minimal disruption of tissue, avoiding opacities and irregularities in the tissue which may result in decreased visual acuity [75]. Laser welding has also been studied in cataract surgery and penetrating keratoplasty [177].

Laser welding of corneal tissue with a diode laser at 810 nm has also been proposed as an alternative to conventional suturing procedures. Laser welding by a 800-nm AlGaAs diode laser (80 mW and 16.7 W/cm^2) in association with the topical application of ICG was found a valid method for the closure of corneal tissues without causing thermal injuries [108].

Data from untreated and laser-welded corneas were compared using multispectral imaging autofluorescence microscopy (MIAM) after 7, 15, 30, 60, 90 post-operative days. After only 7 and 15 days for the laser-welded samples, collagen fibers appeared organized in bundles. After 60 days, the laser-welded corneas were fully recovered, while the untreated corneas still showed irregular epithelium and wavy connective-tissue structures [178].

2.2.9.1 Tissue Welding by 2-μm Lasers.

Tissue welding studies have been performed with a mid-infrared 2.15 micron thulium-

holmium-chromium:YAG laser and it has been offered as a useful technique in future developments by 2 μm lasers [179]. The laser tissue welding using a 1.9-μm diode laser has produced a tensile strength equivalent to suture [86].

An experimental work has been performed in evaluating a 1.9 μm laser coupled to an infrared thermometer system [180]. A 1.95 μm diode laser (300 mW) has been used in a system consisted of a direct view infrared thermometer for monitoring the laser heated spot and a microprocessor for data acquisition and feedback control of the laser power to maintain a constant tissue temperature. Rat aortas are welded under constant surface temperature conditions [181].

The (THC):YAG (2.15 μm) and argon ion (488-514 nm) lasers are studied to define suitable parameters for tissue welding. Full-thickness tissue fusion and limited collateral thermal damage are observed histologically for both the CW argon and pulsed THC:YAG welds [182].

The bursting pressure and histological appearance of canine gallbladder tissue welded with a THC:YAG laser producing a 2.15 μm pulsed output have also been evaluated. The tissue absorption characteristics at this wavelength as well as the pulsed nature of the output permit tissue welding with limited collateral thermal damage. THC:YAG laser welding is concluded as a useful technique in the clinical development of percutaneous endoscopic biliary surgery [183].

Thulium fiber laser radiation with a wavelength of 1873 nm, power of 550-650 mW, has been successfully delivered to the tissue in continuous-wave mode through a silica optical fiber to weld 1-cm-length incisions in porcine ureters [184]. In addition, Ho:YAG laser at 2.09 μm has been applied to rat intestine in a temperature controlled feedback system [24]. Furthermore, diode lasers emitting at 1.9 μm have been used in tissue welding of vascular anastomosis [185], bladder [86], and carotid artery [87] of dogs.

An experimental device incorporating co-aligned laser delivery and temperature detection has been used to perform continuous-wave Ho:YAG laser-welded enterotomies with and without temperature feedback control. Argon and Ho:YAG laser-welds with and without temperature feedback control and the control sutured anastomoses healed comparably. Laser welds and suture anastomoses are found equally strong by 3 weeks [24].

Using a THC:YAG laser at wavelength of 2.15 μm, microvessels have been repaired with an average wall thickness of 100 μm [186]. The concept of matching laser optical penetration with wall thickness to achieve uniform and transmural heating has been studied by using a Raman shifted Nd:YAG laser (1.9 μm) to weld small vessels [187].

A 1.9 μm laser has been used to investigate the acute weld strengths for anastomoses of rat and rabbit aortas and femoral arteries. A low power (150 mW) 1.9 μm laser is used by silica fiber optics. The studies suggest that a laser wavelength with absorption depth in tissue matches to the vessel wall thickness should yield optimum welds. Therefore, a laser operating near 1.9 μm has been found suitable for small vessel welding [187].

In vitro porcine arteries and veins have been welded end-to-end using either a 808 nm diode laser with an indocyanine green enhanced albumin solder, or with a continuous-wave Ho:YAG laser without biological solder. Water acts as absorbing chromophore in the Ho:YAG experiments, where the tissue are welded without any additional solder. The Ho:YAG laser radiation is absorbed over the whole thickness of the vessel wall [99].

Laser anastomosis of the rat carotid artery has been performed using the pulsed THC:YAG laser (2.15 μm). Unlike the CO_2 laser, the THC:YAG is transmissible through flexible silica fibers, which greatly facilitates delivery of the laser in a microsurgical operative field. The THC:YAG laser provides shallower absorption depth than Nd:YAG and argon lasers but somewhat deeper tissue penetration than CO_2. For mi-

crovessels, the absorption results in full-thickness fusion of the media, with minimal thermal damage to vascular tissue adjacent to the anastomosis [100].

2.2.9.2 Tissue Welding by 2-μm Lasers in Ophthalmology.

Laser welding of corneal incisions has been performed using two different diode laser wavelengths, with direct absorption of radiation at 1950 nm radiation and with ICG dye-enhanced technique at 810 nm. Wound closures obtained using 1950 nm are characterized by superficial welding of corneal layers [188]. The corneal cultures have been exposed to the 2-μm wavelength output of a Thulium fiber laser [189]. A 1.9-μm diode laser has also been evaluated for corneal wound suture. Corneal welding using a 1.9-μm diode laser has been found possible either with laser and stitch or with laser only [190].

The refractive power of the cornea has been adjusted by shrinkage of corneal collagen fibers with Holmium laser emitting around 2 μm [191]. Corneal epithelial damage thresholds for a continuous-wave Tm:YAG laser radiation (2.02 μm) have been investigated on New Zealand white rabbits [192]. In a recent study, a noteworthy corneal welding was obtained with 1070-nm YLF laser and 1980-nm Tm:YAP laser developed in this thesis [193].

3. DEVELOPMENT OF Tm:YAP LASER SYSTEM

Laser systems emitting around 2 μm are gaining importance due to a growing number of applications in medical surgery. Tm:YAP is an efficient source of 2-μm radiation with tunability in the 1.9-2 μm region and with a free-running wavelength (1.94 μm) that overlaps with the absorption peak of water.

Advantages of Tm:YAP lasers include the availability of high-power pump diodes that overlap with the absorption band of the crystal near 800 nm, enhanced pumping efficiency through cross relaxation, broad tunability around 2 μm, and polarized laser emission due to the biaxial nature of the YAP host.

In the literature, several Tm:YAP lasers have been designed. A high efficient diode-pumped Tm:YAP laser was reported with an output power of 5.2 W at 1981 nm [194]. A diode end-pumped Q-switched Tm:YAP laser at 1937 nm was reported with an average output power of 3.9 W [195]. Room-temperature operation of a continuous-wave Tm:YAP laser was reported at 730 mW laser output [13].

3.1 Tm:YAP Laser System Setup

Tm:YAP laser resonators can be designed by using high-power pump diodes that overlap with the absorption band of the Tm:YAP crystal near 800 nm. The power performance of Tm:YAP lasers is determined by the doping concentration Tm3+ ions inside the YAP crystal. Varying the active ion concentration can change the strength of cross relaxation, reabsorption losses, and nonradiative decay rates. Previous spectroscopic measurements and rate-equation analysis suggest that cross relaxation should be effective in samples with 1.5% Tm^{3+} ion concentration. Therefore, a cylindrical 1.5% Tm^{3+} doped Tm:YAP crystal (Crytur, Inc., diameter:5 mm, length:4 mm), was used to obtain optical gain inside the laser resonator in this study. The crystal was

normal cut and both faces had antireflection coatings at 1940 nm [196].

The schematic of the laser resonator setup is shown in Figure 3.1. The resonator consisted of a flat input mirror and a curved output coupler of 6% transmission with a radius of 10 cm. The input mirror was reflective around 1.94 μm and transmitting at 795 nm. The Tm:YAP crystal, which was positioned near the input mirror, was wrapped in indium foil and held between copper holders maintained at 20°C by water cooling. The length of the resonator was 7.5 cm. The Tm:YAP resonator was end-pumped with a fiber-coupled laser diode at 797 nm. An imaging telescope was used to focus the pump beam inside the crystal. The laser wavelength was effectively stabilized at 1980 nm [197]. The output laser radiation was delivered by means of a 200 μm-core fiber. The picture of the Tm:YAP laser setup is in the Figure 3.2 and Figure 3.3.

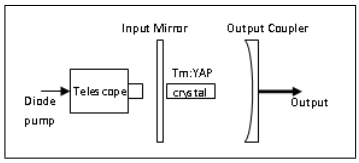

Figure 3.1 Tm:YAP laser resonator setup.

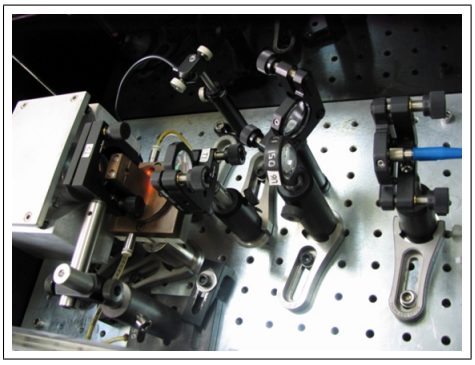

Figure 3.2 Tm:YAP laser setup (side view).

During laser design for medical application, its fiber delivery study and availability of fibers are important. Standard optical fibers are still most used fibers in laser tissue interactions. Lasers operating at wavelengths shorter than 2.5 μm can be transmitted through available silica delivery fibers, unlike the Er:YAG and CO_2 lasers [48]. Silica fibers are made of silica glasses, and they are highly transparent in the visible and near infrared range [198]. A flexible quartz fiber-optic delivery system provides

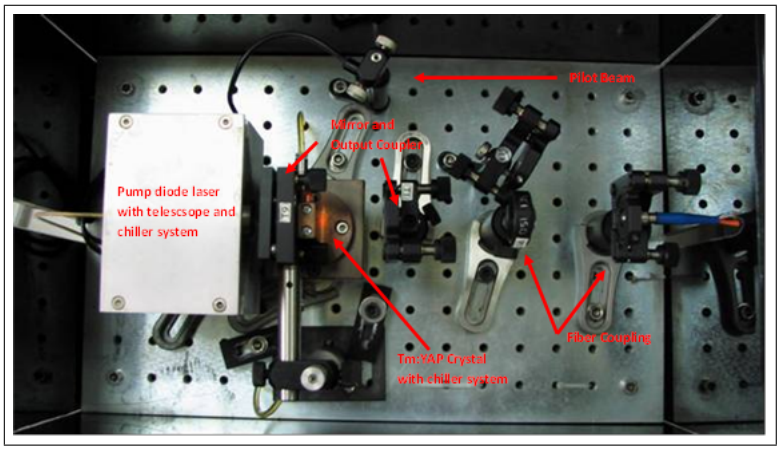

Figure 3.3 Tm:YAP laser setup and its components.

convenient handling of the laser source. The thulium laser developed in this study can be easily coupled to conventional silica fibers. Laser radiation in this study is delivered by means of a 200 μm multimode fiber optic cable.

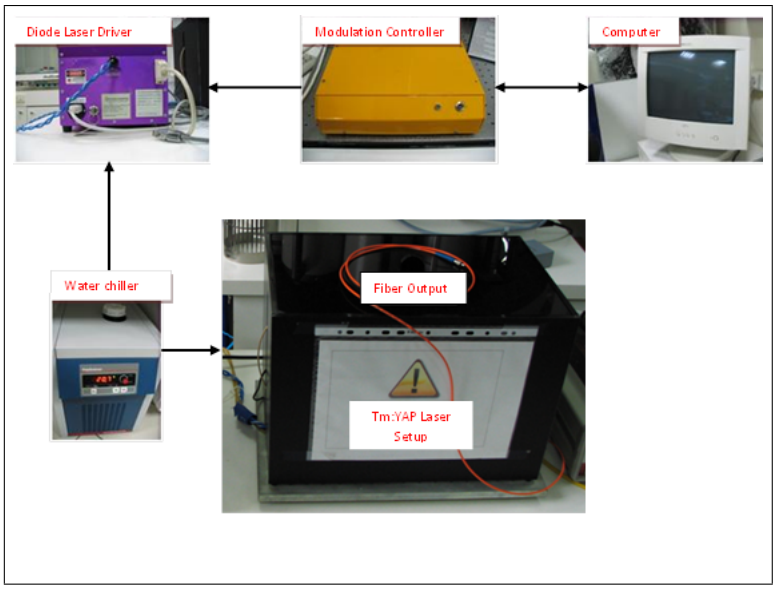

Figure 3.4 Tm:YAP laser system.

The Tm:YAP laser system developed for laser tissue applications includes a Tm:YAP laser resonator setup, diode laser driver, water chiller, modulation controller unit, and acquisition and control software in a personal computer (PC). The schematics of the system can be seen in Figure 3.4.

3.2 Modulation Controller and User Interface

The controller unit that was employed to operate the laser consisted of five blocks as in Figure 3.5 [117]: (1) microcontroller unit, (2) analog-to-digital converter, (3) RS 232 serial communication unit, (4) digital-to-analog converter, and (5) relay controller switching unit. (1) In the microcontroller unit, an 8-bit microcontroller PIC16C84 (Burr Brown Texas Instruments, TX) was used. The control software developed in assembly language was compiled and loaded into PIC16C84 in MPLAB Integrated Development Environment (Microchip Technology Inc., AZ). The application software processes data received from the diode laser power supply and user interface program, while the microcontroller waits for commands from the user interface by checking the diode laser status. (2) The analog to digital converter block converts the analog signals of the diode current and diode temperature values to digital signals to be processed by the microcontroller. For the analog-to-digital conversion, a 4-channel 16-bit sampling converter (ADS7825 IC; Burr Brown Texas Instruments, TX) was used with ± 10 V input range for each channel with a resolution of 305 μV/bit. (3) RS-232 serial communication unit enabled the microcontroller unit to communicate with a PC by performing asynchronous communication in RS-232 communication protocol (developed by the Electronic Industries Association, South Australia, EIA232). As a multi-channel RS-232 driver/receiver with two receive-transmit channel pairs, MAX232 IC (Maxim, Integrated Products, CA) was used via serial port of the PC. Half duplex RS232 serial communication mode was implemented by setting the baud rate to 9600 bps. (4) Digital to analog converter (DAC714 IC, Burr Brown Texas Instruments, TX) was used to convert digital signals taken from the user interface program to analog signal in order to set the diode laser current in the laser power supply. (5) Relay controlled switching unit has four independent relays that can be activated by the user for complete galvanic power isolation.

The acquisition and control software was developed in Labview 6.0 (National Instruments, TX) programming environment. The date flow and all units of the controller circuit were controlled by subprograms in the user interface. All the subprograms were then combined into one main user interface according to the algorithm of the laser

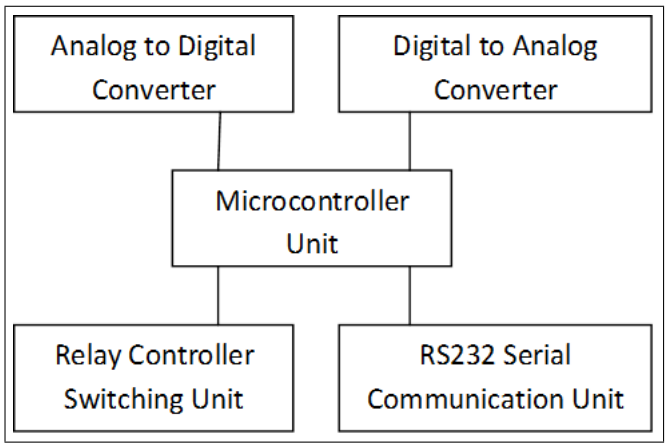

Figure 3.5 Block diagram of the controller.

operation. Both continuous and modulated laser output with different parameters was provided by the user interface software. The user interface program communicates with the laser diode via the controller circuit in order to set the operating parameters of the laser including power, duration and pulsed mode cycles. The user can switch on and off the laser and set the diode current to attain desired power level and duration of operation with a particular duty cycle (20 Hz maximum). In the modulated mode of operation, the controller communicates with the laser diode and switches the diode current on and off as a square wave.

The modulation microcontroller unit provides the modulation the Tm:YAP laser output. The microcontroller unit can operate the laser in pulsed mode up to frequency of 50 Hz. The user interface designed by Labview 6 software sets the duration of the emission, on cycle, off cycles, and number of cycles. In addition, the diode current and the corresponding laser output power can be set via the user interface on PC as in Figure 3.6.

Figure 3.6 User interface of the Tm:YAP laser system.

3.3 Power and Intensity Measurements of the Laser System

Power measurements of the Tm:YAP laser are sampled for each diode current and the laser output powers are obtained as in Table 3.1 and Figure 3.7. The power measurements are performed by a power meter (Newport 1918C) while the Tm:YAP crystal and pumping diode laser are water-chilled at 20° by a chiller (Polyscience MiniChiller 5005). The maximum standard deviation of power measurements are found as 0.01 W, which shows that the Tm:YAP laser is highly stable.

Diode Current (A)	**Laser Output Power (W)**
10.0	0.05
10.5	0.10
11.0	0.16
11.5	0.23
12.0	0.30
12.5	0.38
13.0	0.46
13.5	0.55
14.0	0.63
14.5	0.72
15.0	0.81
15.5	0.90
16.0	0.99
16.5	1.06
17.0	1.14

Table 3.1
Diode current vs laser output power of Tm:YAP laser.

The Tm:YAP spot size changes with respect to the distance between target tissue and the fiber output. This situation makes the average light intensity different for each distance. The laser spot size and the average light intensity on the target

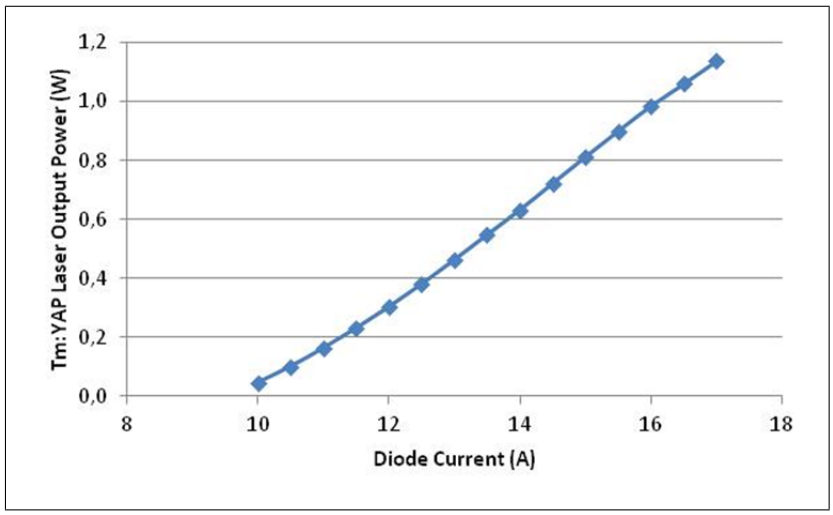

Figure 3.7 Diode current and power curve of Tm:YAP laser system.

tissue were measured by using M^2 method. When the laser output power is 0.70 W, fiber tip was horizontally scanned close to the knife with different distances. When the laser power is at 84% and 16% of its original power, the position difference was obtained by a micrometer as in Figure 3.8.

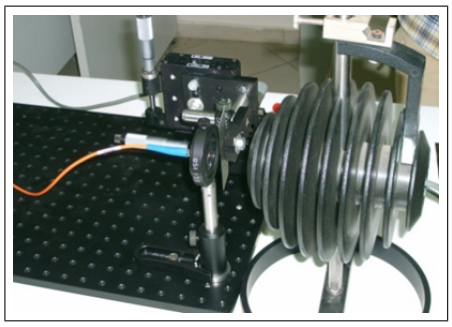

Figure 3.8 Measurement of laser spot size and intensity by knife and M^2 method.

The Gaussian beam M^2 value was calculated as 22.7. M^2 value shows the divergence of the laser light from ideal Gaussian (TEM00) beam. M^2 value for TEM00 is 1. M^2 value increases with increasing the divergence or mode numbers. Since the fiber core diameter is 200 μm with a numerical aperture of 0.22, the laser spot size was calculated with respect to the distance from the fiber tip by the equation in the Figure 3.9. The laser spot diameter with respect to the distance from the fiber tip is figured in Figure 3.10. The laser spot diameter is increasing by increasing distance from the fiber tip.

$$w(z) = w_o \sqrt{1 + \left(\frac{\lambda M^2 z}{\pi w_o^2}\right)^2}$$

w_o = 100 μm, λ = 1980 nm, M^2 = 22.7

z: distance to the fiber tip [μm]

Figure 3.9 Laser spot size calculation by M^2 method.

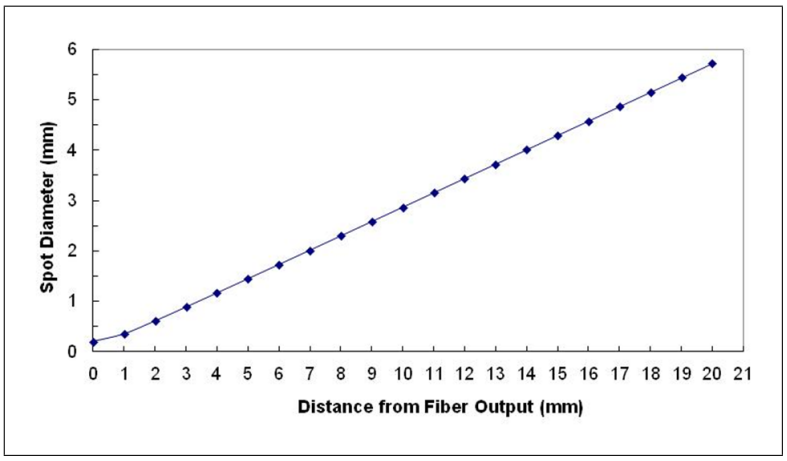

Figure 3.10 The spot diameter of the Tm:YAP laser by the distance from the fiber tip.

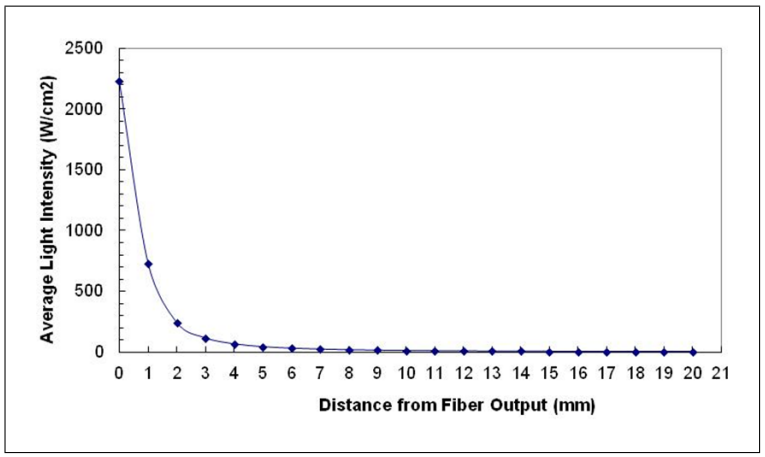

Figure 3.11 The average light intensity of the Tm:YAP laser with respect to the distance from the fiber tip when the laser output power is 0.7 W.

Distance (mm)	Spot Size (mm)	Average Light Intensity (W/cm^2)
0	0.20	2229.30
1	0.35	731.68
2	0.61	242.65
3	0.88	114.79
4	1.16	66.05
5	1.44	42.73
6	1.73	29.85
7	2.01	22.01
8	2.30	16.89
9	2.58	13.37
10	2.87	10.84
11	3.15	8.97
12	3.44	7.54
13	3.73	6.43
14	4.01	5.54
15	4.30	4.83
16	4.58	4.25
17	4.87	3.76
18	5.15	3.36
19	5.44	3.01
20	5.73	2.72

Table 3.2
Tm:YAP laser spot size and average light intensity with respect to the distance from the fiber tip when P = 0.7 W.

Average light intensity is directly proportional to laser power. The average light intensity can be calculated for other laser output powers before each laser application by the distance from the fiber tip. The average light intensity is decreasing by increasing the distance.The average light intensity was calculated by the equation $Pav(z)=Po/\pi w^2(z)$.

When Po = 0.7 W, the average light intensity values are given Figure 3.11 and in Table 3.2. For each experiment, the average light intensity values were calculated by using the power applied (Po).

4. DOSIMETRY APPLICATIONS of Tm:YAP LASER SYSTEM

4.1 In vitro Dosimetry Studies on Liver, Heart, Kidney and Brain

Choosing the optimal combination of laser generator, wavelength, delivery system and desired outcomes requires a thorough understanding of the interaction between the laser energy and the tissue of interest. Determination of the optimal laser wavelength requires knowledge of the tissue absorption and scattering characteristics, the depth of penetration within the target tissue and in surrounding tissues, and the ablation threshold. Careful in vitro studies can serve as the basis for system design and choice of laser; however, testing in animal models and careful clinical trials are often required to achieve optimal results.

4.1.1 Materials and Methods

In this thesis, after the laser system was setup and its stability was confirmed, the first-step experiments were performed on in vitro fresh lamb tissue samples of liver, heart, kidney, and brain. These experiments were performed to see the effect of the laser on biological tissues and determine the dosimetry for the future in vivo studies. The experiments were sampled for three times by increasing the power and light intensity of the laser.

The laser parameters of both continuous wave (CW) operation mode and modulated mode of operation were applied on the tissue samples and the effects were comparatively analyzed. The experiment setup is shown in Figure 4.1 and Figure 4.2. The laser fiber output was applied on the tissue samples from the distances of h = 5 mm and h = 10 mm. The fresh tissues were placed on a vertical stage.

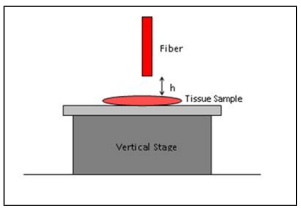

Figure 4.1 The experimental setup for in vitro studies.

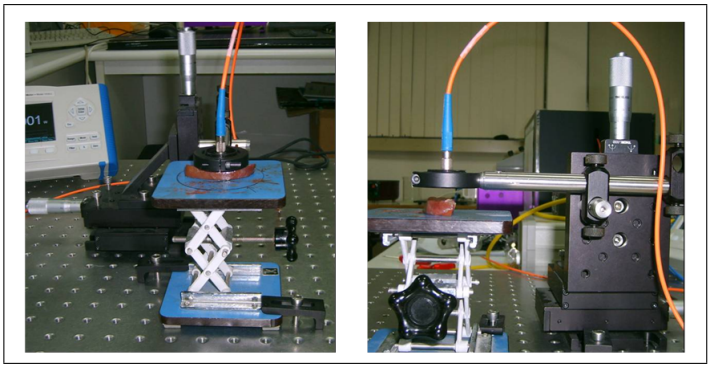

Figure 4.2 The experimental setup pictures for in vitro studies.

After the Tm:YAP laser with predefined parameters was applied on the tissue samples, the thermally altered areas and penetration depths of each tissue were measured by a digital micrometer. The durations of the laser applications were 5 sec and 10 sec in both CW and modulated mode. The applied laser parameters are summarized in Figure 4.3.

Diode current (A)	Laser power (W)	Distance (mm)	Laser spot size (mm)	Average light intensity (W/cm^2)
17 A	1.14	5	1.44	69.59
17 A	1.14	10	2.87	17.65
16 A	0.99	5	1.44	60.43
16 A	0.99	10	2.87	15.32
15 A	0.81	5	1.44	49.44
15 A	0.81	10	2.87	12.54
14 A	0.63	5	1.44	38.45
14 A	0.63	10	2.87	9.75

Figure 4.3 Tm:YAP laser parameters applied on in vitro tissue samples.

4.1.2 Results and Discussion

The macro pictures of the thermal effects on the tissues where the laser parameters were applied from 5 mm distance are given in Figure 4.4.

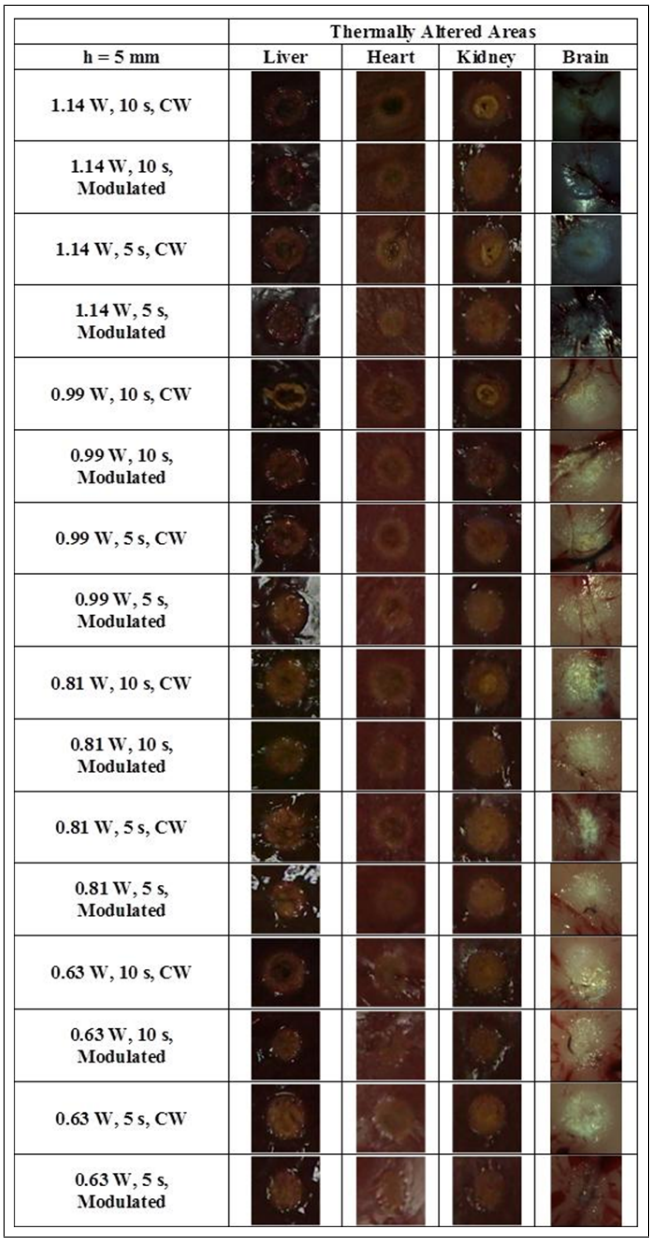

Figure 4.4 Pictures of thermally altered diameters on the tissues when the laser parameters are applied from h = 5 mm.

The water constitutes of the different tissue types differs the laser effects on the tissues. At the maximum dose at 1.14 W at 10 second, serious carbonization effects were observed in both CW and modulated mode of operation. At 5 second, the carbonization effect decreases in modulated mode. The minimum carbonization is observed on heart and brain tissue samples. The measured thermally altered diameters are given in Figure 4.5. The thermally altered areas and carbonization effects are decreasing when the power of the laser is decreasing. The bursting of the tissues when high powers

are applied affects the thermally altered diameters. The bursting effect decreases the thermally altered diameters because the heat is mostly populated in the middle of the application center without spreading the surrounding tissues. The results show that the modulated mode of operation makes the thermally altered diameters smaller. The maximum standard deviation found in the measurements is 0.15 mm.

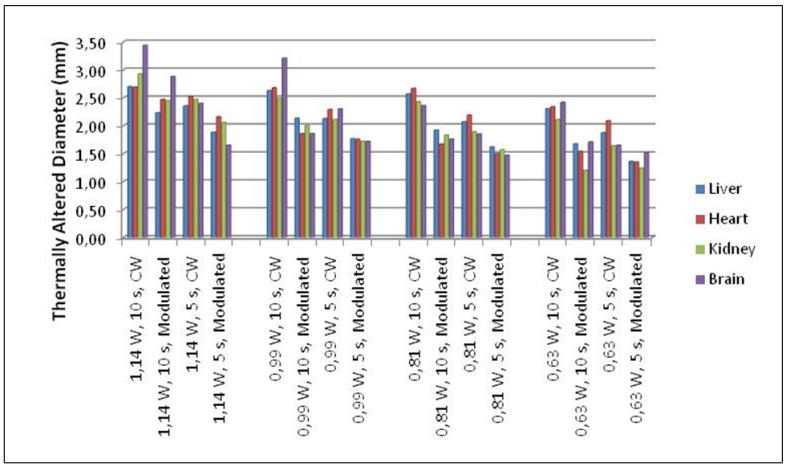

Figure 4.5 Thermally altered diameters on the tissues when the laser parameters are applied from h = 5 mm.

The same experiments were repeated when the distance to the tissue is h = 10 mm. Figure 4.6 shows the macro-pictures of the tissues. The increased distance to 10 mm decreases the carbonization effects seen in the previous experiments. Minimal carbonization effects were observed at power of 1.14 W at 10 second. Figure 4.7 also gives the thermally altered diameters. Decreasing laser powers lessens the thermal effects on the tissues.

Figure 4.8 and Figure 4.9 give the penetration depth measurements on the tissue samples when the laser parameters are applied from h = 5 mm and h = 10 mm respectively. Decreasing laser powers decreases the penetration depths on the tissues. With the same application parameters, modulated mode of operation provides less penetration depth compared to CW mode of operation. The penetration depth of the Tm:YAP laser in liver tissue was found larger than the other tissue types.

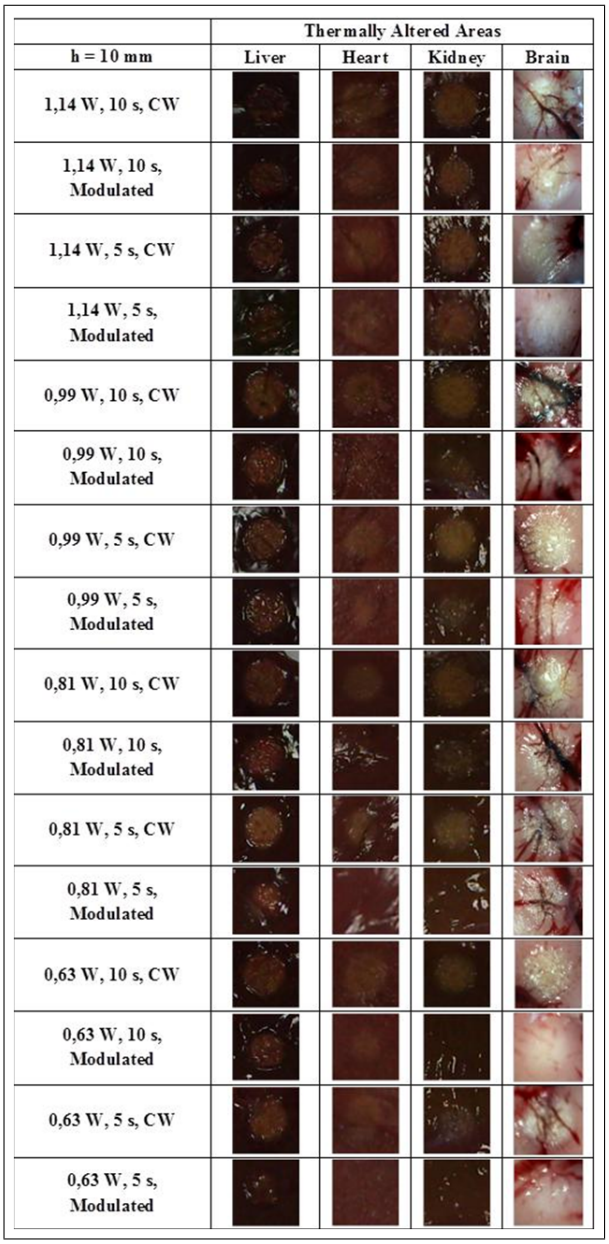

Figure 4.6 Pictures of thermally altered diameters on the tissues when the laser parameters are applied from h = 10 mm.

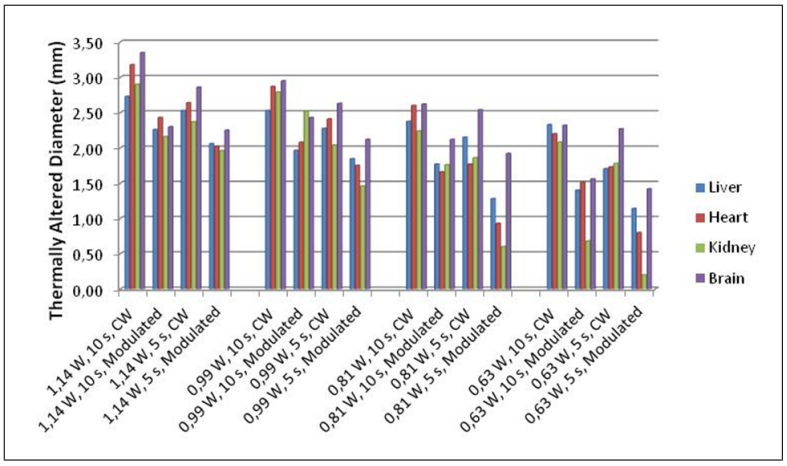

Figure 4.7 Thermally altered diameters on the tissues when the laser parameters are applied from h = 10 mm.

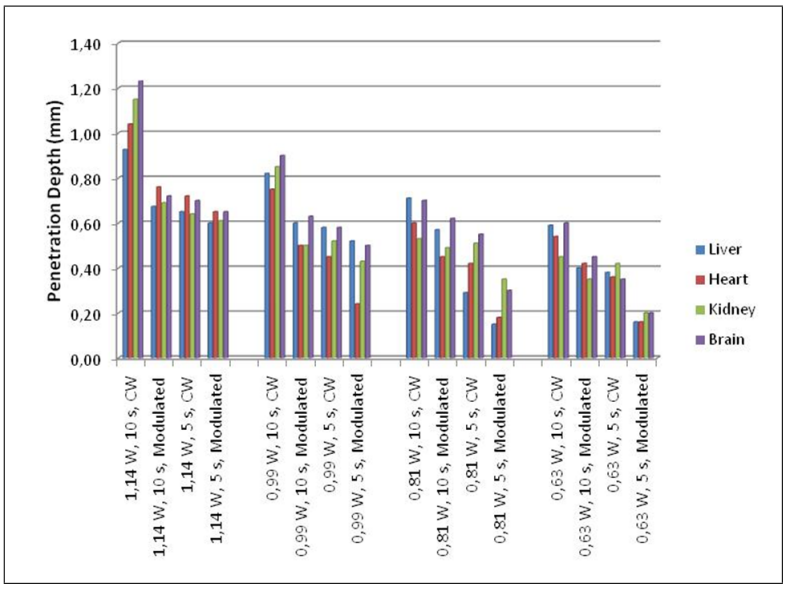

Figure 4.8 Penetration depths on the tissues when the laser parameters are applied from h = 5 mm.

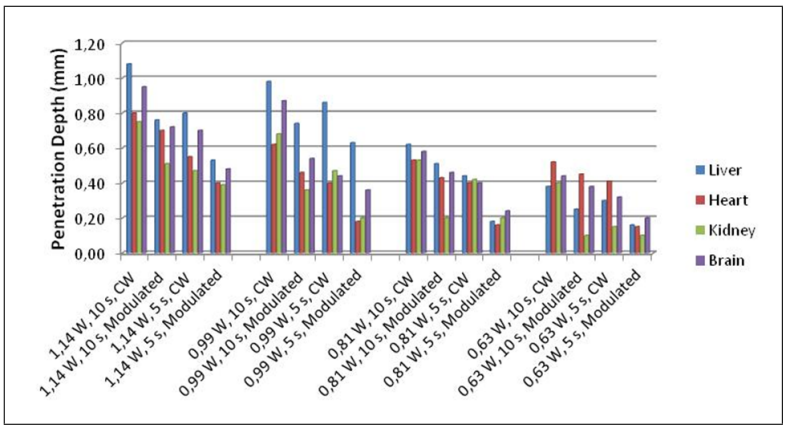

Figure 4.9 Penetration depths on the tissues when the laser parameters are applied from h = 10 mm.

The macropictures of the tissues where the laser parameters are applied from h = 10 mm are given in Figure 4.10 . The penetration depths are found smaller than the thermally altered diameters due to the strong absorption coefficient of the 1980 nm by water. Since Tm:YAP laser at 1980-nm wavelength is strongly absorbed by water, the laser effects are observed on the surface of the tissues.

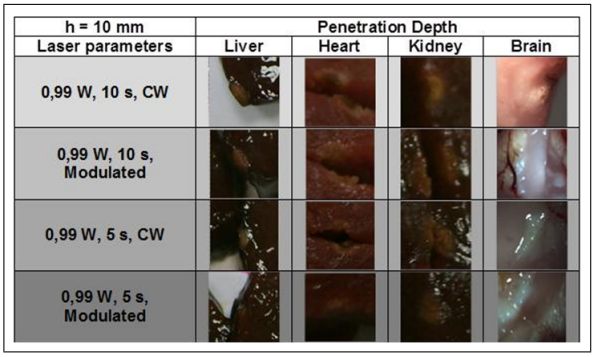

Figure 4.10 Penetration depth pictures on the tissues when the laser parameters are applied from h = 10 mm.

The Tm:YAP laser system at 1980-nm will be experimented for ablation and welding applications due to the strong absorption by the tissue surface. The results on brain and skin samples will be analyzed by histology and light microscopy.

4.2 Brain Tissue Ablation by Tm:YAP Laser System

The aim of this part of the thesis is to develop a Tm:YAP based laser system for brain tissue ablation. The ablation efficiency of the developed laser system was experimentally tested on brain tissue ex-vivo as a predosimetry ablation study. Thermal changes were quantified in terms of ablation efficiency. Minimal thermal damage to the surrounding tissue was aimed. Carbonization should be avoided, thus controlling the laser duration is very crucial. The effects of different power and duration parameters of the surgical laser system on ex vivo tissue samples were investigated in terms of the thermal alteration of target tissue.

4.2.1 Background

Laser tissue ablation is a complicated process, involving multiple thermal effects, such as coagulation, dehydration and carbonization, which are affected by many parameters, including the laser parameters (such as laser type, power, pulse duration and pulse repetition), tissue parameters (such as tissue density, thermal conductivity and absorptivity) and environmental parameters (such as environmental medium like air, water or cryogen, medium velocity and temperature [199].

Thermal properties for tissue vary with temperature and water content. Increasing the tissue temperature may cause denaturation of molecules, coagulation, vaporization, or ablation. The laser irradiations vaporize water in the tissue causing sharp increases in temperature beyond 100°C, and continued irradiation causes ablation of the tissue [1].

The laser-tissue interaction was characterized by three distinct stages. In the first stage, a region of dehydrated tissue instantaneously formed. A high temperature would need to evaporate the substantial water in the tissue, if the heat time is short. During the tissue dehydration period, some protein structures can change. Water is intimately involved in the collagen structure [145]. The second stage followed with water

vaporization and bubbling observed at the tissue surface, accompanied by a popping and crackling sound and visible tissue rupture. The third stage of the interaction process began with the first signs of tissue browning, which became progressively darker until a black char formed around the edge of the ablation crater [23].

If laser intensity is high enough, the ablation process is usually mediated by mechanical effects. If laser intensity is quite low, the ablation process is mainly mediated by thermal effects. In an ablation process mediated by mechanical effects, tissue water is ejected in the form of liquid droplets or solid particles induced by thermoelastic tensile stress, which is induced by material expulsion. For an ablation process mediated by thermal effects, tissue removal will not happen until temperature reaches the ablation temperature. In addition, heat diffusion is always significant during the ablation process by thermal effects, resulting in much larger ablation threshold and depth of the thermally damaged zone [199].

The ablation threshold is dependent on the laser pulse duration. A potential explanation for the dependence of the ablation threshold on the pulse duration is that the thermal loss mechanism is a function of time. With increasing exposure time, the rate of growth of thermally altered tissue zone decreases as tissue water is removed, decreasing local thermal conductivity and resulting in reduced conduction of heat to surrounding areas. At longer pulse durations the ablation threshold is expected to increase because of the conductive loss of heat from the interaction layer. By using of shorter pulse durations, the ablation threshold reached with less energy [48].

In the literature, there is a wide range of applications of 2-μm lasers in tissue ablation. The ablation rates and tissue effects produced by a pulsed holmium laser with a wavelength of 2.12 μm and a pulsed thulium laser with a wavelength of 2.01 μm were compared in vitro and the thulium laser was found to yield a significantly lower threshold of ablation with far less residual thermal injury. The zone of residual thermal injury produced with the thulium laser was found to be slightly less than that produced by the holmium laser [31]. In addition, the CW thulium laser was used in the enucleation of the prostate with no collateral damage to adjacent tissue [47].

Neuroendoscopy study with a 2.0-μm near infrared laser system was also performed [30].

Lasers in neurosurgery provided precise tumor ablation by making spherical lesions without carbonizing. Brain tissue ablation has been investigated with different laser sources, such as 980-nm diodes [200] and 2.94-μm Er:YAG [201] lasers, as alternative tools to conventional electrosurgical units. Histological examinations showed that both 980-nm diode laser system and Er:YAG laser have a remarkable ablation performance with minimal thermal damage of nearby tissue. In this study, a Tm:YAP laser system is employed for ablation applications due to the strong absorption of its output radiation in water. The Tm:YAP laser at 1.98 μm has stronger absorption coefficient in liquid water than that for Tm:YAG and Ho:YAG lasers around 2 μm [33].

4.2.2 Materials and Methods

The experiments were aimed at investigation of dosimetry levels of Tm:YAP laser system for brain tissue ablation applications. In the in-vitro trials, it was observed that the Tm:YAP laser radiation was mostly absorbed at the surface of the tissues. Thermal alterations led to changes of optical properties of the tissue at the surface and this changed the penetration depth of the laser inside the tissue. In addition, increasing the laser power increased the thermally altered areas and penetration depths. By increasing the average light intensity (W/cm^2) of the laser system, the thermal and carbonization side effects were observed even in shorter time durations.

The ex vivo experiments were conducted under a protocol approved by the Institutional Animal Research and Care Ethic Committee at Boğaziçi University. Brain samples from male Wistar rats (5-6 months old, weighing 300-350 g) were dissected for the experiments. Rats were housed in plastic cages and maintained on a 12-h-light/12-h-dark cycle in a temperature-controlled vivarium ($22\pm2^{\circ}C$) in the Psychobiology Laboratory of Boğaziçi University. Food and water were available ad libitum. Rats were anesthetized with ketamine (10% ketamidor, RichterPharma, AG, Wels, Austria) by

intraperitoneal injection (1.65 ml/kg).

The coronal brains were sliced in 4-5 mm samples. The Tm:YAP laser was applied from a distance of 2 mm to cortical (grey matter) and subcortical (white matter) regions. Different exposure times were applied to compare the thermal effects. The selected Tm:YAP laser doses were determined from the efficient results obtained in the in-vitro studies. The Tm:YAP laser doses and the sample sizes were tabulated in Figure 4.11.

Zone	Laser power	Average light intensity	Duration (sample size)
Cortical	200 mW	69 W/cm^2	3 s (n=13), 6 s (n=8), 10 s (n=10), 15 s (n=24)
Cortical	400 mW	139 W/cm^2	1 s (n=8), 3 s (n=15), 6 s (n=16)
Cortical	600 mW	208 W/cm^2	1 s (n=8), 3 s (n=12), 6 s (n=10)
Subcortical	200 mW	69 W/cm^2	3 s (n=8), 6 s (n=8), 10 s (n=13), 15 s (n=12)
Subcortical	400 mW	139 W/cm^2	1 s (n=8), 3 s (n=13), 6 s (n=8)
Subcortical	600 mW	208 W/cm^2	1 s (n=8), 3 s (n=11), 6 s (n=8)

Figure 4.11 Tm:YAP laser dosimetry levels applied to ex vivo brain tissues for ablation analysis.

The total coagulation diameter (CD) and ablation diameter (AD) of each sample (Figure 4.12) were measured under a light microscope (Eclipse 80i, Nikon Co., Tokyo, Japan). The ablation efficiency (AE) was determined from AE = 100 x AD / CD. All data were expressed as mean ± standard deviation. The data were analyzed by Student's t-test, where a value of $p<0.05$ is considered to be statistically significant.

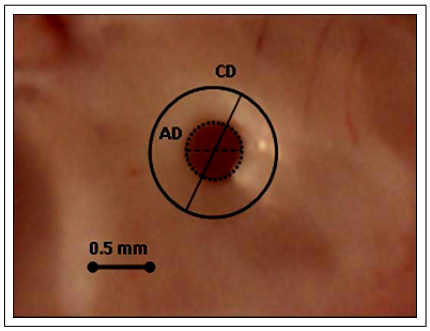

Figure 4.12 A brain tissue sample exposed to Tm:YAP laser.

4.2.3 Results and Discussion

4.2.3.1 Brain Ablation by the Tm:YAP Laser at 200 mW.

Coagulation and ablation diameters of both cortical and subcortical samples exposed to 200 mW (69 W/cm^2). Tm:YAP laser are given in Figure 4.13. There is no statistically significant difference between coagulation diameters of cortical and subcortical samples at 3 seconds (p=0.98), 6 seconds (p=17), and 10 seconds (p=0.5) of laser exposure. However, at 15-second application, coagulation diameters were statistically significant (p<0.01). There were statistically significant ablation diameters among cortical and subcortical samples found only at 10-second (p=0.037) and 15-second (p=0.04) exposure.

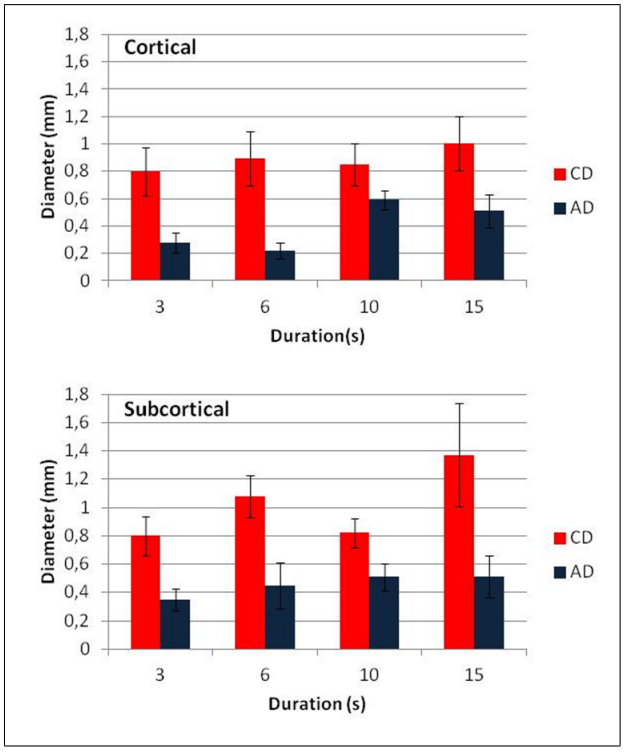

Figure 4.13 Coagulation and ablation diameters of cortical and subcortical brain tissue exposed to Tm:YAP laser at 200 mW.

For cortical tissue samples, the increase in laser application duration from 3 seconds to 6 seconds and from 6 seconds to 10 seconds did not differentiate the coagulation diameter statistically (p=0.31). However, at 15-second application differentiated

the coagulation diameter statistically ($p<0.001$). Increase in laser application duration increased the ablation diameters, which are statistically significant among 3-second and 6-second applications ($p = 0.0025$), among 6-second and 10-second applications ($p = 0.024$). There is no statistical significance for ablation diameters among 10-second and 15-second laser applications ($p = 0.06$). For subcortical tissue applications, the increase in duration from 3 seconds to 6 seconds increased the coagulation diameter ($p=0.053$). The duration increase from 6 seconds to 10 seconds ($p=0.006$) and from 10 seconds to 15 seconds ($p<0.001$) provided statistically significant coagulation diameters.

4.2.3.2 Brain Ablation by the Tm:YAP Laser at 400 mW.

Coagulation and ablation diameters of both cortical and subcortical samples exposed to 400-mW (139 W/cm^2) output of the Tm:YAP laser are given in Figure 4.14. Since the average light intensity at 400 mW was much higher, the experiments were performed from 1-second application duration to 6-second application duration until the carbonization effect was observed. Coagulation effects were observed even at 1-second exposure.

Among cortical and subcortical tissue samples, coagulation diameter for subcortical samples was statistically higher ($p=0.03$) than coagulation diameter for cortical samples at 6-second application. Ablation diameters were not found to be statistically significant among cortical and subcortical samples at 1-second ($p=0.92$), 3-second ($p=0.08$), and 6-second ($p=0.06$). For both cortical and subcortical tissue samples, increasing duration from 3 seconds to 6 seconds made the coagulation diameters higher and statistically significant ($p=0.03$). On the other hand, ablation diameters were found to be higher and statistically significant when the application duration was increased from 1 second to 3 seconds ($p=0.024$) for subcortical samples. For cortical samples, increasing application duration from 1 second to 6 seconds at 400 mW, made ablation diameters statistically significant ($p=0.008$).

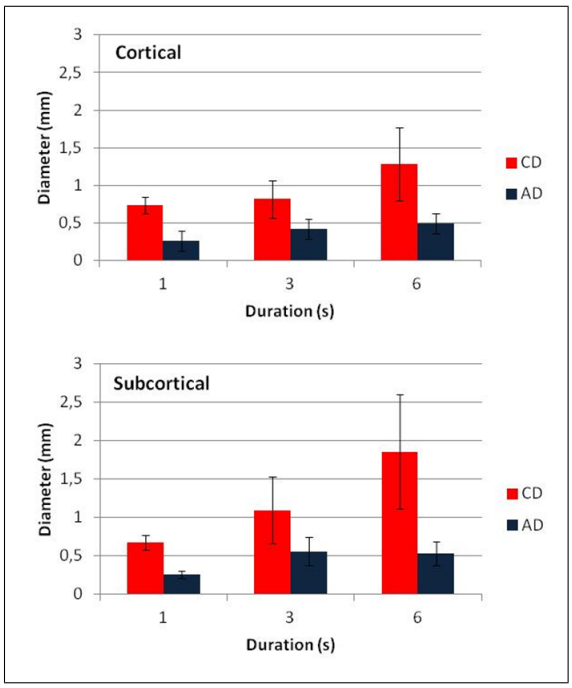

Figure 4.14 Coagulation and ablation diameters of cortical and subcortical brain tissue exposed to Tm:YAP laser at 400 mW.

4.2.3.3 Brain Ablation by the Tm:YAP Laser at 600 mW.

Coagulation and ablation diameters of both cortical and subcortical samples exposed to 600 mW (208 W/cm^2) Tm:YAP laser are given in Figure 4.15. At the laser power of 600 mW, there were no statistically significant coagulation and ablation diameters among cortical and subcortical samples. For cortical samples, coagulation diameters among 3-second and 6-second durations were found statistically significant (p=0.01). On the other hand, ablation diameters were not found statistically significant among 1-second and 6-second durations (p=0.32), among 3-second and 6-second durations (p=0.25), and among 1-second and 6-second durations (p=0.84). For subcortical samples, increasing the duration from 3 seconds to 6 seconds made coagulation diameter higher and statistically significant (p=0.02). Ablation diameters were not found to be statistically significant from 1-second to 3-second durations (p=0.12), from 3-second to 6-second durations (p=0.24).

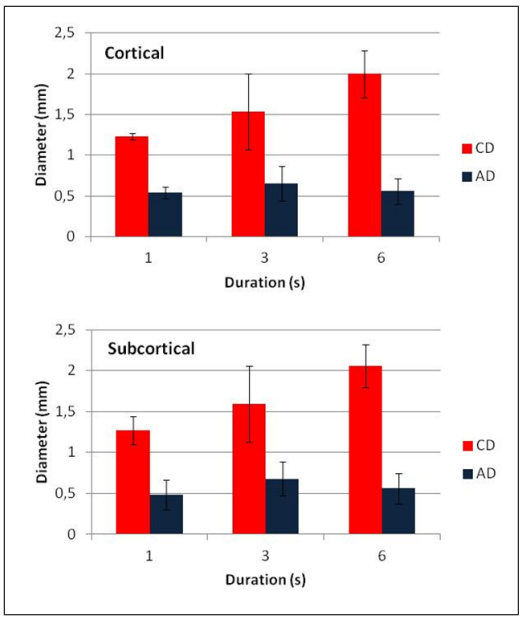

Figure 4.15 Coagulation and ablation diameters of cortical and subcortical brain tissue exposed to Tm:YAP laser at 600 mW.

4.2.3.4 Discussion.

Laser tissue interactions are thermal and highly nonlinear time-varying dynamic processes [137]. Photothermal interactions result from the transformation of absorbed light energy into heat. The heat deposition in tissues by laser application is strongly dependent on optical tissue properties like scattering, and absorption as well as thermal properties. The optical absorption coefficient strongly depends on the wavelength of the laser radiation applied. The heat storage and transfer are also dependent on thermal tissue properties, such as heat capacity and thermal conductivity. The interaction of a laser light with tissue, therefore, depends on the wavelength of the laser, exposure time and the optical properties of the tissue, which are determined by the structure, water content, blood circulation, heat conductivity, heat capacity, and density of tissue. However, optical and thermal properties of tissue are not constant and change during laser irradiation. Thermal conductivity is decreased due to dehydration and heat diffusion is consequently reduced and tissue temperature is increased. Depending on the duration and peak value of the temperature achieved, different effects like coagulation, vaporization, melting or carbonization may be observed. The temperature rise leads to protein dehydration, denaturation, coagulation, and/or ablation [114].

In tissue ablation, the aim is to remove the target tissue without any thermal damage to the surrounding tissue. Energy is dissipated primarily close to the tissue surface. Once the tissue surface is broken, the ablation spreads in deeper layers of the tissue. As absorption increases, propagation of thermal energy is reduced to the edge of the dehydrated zone [23].

2-μm lasers suggest the potentials for accurate tissue removal by thermally induced coagulative and haemostatic effects. Water is the primary absorbing component in tissue at wavelengths above 1.4 μm, leading to efficient conversion of light into heat. Longer infrared wavelengths heat the surface layer of water on the irradiated tissue, with subsequent heat conduction to the tissue elements below this surface. As water is removed from the tissue, local thermal conductivity decreases. This results in reduced heat conduction to the surrounding area.

The water absorption at 1980 nm is 89 cm^{-1}. The optical penetration depth of 2-μm lasers was found to be about 300 μm [41]. However, water absorption around 2 μm is strongly temperature dependent and tissue ablation is highly temperature dynamic process. At wavelengths between 1.85 nm and 2.15 nm, the absorption coefficient decreases substantially as temperature increases. In the inner structure of water, intramolecular and hydrogen bonds are affected by temperature changes. Therefore, the corresponding absorption bands and their harmonics shift in the center wavelength and intensity [40]. To avoid the thermal damage and carbonization of the target tissue, controlling the laser parameters and dosimetry studies are very crucial.

The surgical Tm:YAP laser system was developed in this study and the system produced laser beams with adjustable parameters by communicating accurately with the user interface program. Users can adjust the power and laser duration in on/off cycles. Controlling the mode of operation can change the photothermal effect on soft tissue. Before any clinical applications, the dosimetry study can be performed in terms of power, duration, and modulation parameters. Depending on laser parameters, the dimension of the thermally altered areas is changed from coagulation to carbonization. Diameters of lesions increase with increasing power and duration. The system perfor-

mance and ablation characteristics were tested on Wistar rat brain tissue ex vivo with different power levels of the Tm:YAP laser.

The coagulation and ablation diameters found in the experiments were used to calculate the ablation efficiency for each Tm:YAP laser power level. Ablation efficiencies are shown in Figure 4.16 for 200 mW (69 W/cm^2), 400 mW (139 W/cm^2), and 600 mW (208 W/cm^2) power levels.

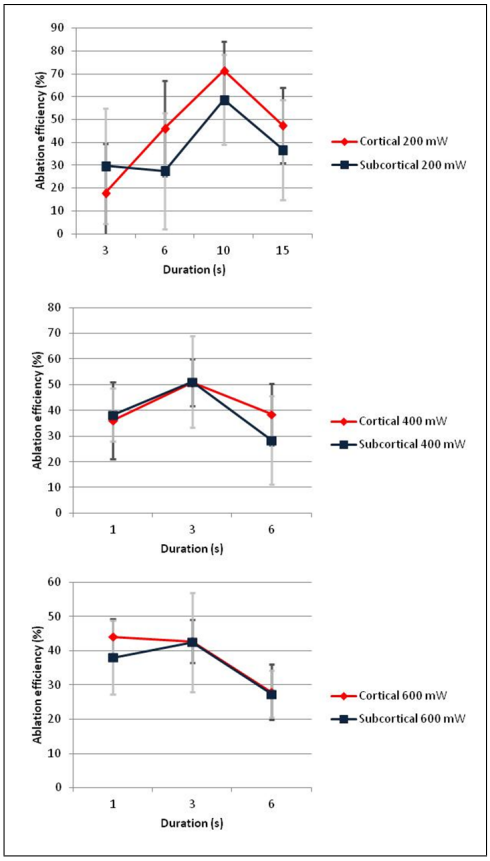

Figure 4.16 Ablation efficiencies of cortical and subcortical brain tissues exposed Tm:YAP laser at 200 mW, 400 mW, and 600 mW of output power.

The maximum ablation efficiency was obtained at 200 mW of Tm:YAP laser application for both cortical and subcortical tissues. At 400 mW Tm:YAP application, the duration of 3 seconds provided the maximum ablation efficiency, however it is lower than the maximum ablation efficiency at 200 mW. There were no statistically significant ablation efficiencies among the application durations at 600 mW. As a result, the maximum ablation efficiency was obtained at 200 mW Tm:YAP laser application for a duration of 10 seconds for both cortical and subcortical brain tissues.

The ablation characteristics of brain and Tm:YAP laser interactions are worth being performed in future studies to maximize the ablation efficiency since thermal injury of surrounding tissues was minimized by using pulsed radiation due to cooling of the tissue between pulses [135]. When the laser pulse width was less than the tissue thermal relaxation time, thermal diffusion outside the application area was reduced and the thermal injury of the surrounding tissues was minimized. In addition, the instrumentation and dosimetry study presented here can be expanded with histological examination in order to understand the limits of the thermal effects that the laser system creates.

Around 2-μm wavelengths, lasers coupled through a fiber offer good coagulation properties. At higher wavelengths, like Er:YAG and CO_2 lasers, lasers offer similar coagulation properties with high absorption by water as 2-μm lasers; however, the optimization of fiber delivery of Er:YAG and CO_2 lasers is difficult in clinical use [27].

The experiments suggest an efficient starting point for a clinical dosimetry study for brain tissue ablation. Further experiments should be performed on higher animals in order to bring this technique to clinical practice. The ablation efficiency can be further increased by optimizing the laser pulse duration and energy density for each kind of biological tissue through histology studies.

In conclusion, the system performance and ablation characteristics of the Tm:YAP laser system were performed by sampled ex vivo experiments on Wistar rat brain tissue. Optimization of the Tm:YAP laser ablation efficiency for cortical and subcortical brain tissues was performed by maximizing the therapeutic effect and minimizing unwanted side effects with different power levels of the Tm:YAP laser. The maximum ablation efficiency was obtained when the Tm:YAP laser was applied at the power level of 200 mW with a duration of 10 seconds (2 J). At this laser dose, the ablation efficiency was obtained as 71.4% for cortical region and 58.7% for subcortical region. The fiber-coupled Tm:YAP laser system was found to be promising for photo-ablation applications. Further investigation of Tm:YAP laser applications has been warranted.

4.3 Skin Tissue Ablation by Tm:YAP Laser System

4.3.1 Background

4.3.1.1 Structure of Skin and Skin Optics.

Skin is the largest organ of the body, making up approximately 14-16% of human adult body weight. It generally consists of three layers: epidermis, dermis and subcutaneous tissue (Figure 4.17). The thickness of these layers varies depending on the location of the skin. Epidermis with thickness of 0.1 mm, dermis with thickness of 1.5 mm, and subcutaneous fat with thickness of 4.4 mm were used in a modeling study [149].

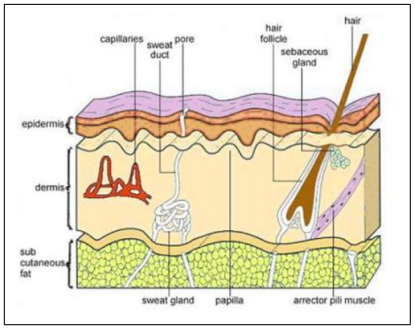

Figure 4.17 Structure of skin [149].

The epidermis is a 0.027 - 0.15 mm thick structure. It is mostly made of keratinocytes cells which produce fibrous protein keratin. Deeper layers are made of younger cells, which gradually travel outwards, transforming into a hard protective layer along the way. The epidermis absorbs light. The absorption property comes mostly from water and melanin pigment. However, for wavelengths longer than 1100 nm, both skin transmittance and remittance are not affected by melanin pigmentation [38]. The dermis is a 0.6 - 3 mm thick structure which also absorbs light. Most of the dermis, around 75%, is made of two proteins: collagen and elastin, providing skin's strength and elasticity. There are many structures in the dermis: tiny loops of blood vessels with important role in regulation of body temperature, glands, receptors for various stimuli, and hair follicles. These layers are primarily composed of dense, irreg-

ular connective tissue with nerves and blood vessels. In the blood cells, there is natural chromophore, hemoglobin, which absorbs light and gives blood its reddish color. The subcutaneous tissue presents significant deposits of white fat. Due to the presence of these white fat deposits, most of the visible light that reaches this tissue is reflected back to the upper layers [202].

One of the most important roles of skin is thermoregulation. Skin functions thermally as a heat generator, absorber, transmitter, radiator, conductor and vaporizer, thus acting as an important barrier for the human body to various outside conditions. However, skin fails to protect the body when the temperature lies outside the normal physiological range. The transfer of heat in skin is mainly a heat conduction process coupled to complicated physiological processes, including blood circulation, sweating, metabolic heat generation and, sometimes, heat dissipation via hair or fur above skin surface [203].

The mechanical behavior of skin tissue is found to be heterogeneous, anisotropic, non-linear, and viscoelastic in vivo because of its non-homogenous structure and composition. The major constituent skin is collagen. During heating, when the temperature exceeds a certain threshold, thermal denaturation of collagen occurs. Furthermore, not only the structure, but also the hydration of collagen changes during denaturation. Thermal denaturation of a collagenous tissue can therefore lead to remarkable changes in skin mechanical, thermal, electrical, and optical properties [149].

When a laser beam strikes the skin, there are four possible outcomes: reflection, scattering, transmission, or absorption of light. A tissue effect can only occur when light is absorbed. The skin contains several chromophores that selectively absorb light at certain wavelengths. The main chromophores of the skin are water, melanin, and hemoglobin. When these chromophores absorb laser energy, their molecules become excited and create a photochemical reaction or dissipating their energy as heat. In most cases the absorbed energy is converted to thermal energy. The depth of light penetration in the skin or the optical penetration is affected by two essential processes: absorption and scattering of light. In the epidermis, absorption is the dominant pro-

cess over most of the optical spectrum, whereas in the dermis optical penetration is largely dominated by scattering due to the high collagen content. The dermis may be considered a turbid tissue matrix with which optical scattering is an inverse function of wavelength and largely defines the depth of optical penetration [37].

4.3.1.2 Skin Ablation.

The ablation of skin tissue has been investigated extensively in the literature. Results of these studies have led to the wide acceptance of clinical procedures using modulated laser pulses to treat disorders of cutaneous pigmentation. Ablation-based laser surgery using visible or near-infrared laser pulses has gained significant recognition owing to the potential to achieve precise ablation and reduce collateral tissue damage. These capacities are especially desired in dermatology and cosmetic surgery [48].

In the cellular level, hyperactivity of Calcium-ATPase calcium pumps produces much calcium influx during ablation. This process exhausts the cell energy and the increased intracellular osmotic pressure eventually explodes the cell. The cell death induced by a laser irradiation has been explained by photothermal effect which results in desiccation, protein denaturation, coagulation, evaporation of soft tissue, as well as biochemical alteration in cell metabolism [204].

Photothermal interactions of Ho:YAG laser at 2.12 μm on tissue damage and recovery were studied for rabbit skin with different operating parameters by measurement of the lesions and by tissue histology. The lesion size on the surface, the photocoagulation depth and the thermal damage depth were recorded as functions of irradiation parameters. The lesion width and the photocoagulation depth increased with the beam energy while the area of thermal damage remained relatively unchanged. The thermal damage on rabbit skin began recovery within a short period and new epithelial growth was clearly seen at day 3. By 7 days, most of the photocoagulated zone was separated from the main body and was replaced by a new layer of epithelium [52].

Some studies also used mass loss experiments to analyze the ablation rate. The ablation rate was calculated by dividing the mass loss by the number of laser pulses and expressed in micrograms per pulse. The linear dependence of ablation rate on radiant exposure was found in agreement with the mass loss measurements. The threshold radiant exposure was found inversely proportional to the absorption coefficient [31]. Although typically an order of magnitude lower than at the CO_2 wavelength, tissue absorption coefficients in the 2-μm wavelength region are still significantly higher than at near-infrared and visible wavelengths [23].

The laser-tissue interaction experiments were also reported with a novel short pulse high-peak power, tunable Qswitched Tm^{3+}-silica fibre laser and a CW fibre laser operating at wavelengths ranging from 1.94 to 1.99 μm. Comparisons were made of crater depths, zones of secondary damage, and heat of ablation for soft tissues [48]. In addition, the findings of preliminary experiments by 2-μm fiber laser were described investigating the interaction by microscopic images of surfaces and histological sections of craters and slots cut in tissue [23].

Histology studies of skin damage were performed at 48 hours after irradiation with a 2.0 μm Thulium continuous-wave laser to determine the mechanisms of laser effects in the skin. For each threshold lesion, the widths of epidermal necrosis at the surface, the outer boundary of the thrombosis zone, the depth of vascular thrombosis, and the depth of perivascular inflammation and edema were measured to predict various types of thermal injury in the skin [37].

4.3.2 Materials and Methods

4.3.2.1 Ablation of ex-vivo Skin Tissues.

In this part of the study, the effects of Tm:YAP laser doses on ex-vivo skin samples were investigated. The fiber tip from both 10 mm and 5 mm was positioned on the skin samples dissected from discarded Wistar rats. The laser doses of CW mode

were applied (Figure 4.18). The applications were sampled by two tissues for each application distance of 5mm and 10 mm. The thermally altered diameters on the skin samples were measured and the average values of the sampled tissues are reported.

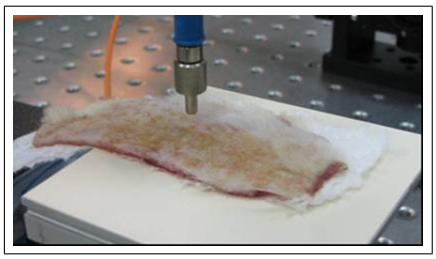

Figure 4.18 Tm:YAP laser application on ex-vivo skin samples.

The thermally altered areas on the ex-vivo skin samples after the laser application were photographed. The thermally altered diameters of each sample were measured by a micrometer. The penetration depths of the skin samples by the Tm:YAP laser doses from 5 mm were also measured.

4.3.2.2 Ablation of in-vivo Skin Tissues.

In addition to macroscopic analysis, it is necessary to analyze the thermal effects under light microscopy by histology. The experiments were conducted under a protocol approved by the Institutional Animal Research and Care Ethic Committee at Boğaziçi University. Healthy male Wistar rats, 5-6 months old, weighing 240-250 g, were randomly selected from Psychobiology Laboratory of Bogazici University for in vivo experiments. Rats were housed in plastic cages and maintained on a 12-h-light/12-h-dark cycle in a temperature-controlled vivarium (22±2°C). Food and water were available ad libitum. Rats were anesthetized with ketamine (10% ketamidor, Richter-Pharma, AG, Wels, Austria) by intraperitoneal injection (1.65ml/kg). Hair at the site of application of each subject was shaved.

All the laser application procedure was conducted by one operator to in vivo Wistar rat skin. Laser protective glasses were used when the laser was active. Power, duration, and mode of operation (modulated and CW) parameters were set by another

operator through the user interface on the PC. Laser output power was checked with a powermeter (Newport 1918-C, Irvine, CA, USA) before each application. The laser application was sampled at a distance of 2 mm above to each spot. The laser spot diameter was measured from 2 mm as 0.6 mm by using the knife-edge technique.

In modulated mode of operation of Tm:YAP laser system, a laser pulse duration of 200 msec was chosen in this thesis to confine heating to the application site and reduce the temperature rise in the surrounding tissue. Previous studies have shown that, 200 ms pulse duration limited thermal diffusion during the laser pulse to a lateral zone of around 200 μm from the application site. If the thermal damage zone is much greater than 200 μm, then the amount of scarring increases significantly during wound healing [18].

4.3.2.3 Histology Procedure.

The skin tissue samples exposed to Tm:YAP laser (Figure 4.19) were dissected in in-vivo experiments. The samples were then fixed in 10% formalin and processed by Leica TP1020 tissue processor (Figure 4.20). Dehydrated procedure is given in Table 4.1. Dehydrated tissues were embedded by Leica EG1150H into paraffin (Figure 4.21). 5-10-μm-thick tissue sections were obtained via microtome of Leica RM2255 (Figure 4.22). Tissue sections were obtained from removal of paraffin over tissues by inserting into 40°C water-bath (Figure 4.23). Tissues were aligned on top of glass slides. These slides were kept in etuve overnight in order to remove remaining paraffin.

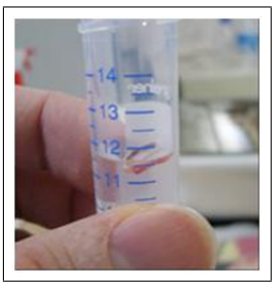

Figure 4.19 The tissue samples fixed in formalin (10%) before dehydration procedure.

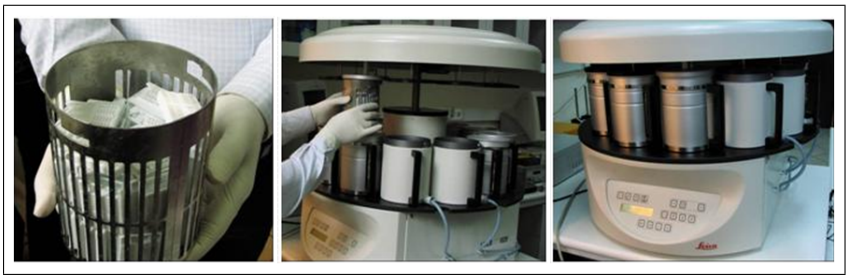

Figure 4.20 Dehydration process by Leica TP1020, Tissue Processor.

Dehydration Procedure		
ALCOHOL	70%	1 hour
ALCOHOL	70%	1 hour
ALCOHOL	80%	1 hour
ALCOHOL	80%	1 hour
ALCOHOL	90%	1 hour
ALCOHOL	90%	1 hour
ALCOHOL	100%	1 hour
ALCOHOL	100%	1 hour
XYLENE		1 hour
XYLENE		1 hour
PARAFFIN	60^oC	1.5 hour
PARAFFIN	60^oC	1.5 hour

Table 4.1
Tissue dehydration procedure.

Figure 4.21 Dehydrated tissues embedded into paraffin by Leica EG 1150 H, Paraffin Embedding System.

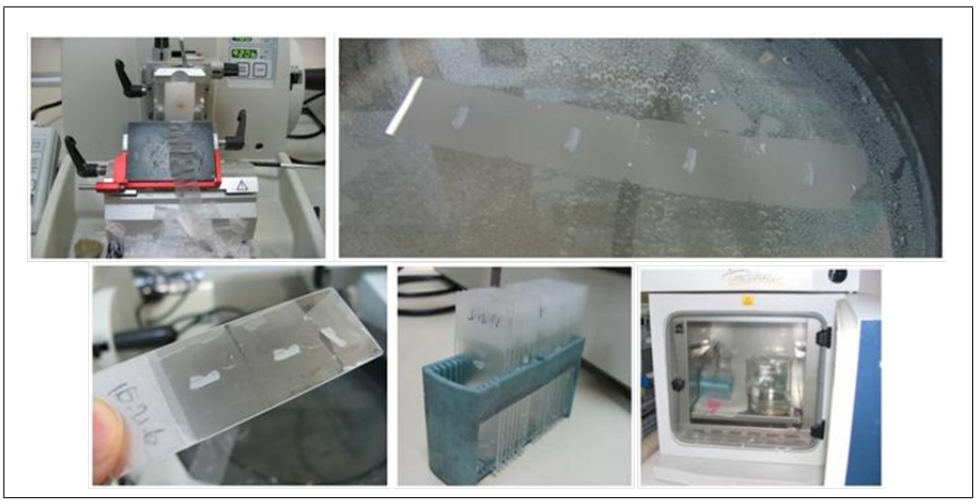

Figure 4.22 Tissue sectioning by Leica RM2255, Rotary Microtome.

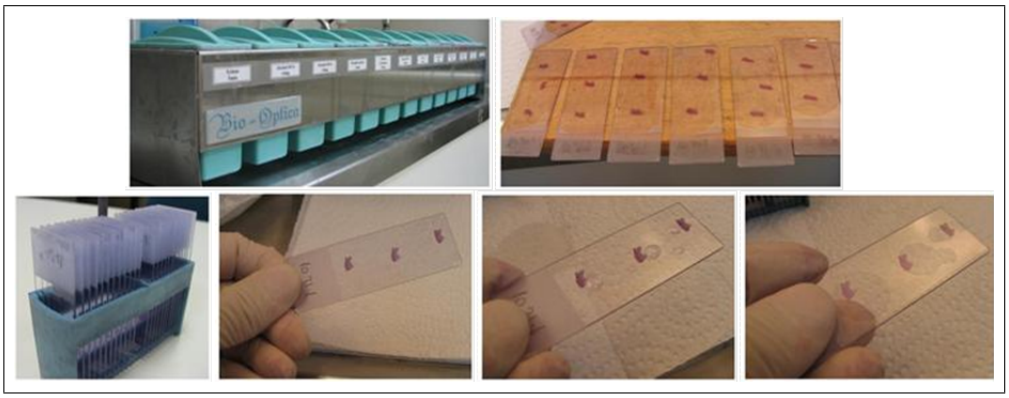

Figure 4.23 Haematoxylin and Eosine stain procedure of tissue samples.

The skin tissue samples were analyzed after hematoxylin and eosine histology protocol. This protocol gives idea about general tissue structure. The staining method involves application of the basic dye haematoxylin, which colors basophilic structures with blue-purple hue, and alcohol-based acidic eosin Y, which colors eosinophilic structures bright pink. Eosinophilic describes the appearance of cells and structures seen in histological sections which take up the staining dye, eosin. This is a bright pink dye that stains the cytoplasm of cells as well as extracellular proteins such as collagen. This procedure will give the idea about carbonization, infections, and healing quality of the tissue samples under light microscopy.

The bright areas in the polarized histology pictures under light microscopy (Nikon 80i Eclipse) show the collagens whereas the holes show the fat areas in the tissues. The normal tissue image (x40) under the light microscope is given in Figure 4.24. The collagens can be seen in the image (x100) in Figure 4.25.

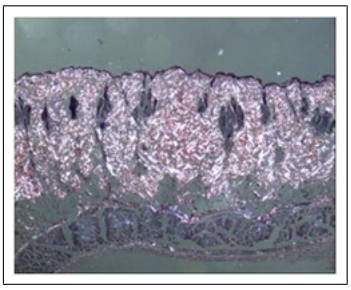

Figure 4.24 Normal skin tissue (x40).

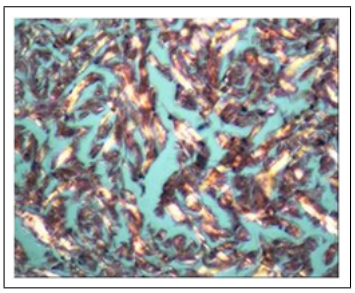

Figure 4.25 Normal skin tissue and its collagens (x100).

A microscopic photomicrograph of thermally damaged skin shows the evaporation zone, the carbonization zone, and the coagulation zone. Morphologic signs of thermal damage including coagulation, vacuolization, carbonization, and ablation can

be examined by nonpolarized light microscopy. On the other hand, polarizing light microscopy has revealed changes in the native birefringence of certain tissues when they are heated. Tissue birefringence is detected by illuminating a microscopic tissue section with incident light polarized 90° to an optical analyzer located above the section creating a dark field. Birefringent tissues will rotate the polarized light to create bright images of the anatomic structures in the dark field. Several types of tissues including collagen can be examined with transmission polarizing microscopy. Changes and/or loss of birefringence of collagen were detected using polarizing microscopy. The sharp boundary of color change corresponded to the boundary between the thermally coagulated collagen and the undamaged fibrillar collagen [205].

4.3.2.4 Ablation Analysis Parameters.

The histology pictures were selected and sampled from tissue sections where the laser ablation was found maximum for each sample. Figure 4.26 shows the ablation analysis parameters under light microscope.

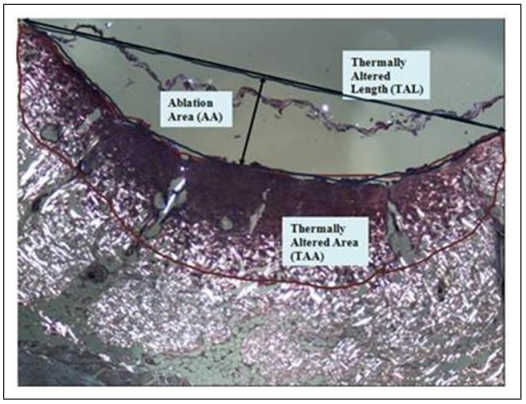

Figure 4.26 Ablation analysis parameters.

In this polarized picture of the tissue sample, the bright areas include collagens of the skin. The holes in the pictures are fat areas of the skin tissue. The thermally effected area is simply distinguished by normal tissue. There is an ablation zone where the laser is applied. The area of this blue-boundary zone, ablation area (AA), can be measured by the microscope software. Ablation depth (AD) of this zone can also

be measured. In addition, thermally altered area (TAA) on the tissue is shown by red boundary. Thermally altered length (TAL) is the length on the tissue sample affected by laser application. These parameters will be used to analyze the laser-tissue interactions quantitatively under light microscopy.

4.3.3 Results and Discussion

4.3.3.1 Ablation of ex-vivo Skin Tissues.

The thermally altered diameters on the ex-vivo skin samples after the laser application from 10 mm are shown in Figure 4.27. The carbonization effects were observed for 0.70 W and 15 second laser application.

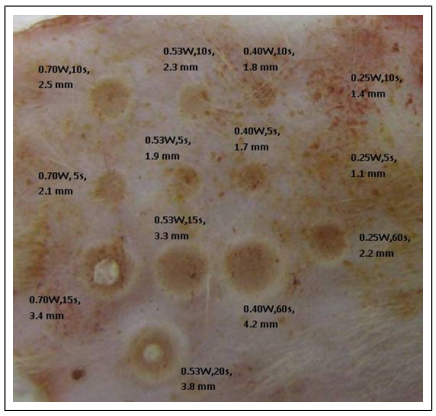

Figure 4.27 The thermally altered areas of ex-vivo skin tissues after he Tm:YAP laser application from 10 mm.

Figure 4.28 shows the results of similar trials when the laser parameters were applied from 5 mm top of the tissue sample. The thermally altered diameters were found larger now because the average light intensity was increased due to the smaller laser spot diameter. The increased average light intensity increases the thermal effects on the samples.

The penetration depths by the Tm:YAP laser doses from 5 mm were also measured by micrometer. Penetration depths of 0.5 mm for 0.25 W - 20 sec., 0.8 mm for 0.40 W - 20 sec., 1.0 mm for 0.53 W - 20 sec and 1.2 mm for 0.70 W - 20 sec were

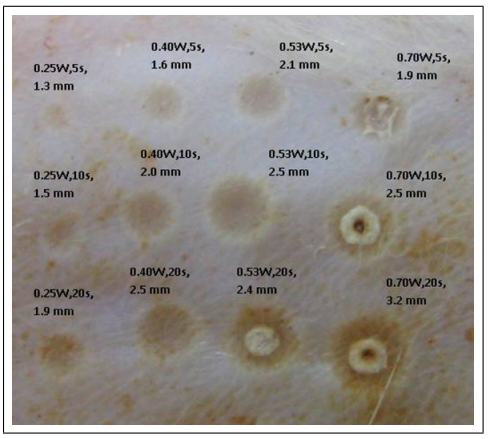

Figure 4.28 The thermally altered areas of ex-vivo skin tissues after he Tm:YAP laser application from 5 mm.

obtained. Figure 4.29 shows the penetration depths after the Tm:YAP laser application of 0.70 W and 20 sec. The similar experiments will be repeated by histology for ablation and welding parameters during the healing period.

Figure 4.29 Penetration depth after the Tm:YAP laser application of 0.70 W 20 s.

4.3.3.2 Ablation Analysis of ex-vivo Skin Samples by Histology.

In the first part of the histology analysis experiments, Tm:YAP laser was applied from 5 mm and 10 mm top of the ex-vivo skin samples. Figure 4.30 shows the laser parameters that were applied for histology analysis. The laser power was set fixed at 0.7 W. Changing the distance to the skin sample is changing the laser spot diameter and average light intensity. The different the time durations are changing the energy density applied to the skin samples. The histological images of the tissue samples with the laser doses in Figure 4.30 were shown in Figure 4.31. The images were 10-μm tissue sections where the laser parameters were applied. The center of each tissue had

maximum damage, these tissue slides were chosen for the data analysis. The histology pictures were selected and sampled from tissue sections where the laser ablation was found maximum for each sample.

Laser Power (W)	Fiber to sample distance (mm)	Duration (s)	Laser spot diameter (mm)	Average light intensity (W/cm^2)
0.7	5	10	1.44	47.61
0.7	5	20	1.44	47.61
0.7	10	10	2.87	12.07
0.7	10	20	2.87	12.07

Figure 4.30 Tm:YAP laser parameters applied on the ex-vivo skin samples.

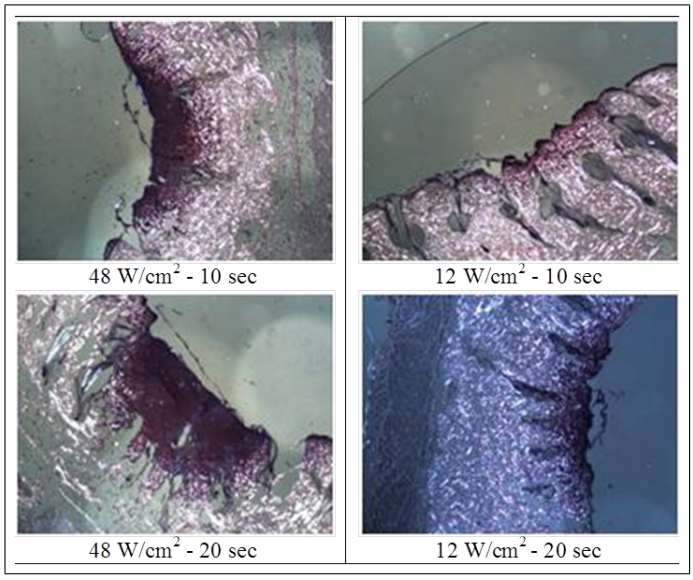

Figure 4.31 Histological images of the tissue samples after Tm:YAP laser applications in Figure 4.30.

The histological images in Figure 4.31 show that Tm:YAP laser doses at 12 W/cm^2 - 10 second give less ablation effect on the tissue. The ablation area on the tissue gets bigger while increasing the duration with the same laser powers. When the laser to the tissue distance is decreased, the laser spot on the tissue is increased. The ablation area and thermally altered area values are found larger. The details of all ablation parameters are given in Figure 4.32 below. The thermally altered lengths are found smaller due to the smaller laser spot with closer application of the laser to the target tissue. Increasing the power and average light intensity makes the thermally altered area bigger on the tissues.

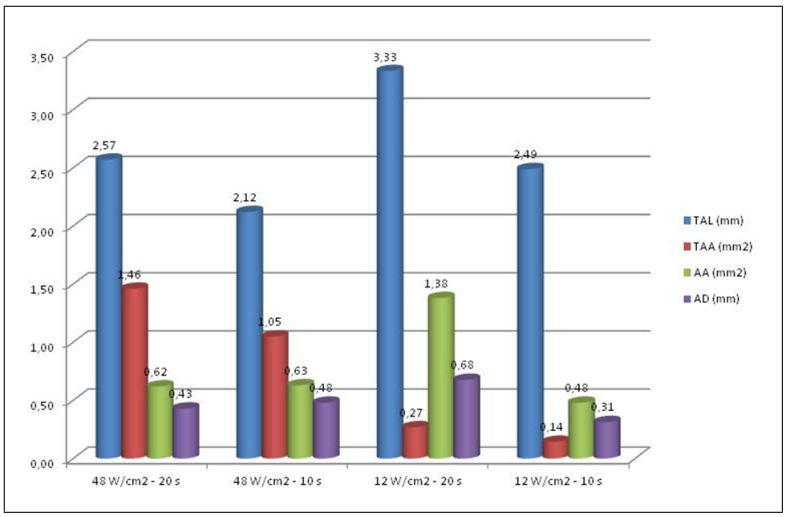

Figure 4.32 Ablation analysis parameters after the laser applications in Figure 4.30.

The second experiment group was performed by fixing the laser to tissue distance at 2 mm. The ex-vivo skin tissues dissected from discarded Wistar rats were used in the experiments. By changing the laser power and duration, different power and energy densities were obtained and the laser parameters in Figure 4.33 were applied to the tissue samples (n=2). Tm:YAP laser (0.7 W and 0.53 W) was pointed from 2 mm top of the skin tissue samples for 5 second and 10 seconds durations. The laser spot on the tissue was measured as 0.61 mm.

Laser Power (W)	Fiber to sample distance (mm)	Duration (s)	Laser spot diameter (mm)	Average light intensity (W/cm^2)	Energy density (J/cm^2)
0.70	2.0	20	0.61	242.65	4853
0.70	2.0	10	0.61	242.65	2426
0.53	2.0	20	0.61	183.72	3674
0.53	2.0	10	0.61	183.72	1837

Figure 4.33 Tm:YAP laser parameters applied on the ex-vivo skin samples from 2 mm.

The different laser power and duration differentiated the power and energy densities. Histology pictures in Figure 4.34 showed significant ablation areas on the skin tissue surfaces, where the Tm:YAP laser radiation was applied. As seen in Figure 4.35, the ablation area of 0.39 mm^2 on the tissue section was found for 4853 J/cm^2 laser radiation. The thermally altered length on skin tissues and thermally altered area inside the tissue were found higher for higher energy densities.

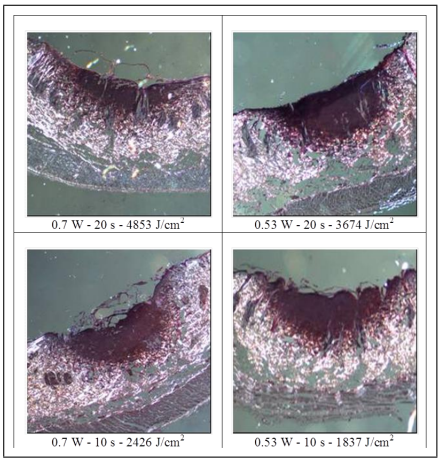

Figure 4.34 Histological images of the tissue samples after Tm:YAP laser applications in Figure 4.33.

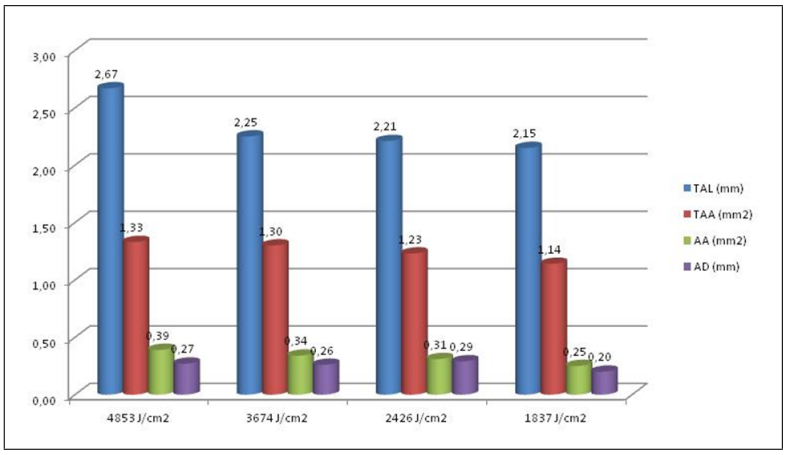

Figure 4.35 Ablation analysis parameters after the laser applications in Figure 4.33.

The center of the applied area showed more severe thermal damage. The thermal damage zones extended deeper into the dermis. When the power was increased, a darker scab-like central area on the skin surface resulted a central shrunken, desiccated epidermis. This area was detached from the underlying dermis. The underlying collagen fibers of the dermis were swollen and hyalinized. The concentric damage zones of thrombosis and perivascular inflammation extended further into the dermis. Increasing the power more produced water vaporization in dermis and ruptured epithelium layers. This thermal damage caused fragmented epidermis with severely thermally damaged hyalinized dermal collagen as seen also in the literature [37].

In the histology sampling analysis, tissue ablation was obtained at various effects of ablation area (AA), thermally altered area (TAA) and thermally altered length (TAL) on the tissue, depending on the tissue and laser parameters and the temperature range achieved. The different laser power and duration differentiated the power and energy densities. Histology pictures showed significant ablation areas on the skin tissue surfaces, where the Tm:YAP laser radiation was applied. The TAL on skin tissues and TAA inside the tissue were found higher for higher energy densities. The results of these experiments suggest that due to strong water absorption, 1980-nm Tm:YAP lasers are promising efficient candidates for efficient skin tissue ablation with minimal depth compared to smaller wavelength lasers. Whereas other types of lasers can penetrate the tissue too deeply, Tm:YAP lasers interact with the tissue surface that enables to cleanly remove the unwanted part of the tissue from the healthy part or strip it layer by layer. In the next part, similar trials are planned for modulated mode of operation during 4-day healing period in vivo.

4.3.3.3 Ablation of in-vivo Skin during 4-day Healing Period.

The fluence effect of the laser system for skin ablation was analyzed by Wistar rat skin tissues during four-day healing period. The laser parameters applied to the in vivo skin tissues were tabulated in Figure 4.36. Serial consecutive histologic sections were cut through selected sample blocks from two different animals and examined to locate the center of the thermal lesion at the microscopic level to determine the maximum histological diameter of the lesion in the skin. Averages of each parameter were used in ablation analysis. The Tm:YAP laser was applied in modulated mode of operation as 200 ms on/off. The histology images of the skin samples at day0 and day4 were given in Figure 4.37

As seen in Figure 4.38, TAA was increasing when duration was increased in the same power level for day0. On the other hand, AA and AD were measured smaller when the laser energy density was increasing. This shows laser parameters should be applied in less powers and energy levels for efficient ablation effect. Similar results were

Laser Power (W)	Average light intensity (W/cm^2)	Duration (s)	Fluence (J/cm^2)
0.99	343	10	3430
0.99	343	20	6860
1.14	395	10	3950
1.14	395	20	7900

Figure 4.36 Modulated laser parameters applied to in vivo skin samples.

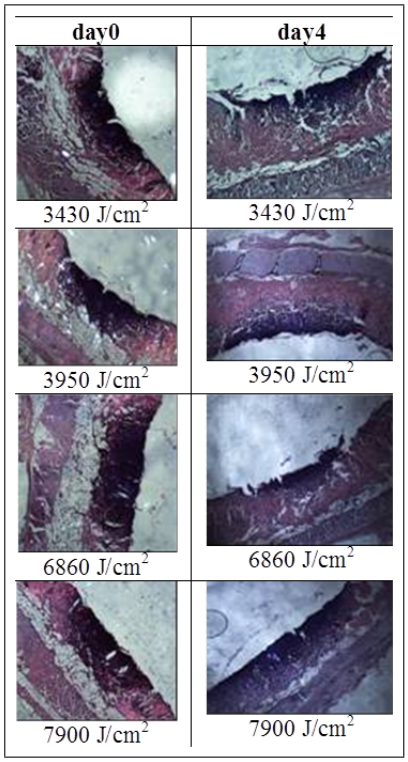

Figure 4.37 Histologic images of the tissue samples after modulated Tm:YAP laser applications in Figure 4.36.

observed for skin samples at day4 (Figure 4.39). However, TAL, TAA, AA, and AD values were found higher than the values at day0. This shows that the thermal effects were spreading to the deeper layers during the healing period. As the power increased, edema, epidermal necrosis and decrease of dermal collagen birefringence were observed.

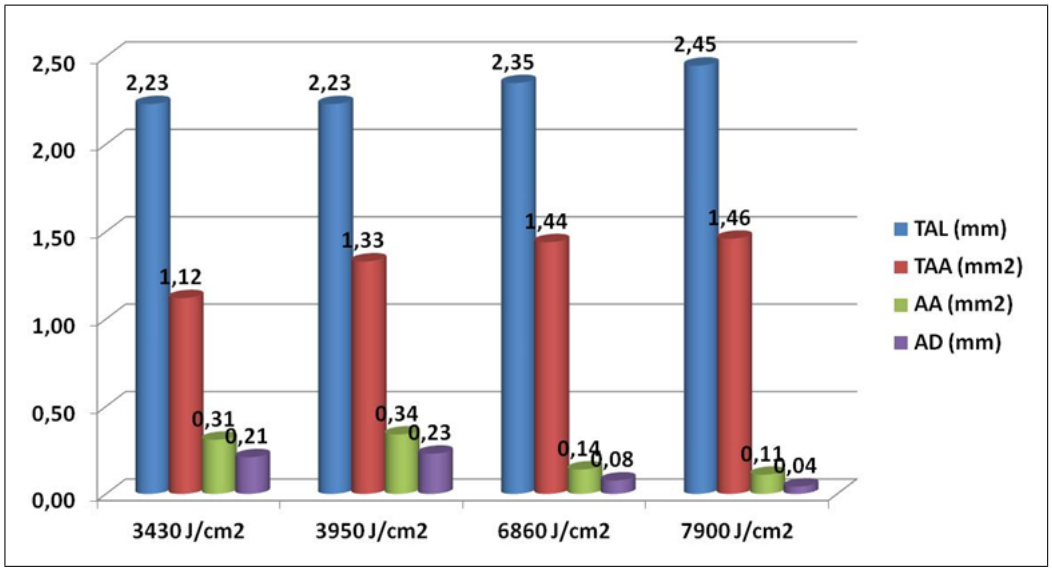

Figure 4.38 Ablation analysis parameters after the laser applications (day0).

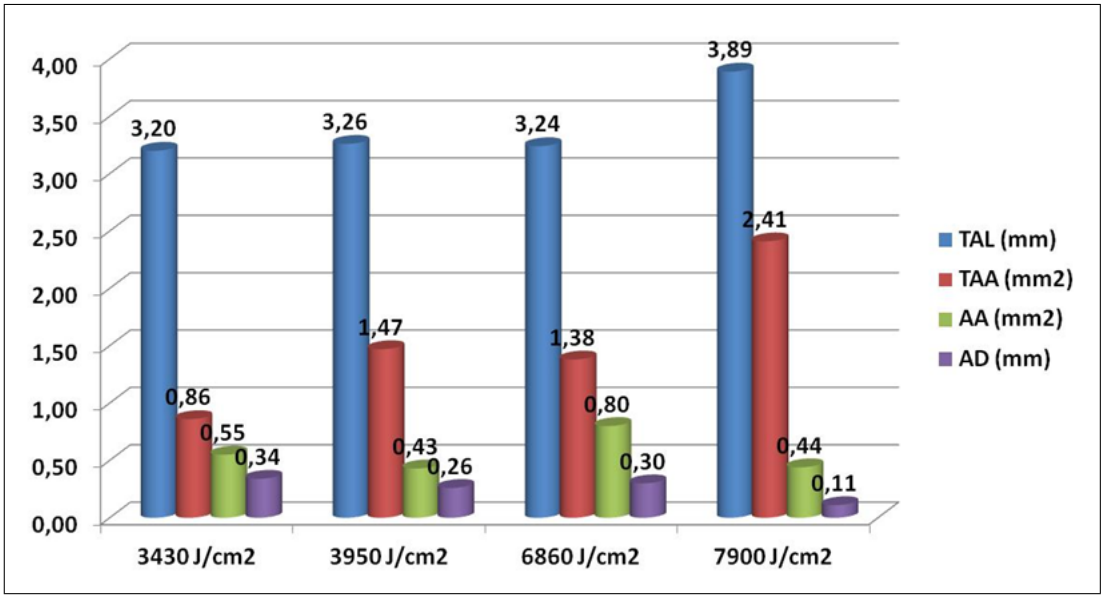

Figure 4.39 Ablation analysis parameters after the laser applications (day4).

In another group of experiment, the same method was applied to another group by using CW mode of operation of Tm:YAP laser. Then, the ablation parameters were compared among CW and modulated modes of operations with the same laser energy levels. The macro pictures of the skin samples at day4 were given in Figure 4.40, whose histology images were given in Figure 4.41. AA and AD were not observed after application of Tm:YAP laser in CW mode of operation at these power levels. This shows that CW mode of operation provides higher thermal effects on the skin samples. TAA and TAL values were also found higher at CW mode of operation (Figure 4.42).

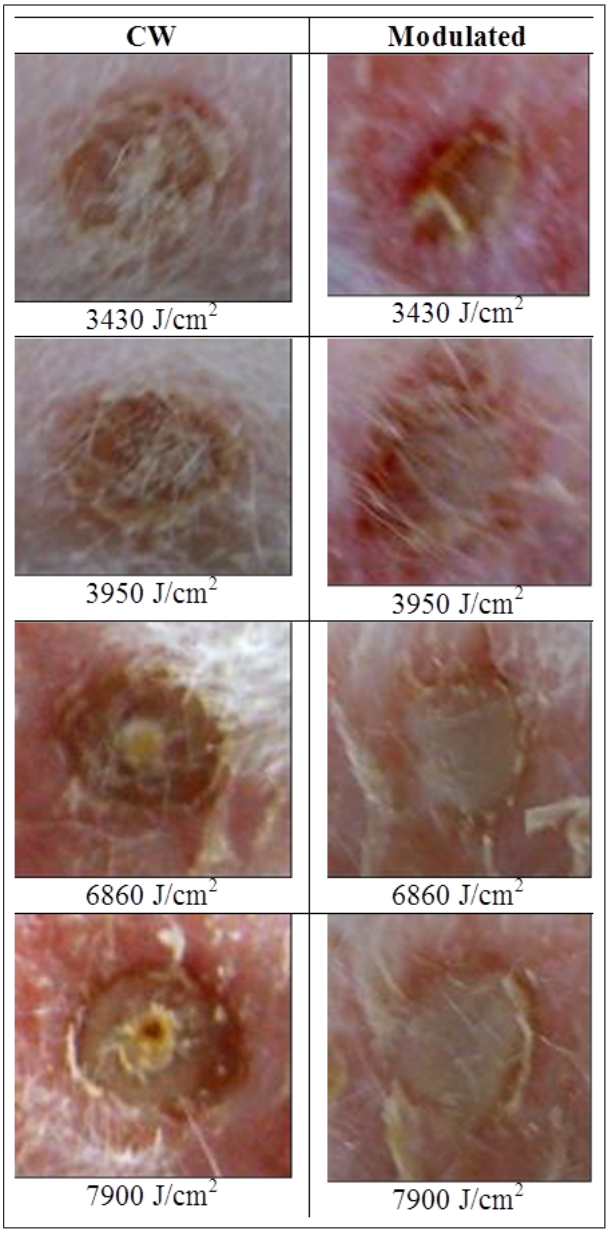

Figure 4.40 Macro pictures of skin samples at day4.

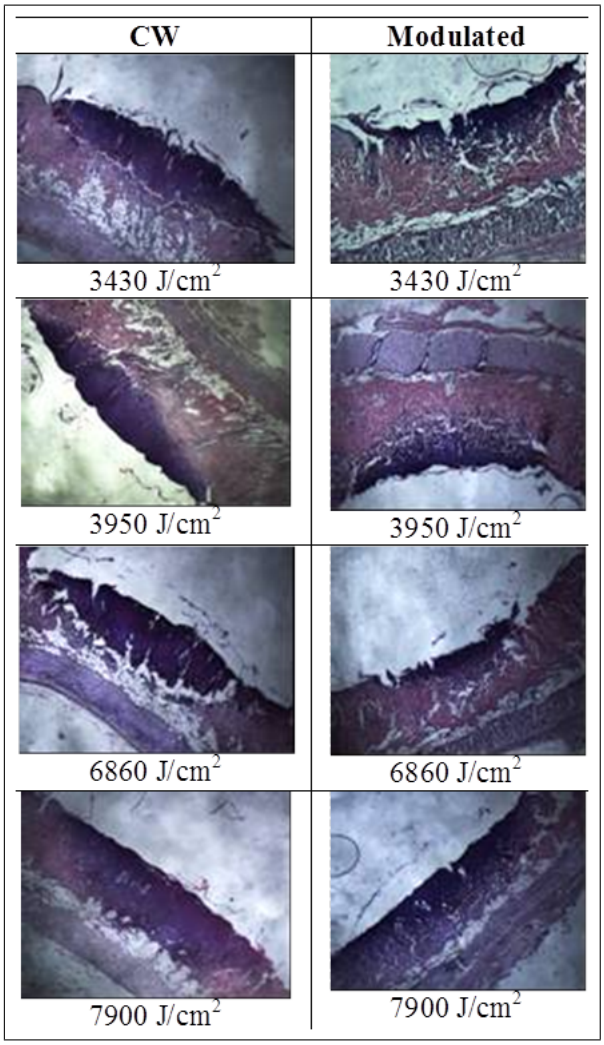

Figure 4.41 Histology images of skin samples at day4.

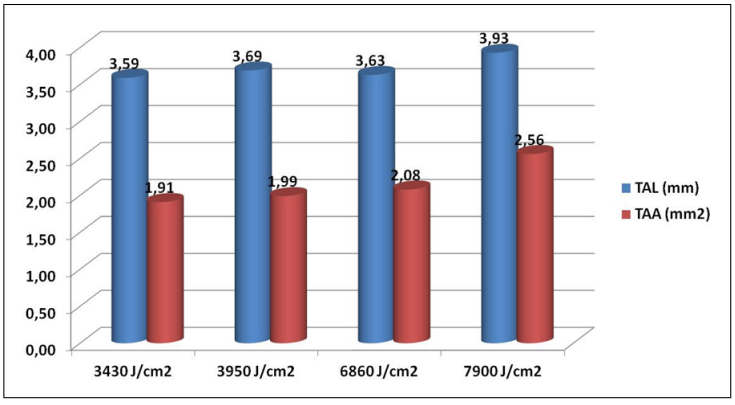

Figure 4.42 Ablation analysis parameters after CW laser applications (day4).

The maximum thermally altered depths of the samples were also compared between CW and modulated modes of operation of Tm:YAP laser. As seen in Figure 4.43, the modulated mode application gives less thermal damage into the deeper part of the skin samples. The depth was increased by increasing the fluence of the laser.

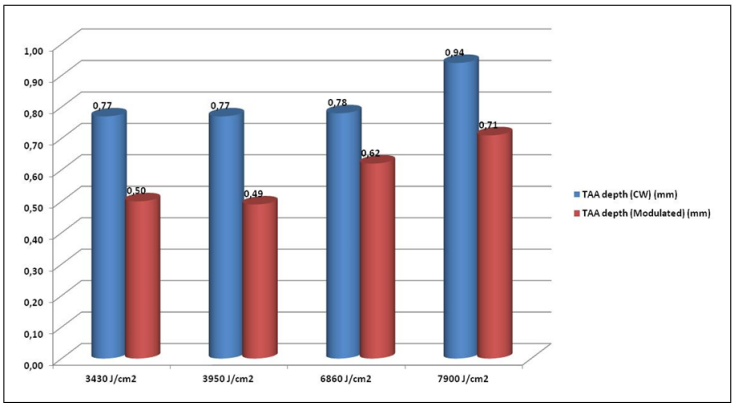

Figure 4.43 Thermally altered area depths among CW and modulated samples (day4).

Depth of injury on histologic examination was much less affected by exposure duration when modulation mode was used. The modulation nature allows tissue cooling between interval pulses hence causing less adjacent tissue injury as seen in the literature [27]. Modulation laser parameters can produce comparable strength with reduction in thermal injury. Thus, mode of operation was found to be an important parameter.

The results of these experiments can be used in dosimetry and comparison among CW and modulated modes of operation of Tm:YAP laser. Due to strong water absorption, 1980-nm Tm:YAP lasers are promising efficient candidates for efficient skin tissue ablation with minimal depth compared to smaller wavelength lasers.

The lasers, whose absorption coefficient for water is high, have been known as purely ablative lasers, resulting in almost no thermal damage to the dermis when fluences are above the ablation threshold [206].

In tissue ablation, cutting is the main mechanism and thermal damage at the boundaries of the ablated zone should be minimized. Heat deposited at the application site is transferred to adjacent structures. It may cause unexpected thermal damage to

otherwise viable tissues adjacent to the irradiation site [28]. Short high-energy laser pulses can provide a fast ablation rate. During this process the exposure time of the boundaries of the ablated zone to heat conduction is short compared to the continuous radiation, so that thermal damage may be almost completely eliminated [48]. Tm:YAP lasers in this thesis, operating near the OH absorption band, around 1.9 μm, suggests the potential for an interaction characterized by accurate tissue removal, accompanied by thermally induced coagulative and haemostatic effects [23].

At the fluences used, intracellular water absorbs the laser energy of the laser with resultant heat production and water vaporization. This is an exothermic reaction that causes tissue ablation. As the dermis is encountered, the relative concentration of water is less and the laser energy is inadequate for complete tissue ablation and more energy is dissipated to the surrounding tissue.

Diameters of lesions tended to increase with increasing power and irradiation duration for both modes of operation. After a certain threshold, carbonization began to dominate the laser-tissue interaction process. The optical properties of the tissue change dramatically; the absorption and the scattering properties of the tissue are altered. Carbonization does not only affect the healing process, but does change laser operation conditions. This is another reason why carbonization of target tissue is the primary damage to prevent [136].

The ablation efficiency can probably be further increased by optimizing the laser pulse duration, energy density and focus size individually for each kind of biological tissue.

4.4 Temperature Measurements by Thulium Laser System

4.4.1 Background

During laser applications, lasers induce heating to levels that can cause immediate irreversible damage through cell necrosis and denaturation of structural proteins in both targeted tissue and surrounding healthy tissue. A common aim in medical laser applications is coagulation of a desired volume of tissue with minimal or controlled thermal effects in the surrounding healthy tissue [68].

In the laser treatments, many medical procedures depend on the thermal response. These procedures involve laser assisted therapeutical modalities, such as laser tissue welding; laser angioplasty and recanalization for cardiovascular diseases [207]; laser interstitial hyperthermia for destroying cancers [208]; photocoagulation for homeostasis and photovaporization for tissue ablation [209]; radiofrequency ablation for treatment of cardiac arrhythmias [210].

Temperature is a crucial factor in tissue welding. Too high a temperature causes irreversible tissue damage, while too low a temperature fails to form a strong tissue bond. The objective is to limit heating of the tissue surface, while creating enough thermal denaturation in the deeper layers of the dermis to produce full-thickness welds.

Excessive thermal damage to tissue is a major phenomenon to overcome in laser welding or soldering. This may contribute to a poor wound healing process and low tensile strength. A large zone of thermal damage may result in a significant amount of scarring during wound healing and therefore may be unacceptable for skin closure applications [18]. To overcome these limitations, some researchers have used different heat-absorbing biological materials (solders) or cryogen spray cooling systems [19]. Some others used feedback systems in order to control the amount of energy delivered to the tissue surface, to keep the temperature below a certain critical value [24].

Recent studies have reported that temperature-controlled laser tissue welding yields increased consistency and strength compared to uncontrolled procedures [211]. Real-time control of the temperature in tissue is important for ensuring the treatment with minimal thermal damage to surrounding normal tissue [91]. These systems are able to decrease temperature variations by adjusting the power output of a laser to maintain constant surface temperatures. By controlling the temperature during welding, an optimal set temperature for tissue welding can be determined, to maximize the weld strength, while minimizing the resulting thermal damage.

Experiments in the literature has shown that excessive irradiation may result in more thermal damage than needed for the laser-induced weld, whereas inadequate heat deposition results in tissue dehydration without effective welding [24]. In the temperature range up to 70°C, the skin samples specimen presented decent histological appearance with no signs of thermal damage. However, the presence of histological signs of thermal damage has been observed at temperatures above 70°C. The temperatures below 60°C have yielded low tensile strength [71]. Irreversible damage occurs when the epidermal temperature rises above 70°C, which is 35°C above normal skin temperature [212]. On the other hand, the melting temperature of collagen is about 60°C, while that of elastin is about 300°C. Thus, the elastin content in the skin requires high irradiation intensity for welding of elastin. Hence the temperature in areas where actually welding occurred can be around 85°C [124]. The temperature of 65°C was considered the minimum tissue surface control temperature for robust welds [24]. The optimal laser-soldering temperature in the rabbit-skin model was also set as roughly 65°C [71].

In another study in the literature, multiple full-thickness skin incisions were repaired by using a 1.32-μm laser at temperatures of 65°C, 75°C, 85°C, or 95°C with and without a 50% human albumin solder. These results suggest that temperatures of 65-75°C with solder provide the optimal conditions for maximizing acute wound strength and minimizing tissue injury [119]. Higher temperature (95°C) welds had lower strengths than repairs completed at lower (65°C or 75°C) temperatures. The histology studies showed that the amount thermal damage was strongly dependent on

the tissue temperature and increased both in tissue depth and lateral to the repair with temperature. The depth of thermal denaturation increased with temperature over the temperature range. The choice of lasers is based on absorption of the laser energy by water, thereby heating proteins within the target tissue or the applied solder, resulting in coagulation around 70°C [95].

A study in the literature suggested that maximum tissue temperature during laser welding with argon wavelengths was 48.8°C, whereas it was significantly higher with the longer wavelength lasers. The accuracy of the argon welding is questionable due to the water irrigation used during argon welding [26].

One method for instant temperature measurements is to use thermal cameras to measure surface temperatures during laser skin welding to provide feedback for optimization of the laser parameters [213]. A thermal camera was used to measure surface temperatures during laser skin welding to provide feedback for optimization of the laser parameters [18].

A welding system based on a CO_2 laser and on infrared transmitting AgClBr fibers were also developed. The fiberoptic system plays a double role: transmitting laser power for tissue heating and noncontact (radiometric) temperature monitoring and control. The system was used for welding of urinary bladders in various animal models and complete closure of the bladder was obtained with a surface temperature of 55 ±5°C [25]. In the following experiments, the feedback loop systems made it possible to control the tissue temperature to an accuracy of ±3°C [105]. In another study, albumin solder was applied onto the approximated edges of cuts created in rat skin. A fiberoptic system was used to deliver the radiation of a CO_2 laser and to control the temperature [29].

In laser assisted anastomosis, reproducible and reliable welds were obtained by temperature feedback systems. Once the optimal temperature range is known, a feedback loop can be employed to modulate the laser power to maintain the tissue temperature within this range during tissue welding. Another study were performed

with a system consisted of a direct view infrared thermometer for monitoring the laser heated spot, a 1.9 μm diode laser, and a microprocessor for data acquisition and feedback control of the laser power to maintain a constant tissue temperature. The study demonstrated that the use of real time monitoring and feedback control results in improved consistency for vascular tissue welding [181].

In some studies, the temperatures that develop at the solder-tissue interface during the welding process were recorded with a thermocouple [214, 107].

4.4.2 Materials and Methods

The focus of the experiments in this part of the thesis is mainly on temperature measurements during the laser application on biological samples. For instant temperature detection, several temperature measurement systems were investigated.

The experiments were performed to see the temperature effect of Tm:YAP laser by direct temperature measurements under skin and on skin surface, to compare the temperature measurements for difference laser parameters and to compare modulated and CW mode of operation of Tm:YAP laser on skin tissue.

4.4.2.1 Instruments for Temperature Measurements.

In the experiments, a thermocouple and a thermal camera system were used. A thermocouple is a junction between two different metals that produces a voltage related to a temperature difference, converts heat into electric power. It undergoes Seebeck effect which can be described such that when any conductor is subjected to a thermal gradient, it will generate a voltage. Type K (chromel-alumel, diameter of 1 mm, and response time of 0.25 s) was used in the experiments, which is the most common general purpose thermocouple. The thermocouples were connected to the recording unit, which is 8 channel OMEGA OM-CP-OCTTEMP (Figure 4.44). It has an RS232

connection to PC by OM-CP-IFC110 software, it records in 2-second intervals with resolution of 0.01°C.

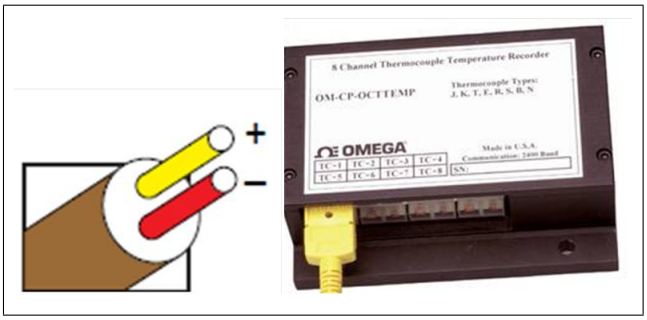

Figure 4.44 Thermocouple and recording unit.

The other instrument for temperature measurement was thermal camera, which was ThermoProTMTP8 by Wuhan Guide (Figure 4.45). Its spectral range is 8-14 μm, temperature range is between -20°C and +800°C. It has a thermal sensitivity of 0.08°C at 30°C with an accuracy of ±1°C. It has a pixel size of 384x288 pixels (35 μm) and field of focus of 35 mm.

Figure 4.45 ThermoPro (TMTP8) thermal camera.

Thermal camera mechanism depends on that all objects emit a certain amount of black body radiation as a function of their temperatures. The higher an object's temperature is, the more infrared radiation as black-body radiation it emits. They undergo the Stefan-Boltzmann law. For any surface, the intensity of the radiation emitted (emissive power) is given by $I=\varepsilon\sigma(T^4\text{-}Ta^4)$, where I is thermal power in watts/meter^2, ε is emissivity, σ is Stefan's constant (5.6703 x 10-8 W/m^{2}xK^4), T is temperature of object in Kelvin, and Ta is temperature of ambient surroundings in Kelvin.

The emissivity ε is determined b the surface properties of the tissue. For tissues, tissues, ε is determined mostly by the water content: if the water content is very high (such as in soft tissues), ε is almost 1, but if the tissue is dry, the emissivity decreases significantly. For most tissues, most of the emitted infrared radiation is in the spectral range between 3-30 μm, and its peak is near 10 μm [24].

An infrared radiometer is an instrument containing an infrared detector to measure the radiation emitted from tissue surface. If the area A and emissivity ε are known, the surface temperature can be estimated [215].

4.4.2.2 Sample Preparations and Data Recordings.

The experiments were conducted under a protocol approved by the Institutional Animal Research and Care Ethic Committee at Boğaziçi University. Healthy Wistar rats, randomly selected, 5-6 months old, weighing 200-300 gr, were supplied from Psychobiology Laboratory of Boğaziçi University. Before each application, rats were anesthetized. Hair at the site of application of each subject was shaved. Temperature measurements were performed under skin of their samples by thermocouples (Figure 4.46) and on skin by focusing the thermal camera (Figure 4.47). During the real-time measurements, the laser was applied to different spots of the skin sample, where the thermocouple tip was placed. In the recorded data, the temperature was increasing when the laser was applied and then the temperature was decreasing. Then, the experiment was sampled for different parts on the skin. On the recorded data, temperature increase, effected duration and full-width at half maximum values were calculated (Figure 4.48) and statistical analysis was applied. Each laser parameters were repeated at least eight times.

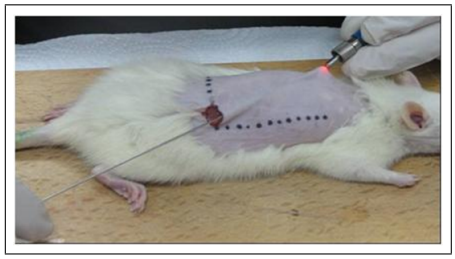

Figure 4.46 Temperature measurements under skin by thermocouples.

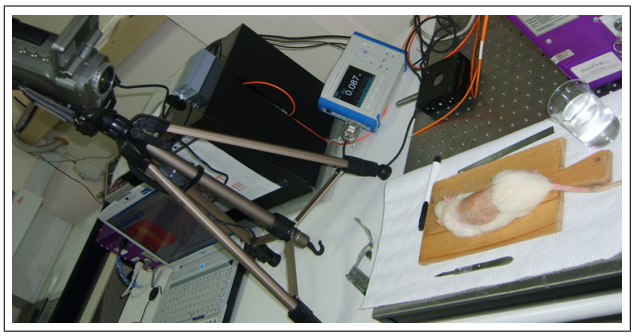

Figure 4.47 Experimental setup for temperature measurements by thermal camera.

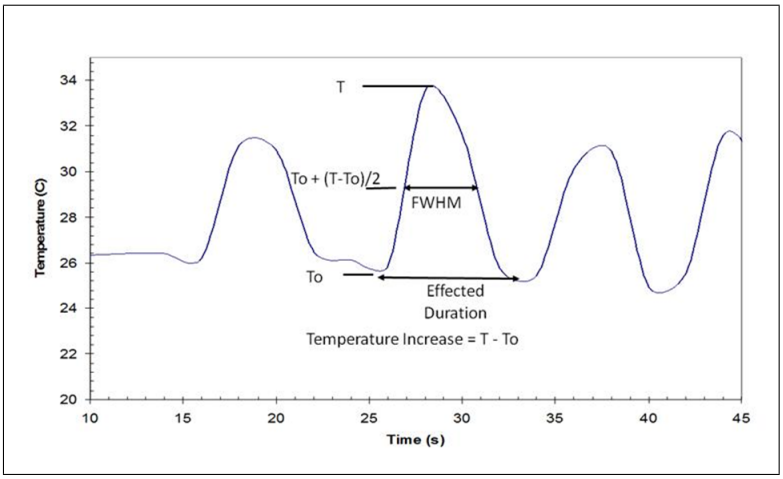

Figure 4.48 Temperature measurement analysis parameters.

4.4.3 Results and Discussion

4.4.3.1 Temperature Measurements by Thermocouples.

The laser parameters in Figure 4.49 and Figure 4.50 were applied on skin samples and the results in Figure 4.51, Figure 4.52, and Figure 4.53 were obtained. The modulated mode was applied as 200 ms on and 200 ms off modulation, which was determined in previous dosimetry studies.

Diode current	Laser output power	Duration	Average	StDev	Average	StDev	Average	StDev
15 A	0.69 W	10 s	7,12	1,27	43,60	5,90	23,60	3,85
16 A	0.87 W	10 s	7,27	0,97	37,20	2,28	19,20	2,28
17 A	1.05 W	10 s	7,51	0,98	34,40	5,37	20,00	3,74

Figure 4.49 Tm:YAP laser parameters for underskin temperature measurements by thermocouples (CW).

Modulated			Temperature Increase (C)		Effected Duration (s)		FWHM (s)	
Diode current	Laser output power	Duration	Average	StDev	Average	StDev	Average	StDev
15 A	0.69 W	10 s	6,69	0,68	30,80	3,03	21,40	0,89
16 A	0.87 W	10 s	7,98	0,73	29,20	5,40	20,40	2,19
17 A	1.05 W	10 s	8,55	1,24	24,80	2,28	17,60	1,67

Figure 4.50 Tm:YAP laser parameters for underskin temperature measurements by thermocouples (modulated).

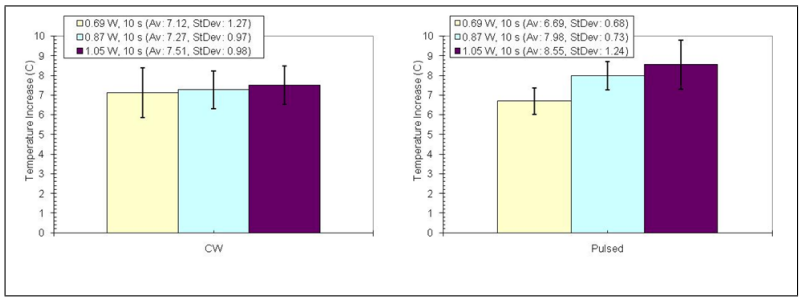

Figure 4.51 Temperature increases measured by thermocouples underskin.

The temperature increase found by CW mode of operation was slightly higher than the temperature increase found by application of modulated of operation of Tm:YAP laser at selected doses. The temperature increase by changing laser parameters were not found significant (pmin=0.08) in both CW and modulated modes. The temperature increases among CW and modulated mode of operations were not found statistically significant (pmin=0.2).

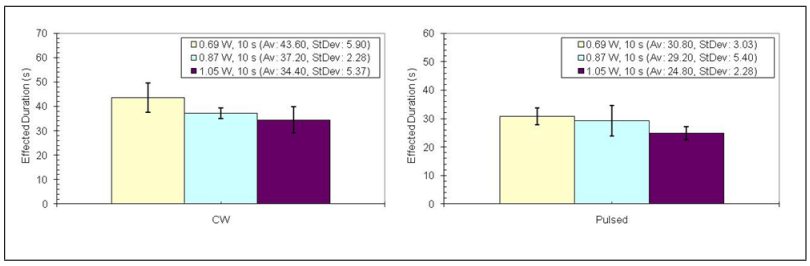

Figure 4.52 Effected durations measured by thermocouples underskin.

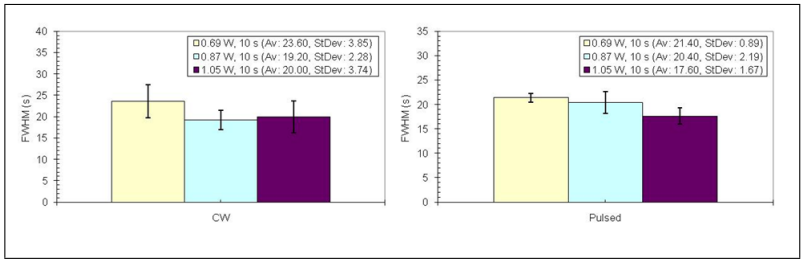

Figure 4.53 FWHM measured by thermocouples underskin.

There was also no statistically significant relation in effected durations and FWHM values by changing the laser parameters from 0.69 W to 1.05 W. However, there was statistically significant relation ($p=0.01$ for 0.69 W, $p=0.02$ for 0.87 W and $p=0.03$ for 1.05 W) between effected duration between CW and modulated mode of operation of Tm:YAP laser applied.

When the real-time data was observed as in Figure 4.54, there was a fast temperature increase in CW mode (10 s, ON) and smooth temperature increase in modulated mode (200ms ON, 200ms OFF, 10 s). There was fast cooling after laser application in modulated mode. The average slopes for temperature increase were 0.89 for CW and 0.54 for modulated mode of operation. The average slopes for temperature decrease were 0.26 for CW and 0.54 for modulated mode of operation. The temperature increase was faster in CW mode and the temperature decrease is slower due to the temperature affected by surrounding tissues in CW mode of operation. The difference between CW and modulated mode of operations were statistically significant ($p<0.05$) for both temperature increase and temperature decrease.

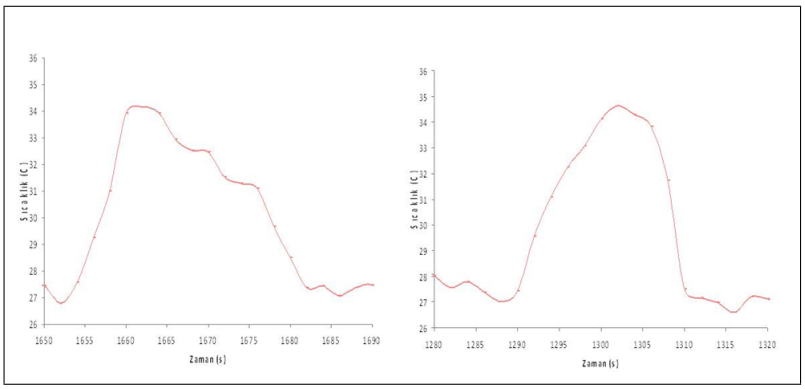

Figure 4.54 Real-time data showing temperature increase and decrease at a laser application in CW (left) and modulated (right) mode of operation.

4.4.3.2 Temperature Measurements by Thermal Camera.

The temperature measurements by thermal camera were performed on skin by focusing the camera on the sample. The laser parameters of 100 mW and 5 sec were applied on different spots on the in vivo skin sample while the thermal camera was recording (Figure 4.55). Then, the data was analyzed to find the temperature increase and affected durations for each application both CW and modulated mode of operation. The maximum values of temperature in the pixels were taken to find the maximum temperature increase.

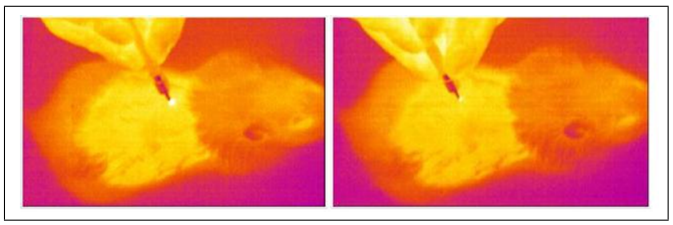

Figure 4.55 Thermal camera images during laser application in both CW (left) and modulated (right) modes.

Figure 4.56 shows the temperature increase measured by thermal camera on skin. The temperature increase was found higher in CW mode of operation than the temperature increase in modulated mode of operation. The difference was a statistically significant ($p<0.01$). This result was also showing the temperature increase difference between CW and modulated mode of operation on skin measured by thermal camera was higher than the temperature increase difference under skin measured

by thermocouples.

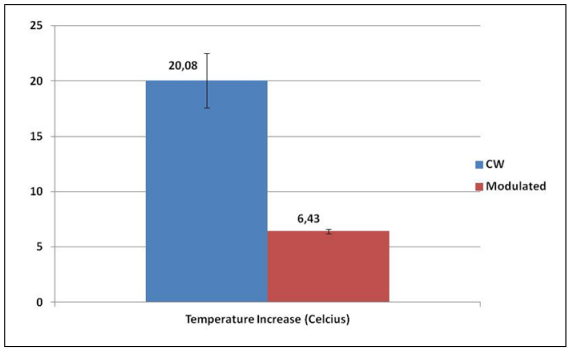

Figure 4.56 Temperature increase measured by thermal camera on skin.

Figure 4.57 below shows the effected durations for both CW and modulated mode of operations. The effected duration for CW laser application is higher than the effected duration measured during modulated mode of operation.

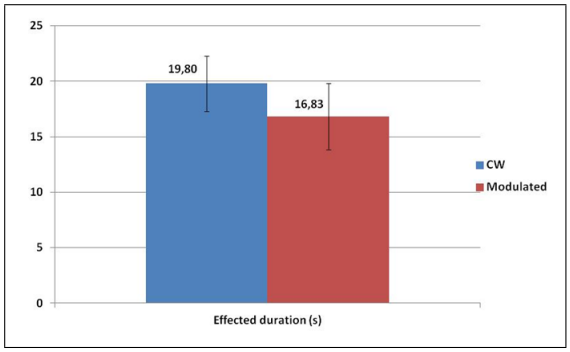

Figure 4.57 Effected duration measured by thermal camera on skin.

4.4.3.3 Limitations of Temperature Measurements.

The absorption of laser light results in temperature increase in target tissue. The resulting temperature profiles are governed by heat conduction relative to the optical penetration depth and thermal boundary conditions in the tissue [24]. Due to tissue inhomogeneity, anisotropy, and variations of the optical and thermal properties of the tissues with temperature, thermo-optical models are not always sufficient to predict the temperature rise within the tissue with the desired accuracy and reliability.

Temperatures generated during clinical or experimental laser irradiation are generally measured with thermocouple probes, infrared optical fibers, optical temperature sensors such as temperature-sensitive fluorescent probes, and MRI monitoring.

Thermocouple probes are reported in the literature as more accurate and less expensive than fiber-optic or fluorescent temperature probes. However, thermocouples consist of thermocouple wires located in a thin needle made of stainless steel, which strongly absorbs near-infrared radiation near 1,000 nm. Because this absorption induces a direct temperature increase of the needle, temperatures measured with thermocouple probes during laser irradiation of tissue may be significantly higher than the target tissue temperature. Therefore, absorption of laser radiation by stainless steel thermocouple probes may induce a significant overestimation of the temperature measured during laser irradiation of tissue [97].

In laser tissue interactions, where differences of a few degrees in temperature are significant to the desired therapeutic results, correction of experimentally recorded thermocouple measurements is necessary in order to predict the treatment effect and accurately to model experimentally recorded temperature data [216]. The tissue temperature can be measured without artifact only if the thermocouple probes have the same thermal and optical properties as the surrounding medium. Thermal conductivities of thermocouple metals are typically two to three orders of magnitude larger than that of human skin. Therefore, inserted thermocouples significantly perturb the thermal distribution in the epidermis. Thermocouple readings represent tissue temperatures only when thermal gradients have become sufficiently small [212].

The radiation from biological tissues is around 10 μm. In order to focus it to the operation regions, where the laser radiation is applied, special fiber optics cables are necessary. There are several types of fiber optics covering the 10 μm. They are Polycrystalline IR (PIR) fibers, AgBrCl fibers [217] and hollow glass waveguides [218]. In the market search, they are found expensive and difficult to handle and calibrate due to their high bending losses.

Accuracy, response time, and sampling errors (both spatial and temporal) are factors affecting the success of such temperature feedback systems. For example, due to thermal conductivity of surrounding tissue and due to laser light scattering and reflection, there are significant problems associated with using surface temperature to indicate what is going on in the depth of the weld. A temperature sensor may give falsely low or high readings depending on its location in relation to the temperature distribution profile within the tissue. In addition, there may not be a single, well-defined temperature at which a total phase transition to denaturation of protein takes place [26]. Furthermore, the feedback systems require several adaptations to the laser set-up, including to the surgical microscope, which ultimately makes its use more cumbersome [91]. One of the major problems in operating such a system in laser tissue interactions is the accurate temperature calibration [219].

Although thermal control was found to improve the tissue welding in some studies, some other studies showed no significant difference between the welds done with and without thermal control [86]. Temperature feedback control during laser tissue welding was implemented to eliminate exponential increases in the rate of denaturation associated with rapidly increasing temperatures. Since rate processes are exponential with temperature, laser tissue welding was performed with and without temperature feedback control to investigate the efficacy of temperature feedback in enhancing the photothermal welding process in vivo. Thermal coagulation of tissues has been described by rate process theory as an accumulation of denatured proteins that is related linearly to time and exponentially to temperature. Constant temperature does provide a more uniform rate of coagulation and it can eliminate carbonization. Temperature feedback control system was also reported as not a satisfactory method to identify completion of a weld in another study [24]. Optical temperature feedback control systems were not reported suitable also when chromophore-doped solders are employed in the tissue welding [97].

Attempts have been made to avoid thermal damage by using a temperature controlled feedback system incorporating infrared detectors or thermocouples, but these devices can only give an estimate of the surface temperature reached [104]. These

methods are also difficult to align because of the small size of the application area [114]. Only the temperature of the central portion of the laser heated spot should be imaged to minimize the effects of slight variations in the imaging angle. Another thermal fluctuation that must be accounted for is the ambient background radiation seen by the camera [181].

5. LASER TISSUE WELDING by Tm:YAP LASER SYSTEM

5.1 Introduction and Background

Laser tissue welding is an alternative method to bond tissues by using laser energy. In the mechanism of laser tissue welding, the photonic energy is converted into thermal energy. Therefore, the choice of laser wavelength for tissue welding is mostly based on the absorption of the laser energy by tissue chromophores. The first use of laser tissue welding was reported in small blood vessels with an Nd:YAG laser [171]. Laser tissue welding has been used for several tissue types including intestine [24], and skin [125], and by using a variety of lasers such as diode [220], Nd:YAG [120], and CO_2 [219] lasers.

Laser tissue welding provides a watertight closure with a reduction in foreign-body reaction, suture and needle trauma, bleeding, surgical times, and skill requirements. The suture technique for closure of wounds by dermatologic surgeons is relatively time-consuming to place for a long wound and provides poor cosmetics. Sutureless methods for closure of surgical incisions such as staples, strips, sealants, and glues are difficult to apply, and they may carry a risk of foreign body reaction [77]. Laser tissue welding prevents foreign body or toxic elements from entering the wounded tissue and improves cosmetic results with no need to use needle and stitch removal. Another important characteristic of laser tissue welding is operation time. Laser tissue welding operation was found 4 times faster than conventional suture technique [221].

The interest in lasers emitting in the 2-μm region has continuously been increasing for tissue welding applications. Laser welding of gallbladder incisions with a mid-infrared 2.15-μm (THC):YAG laser has been offered as a useful technique for future developments of 2-μm lasers [182]. The tissue absorption characteristics by (THC):YAG laser in pulsed mode of operation permitted tissue welding with limited collateral thermal damage in percutaneous endoscopic biliary surgery [183]. On the

other hand, a Thulium fiber laser at 1873 nm with about 600 mW was used to produce full-thickness, watertight tissue closure during microsurgical laser welding of urinary tissues [184]. In another study, tissue welding by a CW Ho:YAG laser was compared to the laser soldering by 808 nm diode laser and both techniques revealed good bursting pressures of anastomoses [99]. A low power 1.95-μm diode laser was chosen to weld small vessels to result in uniform deposition of energy across the thickness of the weld [181].

At 2-μm region, laser energy can be delivered via optical fibers and it can be absorbed very well by water molecules, which is a main constituent of biological tissue. Absorption coefficient at 1980-nm (μa = 92.03 cm^{-1}) was reported as 760 times better than one of the most popular medical lasers at 1064-nm (μa = 0.12 cm^{-1}) [35]. Tm:YAP laser at 1.98 μm has stronger absorption coefficient in liquid water than Tm:YAG and Ho:YAG lasers around 2 μm [33]. The lasers near 3 μm have the highest absorption in tissue because they overlap with the fundamental 0-H vibrational stretch mode of water. However, silica fibers are not transparent at wavelengths longer than 2 μm. Tm:YAP laser at 1.98 μm can be coupled to the conventional silica fibers as opposed to longer-wavelength lasers like CO_2 lasers emitting at 10.6 μm [48]. As an additional advantage, lasers with a wavelength longer than 1.4 microns are in the "eyesafe" band. Hence, laser radiation around 2 μm does not damage the retina because it is absorbed by water in the human eye before reaching the retina [37], and this greatly reduces health risks during the operation of the laser.

The detailed background and literature survey on laser tissue welding is given in Chapter 2. In this main part of the thesis, the objective is to explore the capability of Tm:YAP laser system under different mode of operations for making strong welds. The modulated and CW mode of operations were experimented in vivo and results were analyzed through histological examinations and tensile strength tests.

5.2 Materials and Methods

5.2.1 Animal Preparation

In animal model of the study, the goal is to have a perfect analog of the human clinical situation. Ethics prohibit the use of humans in potentially harmful studies. Tissue welding and soldering studies were widely done on rat models in order to examine the laser-tissue interaction [160]. Many wound healing models have employed rats because of their wide availability, size, and tractable nature [96]. A rat skin model was chosen as rats are relatively inexpensive, easy to handle, and a rat model is an accepted biocompatibility model in the literature [128]. Another reason to consider rats as skin wound healing models is the availability of a broad knowledge base on rat wound healing gained from years of previous research. Furthermore, the rat skin wound healing model was chosen because it is a well used model for characterization of bonding procedures for wound healing response to mimic the properties of human skin. In the literature, rat skin thickness was measured by calipers as between 2.2 and 2.4 mm [81], as 2.28 ± 0.35 mm [96], and 2 mm [93].

One of the advantages of using animals is that the wound healing process is so accelerated in animals that it is possible to study the process over days rather than over the weeks required for humans. Most research in laser tissue welding has been conducted on animals, including rats, dogs, rabbits, pigs, and monkeys. In the literature, the success rate of laser tissue welding studies on rats was found 73%, whereas it is 80% on rabbits, and 100% on cats [219]. Therefore, if a reasonable success on rats have been obtained, the success rate and results will be better on human skin in clinical studies.

Wistar rats were served as animal models in the experiments. The experiments were conducted under a protocol approved by the Institutional Animal Research and Care Ethic Committee at Boğaziçi University. A total of fifty-two healthy male Wistar rats, 5-6 months old, weighing 240-250 g, were randomly selected from Psychobiology Laboratory of Bogazici University for in vivo experiments. Rats were housed in plas-

tic cages and maintained on a 12-h-light/12-h-dark cycle in a temperature-controlled vivarium (22±2°C). Food and water were available ad libitum.

Before the operationRats were anesthetized with ketamine (10% ketamidor, RichterPharma, AG, Wels, Austria) by intraperitoneal injection (1.65 ml/kg). Hair at the site of application of each subject was shaved. Three pairs of 10-mm-long full-thickness incisions bilateral and parallel to the spinal cord were created on each animal using no.11 scalpel [22]. The length of the incisions was sustained via a calibrated micrometer. For the good apposition, incisions were created such that there was no opening of incision after mechanically contacted. The weld strength may depend strongly on the degree of the apposition [222]. It is important to obtain a good and reproducible coaptation of the edges before irradiation [82, 126]. Any blood exposed on the incision surface was cleaned to prevent blood from interfering with the laser welding process (Figure 5.1).

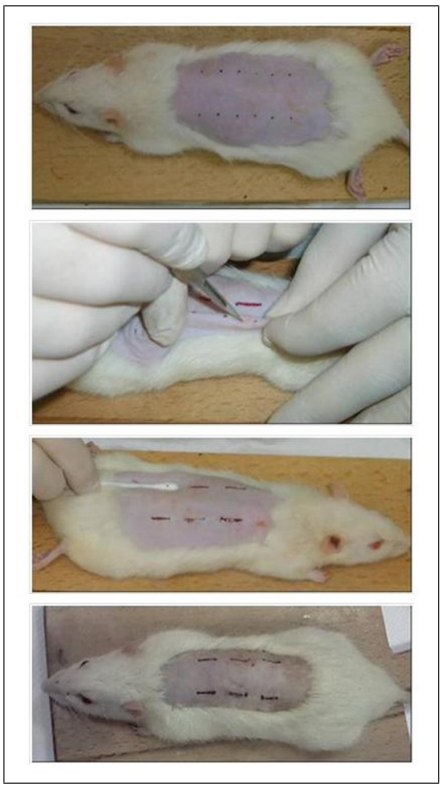

Figure 5.1 Three pairs of 1-cm-long full-thickness incisions before laser welding.

5.2.2 Welding by Tm:YAP Laser System

All the laser application procedure was conducted by one operator. Laser protective glasses were used when the laser was active. Power, duration, and mode of operation (modulated and CW) parameters were set by the user through the user interface on the PC. In the CW regime, the laser beam was delivered continuously during the selected exposure time. The controller designed for this study provided modulation within the limits of laser diode (maximum 20 Hz). Laser pulse duration of 200 ms on and 200 ms off was chosen to confine heating to the weld site and reduce the temperature rise in the surrounding tissue [18]. Laser output power was checked with a powermeter (Newport 1918-C, Irvine, CA, USA) before each application. A red pilot beam (650 nm) allows the surgeon to visualize the spot size of the laser during activation.

The laser application was repeated six times along the incision at a distance of 2 mm above to each incision which was determined for optimal non-contact application to prevent laser divergence and fiber damage. (Figure 5.2). The fiber tip was held approximately 2 mm above the welded site. The laser beam was applied perpendicular to the skin surface so that equal energy can be delivered to both edges. Six spots were applied at a distance of 2 mm above 1 cm-long incisions. Each spot slightly overlapped each other. In some studies, the laser spot was manually scanned back and forth over the incision [78, 96]. However, the most preferred method is applying the laser beam spot by spot along the incision [82]. The laser spot diameter was measured from 2 mm as 0.6 mm by using the knife-edge technique.

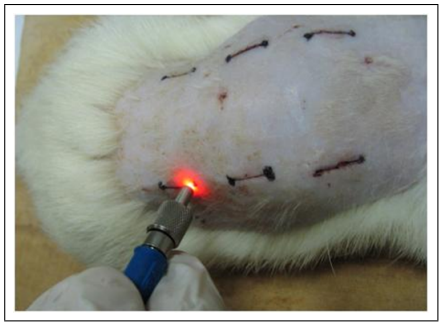

Figure 5.2 Application of Tm:YAP laser to each incision.

Once the rats were fully awake from anesthesia after the operation, they were placed in small cages. The wounds were left uncovered and the rats were housed separately to prevent them from licking and biting each other's wounds. The presence of wound reopening, infection, scar, and hair formation was checked on a daily basis. The wounds on the rats were examined and photographed daily during the recovery period. Their regular diet was gradually resumed 24 hours postoperatively depending on their physical condition. Water was supplied ad libitum starting 24 hours after surgery [105]. The rats were kept under conventional laboratory conditions.

5.2.3 Suture

To compare the histology and tensile analysis of the samples welded by TmYAP laser system with samples closed by conventional suture technique, a total of 120 incisions of twenty Wistar rats were closed by suture. A single suture usp-3/0 metric silk (Dogsan Tıbbi Malzeme San. A. S., Trabzon, Turkey) was placed in the middle of each 1-cm-long incisions. The distance between the needle entrances to the tissue was about 10 mm [160].

5.2.4 Histology Analysis

Laser-welded tissue samples underwent histological analysis to determine the tissue welding success. The wounds on the rats were examined during the recovery period. Presence of wound reopening, infection, scar and hair formation was checked on a daily basis. The rats were sacrificed by cervical dislocation on postoperative days of 1, 4, 7, 14, and 21 for histological analysis study on cross sections of each welded samples. In the literature, histologic study and measurement of tensile strength were performed up to 21 days post-operation to analyze overall healing period [22, 82, 160].

An area of the skin with the repaired (laser-welded or sutured) incision including epidermis and dermis was excised with a scalpel (Figure 5.3) before the rats were

sacrificed by cervical dislocation. The samples were fixed in formalin and processed for histology (Leica TP 1020). The samples were embedded in paraffin blocks (Leica EG 1150 H) and sectioned to 5-8 μm-thick samples with a microtome (Leica RM 2255). Then, they sectioned as longitudinal and cross sections, and stained with hematoxylin and eosin [19, 82]. This procedure gives the idea about carbonization, infections, and healing quality of the tissue samples under light microscopy. The detailed histology procedure was given in Chapter 4.

Figure 5.3 Dissection of incision samples.

After staining, skin samples were examined under a light microscope (Eclipse 80i, Nikon Co., Tokyo, Japan), and images were taken with a CCD camera (DS-Fi1, Nikon Co., Tokyo, Japan). Measurements were performed using Imaging Software (NIS Elements-D, Nikon Co., Tokyo, Japan). Histology of the irradiated tissue was used to determine the extent of thermal injury associated with different tissue welding parameters. Welding success was quantified using numerical parameters. Closure index, thermally altered areas, epidermal thickness, and granulation areas of the stained samples were calculated.

In the literature, epidermal parameters are analyzed if there is any presence or absence of thermal injury, necrosis or carbonization residues. The grading of re-epithelialization is also important. Dermal parameters include the presence of inflammatory reaction, the presence of a foreign-body reaction expressed by the presence of granulomas and giant cells formation, and the types of inflammatory cells (i.e., neutrophils, macrophages or fibroblasts) [223].

Thermally coagulated collagens have variable birefringence color shifts when compared to the adjacent unaffected collagens in stained histologic sections. The birefringence changes seen in intact tissues are gradual and may occur over a range of temperatures. Changes in the collagen-histologic stain interactions produced by thermal alterations of the collagen structure may be responsible for the color shift observed. Variations of color birefringence in routinely stained histologic sections may become a marker of temperature ranges in thermally altered collagens [205].

The visible signs of thermal damage in tissues include apparent drying, shrinkage, whitening, disruption, charring, combustion, and/or ablation. The more accurate observations of light microscopy show that thermal damage frequently extends beyond the boundaries of the lesions. There are several factors that were reported to by the use of light microscopy to determine the extent of the heat damage in tissues, such as artifacts produced by histologic preparation and subtle morphologic changes that require experience on the part of the viewer to obtain reproducible data [205]. However, light microscopy is still an important tool in histology examinations. A transmission light microscope fit with crossed linear polarizers was used to analyze the sections [142].

In the literature, birefringent images were used to measure thermal damage zones in welds processed immediately after surgery. Epidermal thickness was also measured for both lasered and sutured wounds. The depth at which re-epithelialization occurred, and the thickness of necrotic tissue sloughed during wound remodeling were also recorded. Granulation tissue width measurements were performed along the weld site [78]. The area of tissue thermal damage was distinguished by a color change and loss of birefringence under the light microscopy [88].

In this study, histological examination of the wound sites revealed data about the recovery process of the laser welding. Tissue samples taken through the line of incision were also examined histologically for evidence of epithelialization, inflammatory response, thermal injury, necrosis, and scarring. For each dose groups, a quantitative determination of closure index (CI), thermally altered area (TAA), epidermal thickness (ET), and granulation area (GA) was performed. CI is the primary indicator for

skin closure by welding (Figure 5.4). It is defined as the ratio of closed parts to the total incision (CI=closed length/total incision). CI values ranges from zero to one. CI=0 corresponds to no closure and CI=1 means full closure. TAA reveals the thermal changes of a laser welded part (Figure 5.5). The thermal changes are identified under light microscope as color change and morphological degeneration due to the denaturation of cellular structures. ET shows the quality of healing and it depends on the thermal effects and inflammations (Figure 5.6). The ETs were measured at six to eight different points for each sample The ET of the recovered incision showed the success of the welding (or suturing) in terms of scar formation. It normally starts at a higher value and gradually decreases to a certain level, depending on the degree of the trauma [224]. In our study the normal value of the epidermal thickness was approximately 40 μm. GA is the area where new fibroblasts, inflammatory cells, and capillaries are formed along the incisions (Figure 5.7). Then, quantitative histologic analysis is performed under light microscopy.

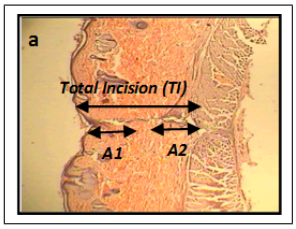

Figure 5.4 Determination of closure index on histology pictures.

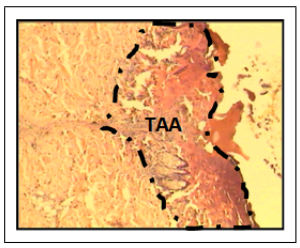

Figure 5.5 Thermally altered area on a skin image by histology.

In these sampling experiments, the success is measured by the histologic parameters described above and statistically analysis is performed. Totally 60 incisions are sampled on ten Wistar rats. Around 20 slides of each incision are histologically imaged under light microscopy.

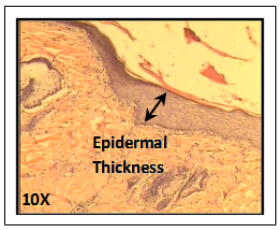

Figure 5.6 Epidermal thickness on a skin image by histology.

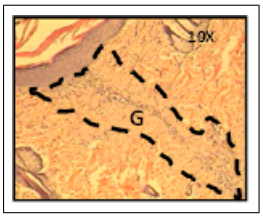

Figure 5.7 Granulation area on a skin image by histology.

5.2.5 Tensile Strength Analysis

Tensile strength tests have been used to quality of laser tissue welding. In the literature, the welding results were tested with a digital force gauge for measuring its tensile strength. The tension force parallel to the welded sample surface was applied, until the fusion site was broken and the maximum force was recorded [134]. In another study, the tensile strength was measured by the burst pressure of the soldered dura [175]. In some studies, tensiometer was used to measure the tensile strength of the samples [82, 83, 118, 119, 123]. The wounds were stressed to failure at a rate and the maximal breaking strength was recorded. The weld strength was defined as the maximum load that was recorded before a complete break occurred. The breaking strength was calculated by dividing the maximum load recorded by the cross-sectional area of the tissue specimen [128].

In most of the studies, the welded skin samples were tested using a loading machine. Samples were inserted into the head of the loading machine and tensile strength measurement was carried out at a specific rate. A plot of the applied force vs. the increasing length of the stretching tissue sample was obtained. The maximum load of the sample was marked at the point of failure, at which the tensile strength sharply

dropped to zero [29]. The tensile strength was calculated by dividing the maximum load at rupture (N) by the cross-sectioned area of the specimen (about 10 mm^2) [71].

In this study, tensile strength measurements were performed at intervals over 1, 4, 7, 14, and 21 days after the operation for each sampled dose. For tensile-test examinations, incision sites were removed at about 5 cm long samples (Figure 5.8). Tensile tests were performed immediately within ten minutes after the sample removal. Samples were locked between the test machine (LF Plus, Lloyd Instruments, Leicester, UK) jigs in such a way that grips (TG34, Lloyd Instruments, Leicester, UK) were as close as possible (about 3 mm) and skin-sample slippage through the jigs was prevented (Figure 5.9). The test machine load cell capacity was 250 N and each sample was tested at 5 mm/min crosshead velocity. Tension was applied until the repair failed, and the breaking force was recorded for each sample (Figure 5.10). The minimum load at which the welded sample failed was recorded by computer-controlled software (Nexygen Plus, Lloyd Instruments, Leicester, UK) [160]. Skin samples after the tensile strength tests can be seen in Figure 5.11.

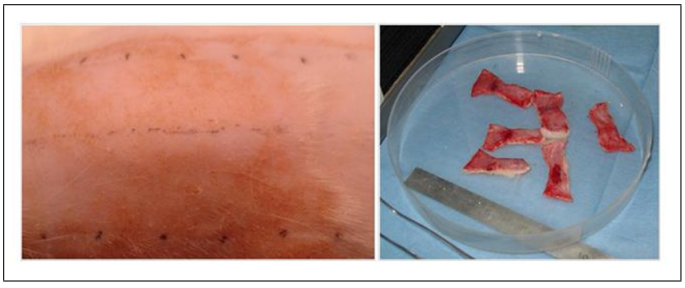

Figure 5.8 Incisions welded by Tm:YAP laser system before tensile strength tests.

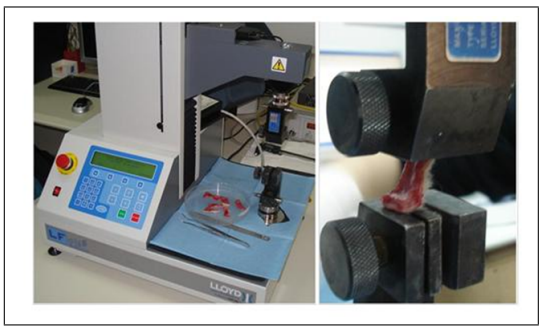

Figure 5.9 Placement of incisions between jigs of the test machine.

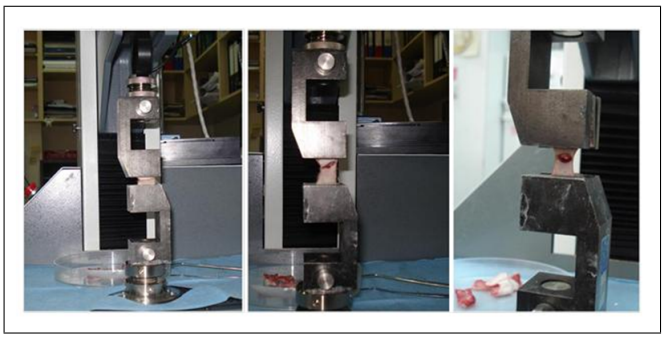

Figure 5.10 Breaking force was recorded for each sample when the repair is failed.

Figure 5.11 Skin samples after tensile strength tests.

5.2.6 Data Analysis

For all groups, the means and standard deviations were calculated. In order to reveal differences between the groups, unpaired Student t-test was performed [139]. A value of $p<0.05$ was considered statistically significant. Some data were expressed as average $\pm$ standard deviation. For ethical reasons, the total animal sacrificed was limited to a fifty-two Wistar rats and each incision sample on each animal was assumed to be statistically independent.

5.3 Results and Discussion

5.3.1 Dosimetry Study

In this first part of the experimental study, several Tm:YAP laser parameters were tested to find the optimum dosimetry for tissue welding before sampling study. The selected doses were applied to two Wistar rats as each dose was sampled by 2.

The healing period for this analysis was determined as 4 days. At day 4, the macro pictures of each incision were recorded and the rats were sacrificed.

The applied laser parameters to each incision are tabulated in Figure 5.12. The table also includes the macropictures of each incision to observe the effects of laser parameters just after the application (0-day) and 4 days later (4-day). The macro pictures offer successful welding at 100 mW, 5 s modulated and CW dose of Tm:YAP laser with maximum closure and minimum thermal side effects. This result is found promising for efficient tissue welding at low powers of Tm:YAP laser at 100 mW in both modulated and CW modes of operation. However, the success should be proven by histology and tensile strength analysis during the healing period until day 21.

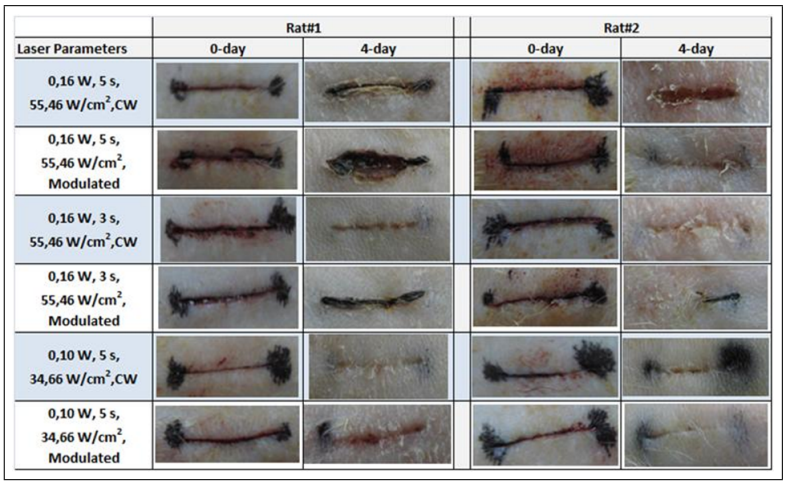

Figure 5.12 Macro pictures of each incision of the two rats and their applied laser parameters for dosimetry study.

5.3.2 Histology Analysis

The laser parameters determined by dosimetry study at modulated and CW operation modes were applied to the incisions on different rat samples. There were six incisions on each rat, incision numbers of 1, 2, and 3 were welded by Tm:YAP laser at 100 mW, 34.66 W/cm^2, CW during 5 sec for each shot. Incisions numbered of 4, 5, and 6 were welded by Tm:YAP laser at 100 mW, 34.66 W/cm^2, modulated (200 ms on / 200 ms off, for a total 'on' duration of 5 sec) mode of operation. The rats were

sacrificed at first (day 1), fourth (day 4), seventh (day 7), fourteenth (day 14), and twenty-first (day 21) recovery days after the laser welding operations. The quantitative histology analysis was performed with an optical microscope. A total of sixty incisions were sampled on ten Wistar rats. Twenty slides of each incision were histologically imaged under the microscope.

During the healing period, macro pictures of rats were taken. Figure 5.13 shows the incisions before the laser application. Figure 5.14 and Figure 5.15 show the incisions 1 day and 4 days after the laser application. No visual difference found between the incisions exposed to CW and modulated mode of operation of Tm:YAP laser. The incisions were successfully welded with no thermal carbonization during the healing period. The macro pictures at day 7, day 14, and day 21 are shown in Figure 5.16, Figure 5.17, and Figure 5.18, respectively.

Figure 5.13 Incisions before the laser application (day0).

Figure 5.14 Incisions after the laser application (day1).

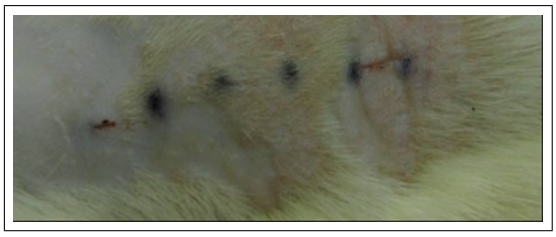

Figure 5.15 Incisions after the laser application (day4).

Figure 5.16 Incisions after the laser application (day7).

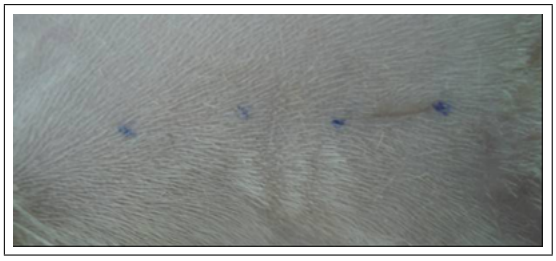

Figure 5.17 Incisions after the laser application (day14).

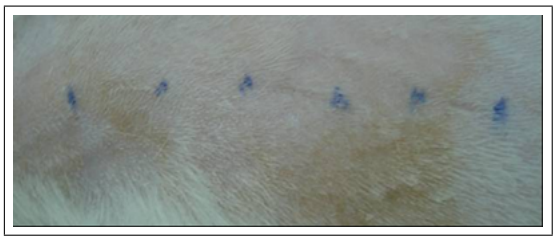

Figure 5.18 Incisions after the laser application (day21).

The sufficient closure on the incisions was observed in the macroscopic pictures and no side effects were observed during the healing period. Charring was observed at day 0 and day 1. Scar formation was noted on day 4. The primary mechanism of instant redness to the skin is the increase of blood flow in the dermis. This is a reversible process without any cell denaturation [146]. In suture samples, needle holes on the skin can also be observed. Macroscopic examinations showed that welding had thinner and minimal scarring with quality healing. No inflammation was evident. It was not found any signs of a foreign body reaction in laser-welded groups, probably because of the absence of carbonized tissue, solders, and suture materials. During the healing period, no anomalies were observed in health conditions, dietary habits, or behaviors of rats.

The selected histology images of samples corresponding to modulated and CW modes of operation of Tm:YAP laser were given in Figure 5.19 during the healing period. Arrows showed the incisions and CI values were embedded into the pictures. According to the histology images taken with the optical microscope, the incisions at day 1 were closed partially for both modulated and CW mode of operations. After day 4, full closure was obtained for both laser operations. Figure 5.19 also included the histology images of samples closed by suture technique. In suture group, closure was not observed for day 1 and day 4. The histological analysis parameters were analyzed for each slide of each incision (n=180) and their average and standard deviation were calculated.

By day 1, in the laser-welded incisions, re-epithelization process started. Welded wounds were closed at the epidermis, but some openings remained in dermis. After day 4, the full closures were observed for both modes of operation (CI=1). At day 1, the CI was higher for modulated mode (CI = 0.12±0.05 for CW and CI = 0.24±0.10 for modulated, $p<0.00$). In suture group, CI value was found to be 0 for day 1, CI = 0.12±0.09 for day 4, and CI = 1 after day 4 (Figure 5.20). TAA values were only observed at day 1 and no thermally altered area was observed after day 1. TAA was found lower for the modulated mode of operation (Figure 5.21). However, TAA values were not significantly different for modulated and CW modes of operation at day 1

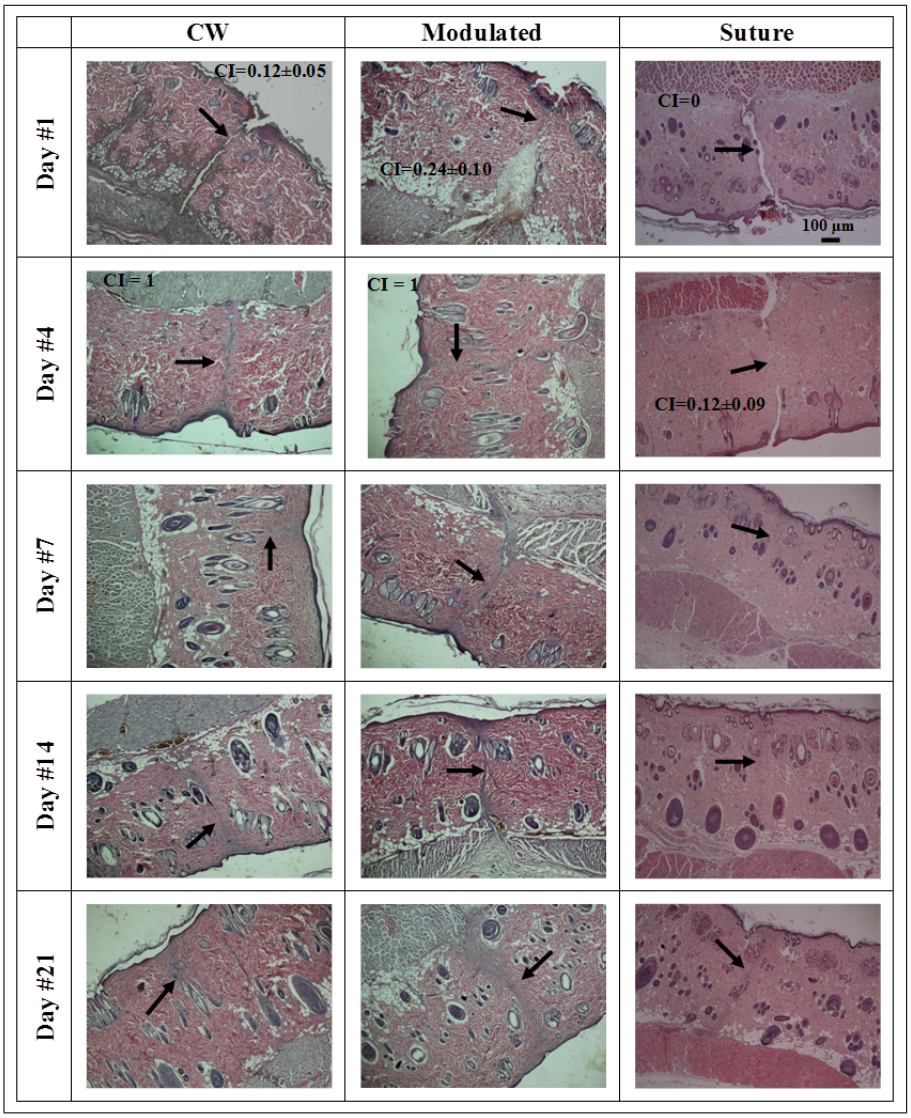

Figure 5.19 Birefringent histology images of samples exposed to CW and modulated mode of Tm:YAP laser.

(TAA = 0.14±0.05 mm^2 for CW and TAA = 0.12±0.04 mm^2 for modulated at day 1, p=0.74). Carbonization was not observed in any of the welded incisions. At day 4 and day 7, re-epithelization was completed, wounds were fully closed. A layer of granulation tissue around full thickness through the skin was observed with deposition of fibroblast cells and collagen formation. By day 14, tissue volume was partially replaced with granulation tissue as the epidermal hyperplasia began to decrease. By day 21, for the sutured wounds, a full-thickness layer of granulation tissue was observed. The epidermal hyperplasia decreased and the epidermal thickness reached normal width. In both groups, the granulation zone was broad near the epidermis and disappeared in

the mid-dermis as a result of the decreased thermal effect on the mid-dermis.

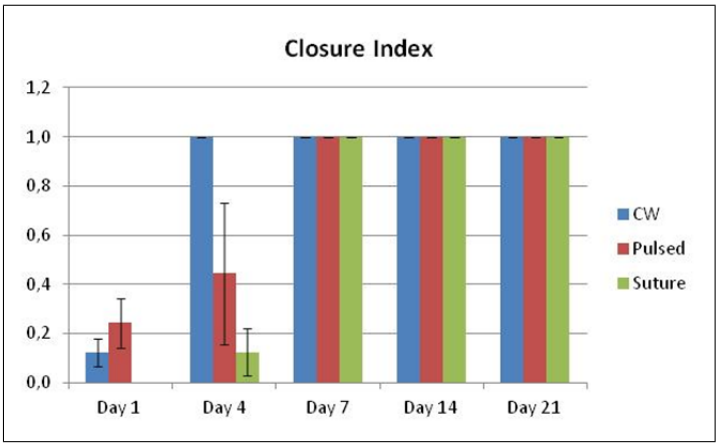

Figure 5.20 Closure index values during 21-day healing period.

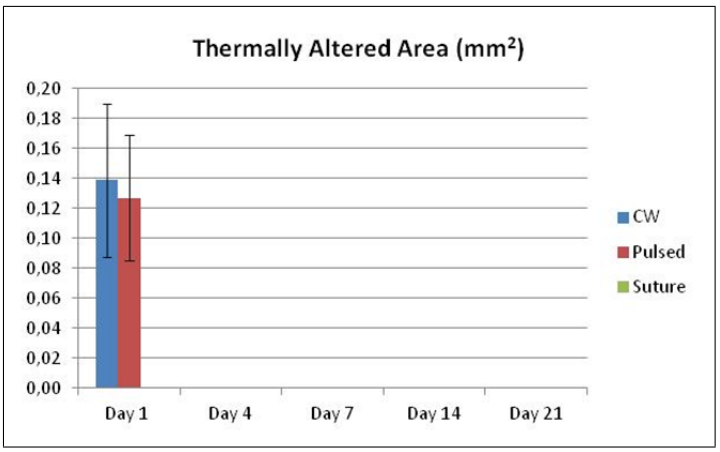

Figure 5.21 Thermally altered areas during 21-day healing period.

ET was observed after day 4 on the incisions (Figure 5.22). ET was found less ($p<0.05$ for day4, day7, and day14) in modulated mode of operation. ET was decreasing during the healing period and recovering its normal thickness. ET values in suture samples were found significantly higher at day 7, day 14, and day 21 than the samples welded by modulated and CW modes of operation of Tm:YAP laser. GA values were given in Figure 5.23. GA was found as 0.04 ± 0.02 mm^2 for modulated mode whereas GA was found to be 0 for CW at day 1. At day 4, day 7, and day 21, there was no statistically significant difference between modulated and CW modes of operation. At day14, GA value was found higher for the samples exposed to the modulated mode of operation (GA = 0.39 ± 0.03 mm^2 for CW and GA = 0.48 ± 0.02 mm^2 for modulated, $p<0.05$). In suture group, GA was observed at day 7, day 14, and day 21. GA values

in the suture group were found less than both modulated and CW modes of operation ($p<0.05$).

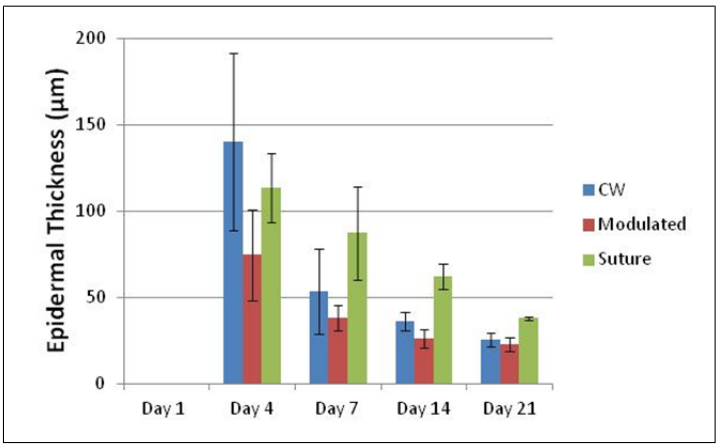

Figure 5.22 Epidermal thicknesses during 21-day healing period.

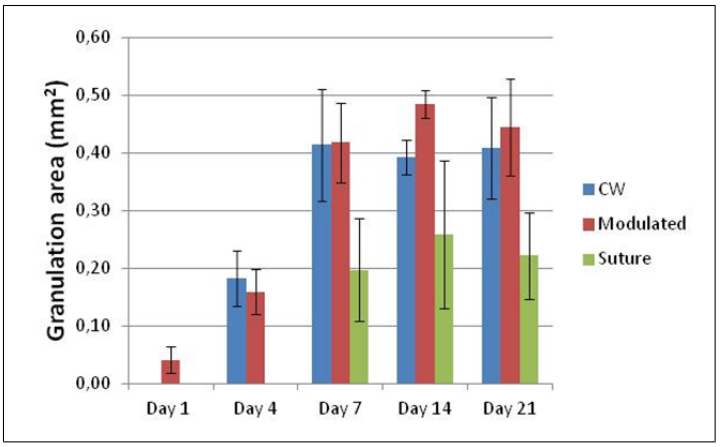

Figure 5.23 Granulation areas during 21-day healing period.

By histology, inspected incisions were closed tightly at the skin surface with welding applications on day 1. Some thermal effects were observed for some samples. No closure was noted in sutured incisions. For the sutured incisions, wounds remained open at the epidermis and dermis at day1. The dermal layers were traumatized by the suturing needle. Signs of edema were seen around the stitches of suture, representing possible local wound ischemia. The suture material inside the reparative tissue behaved as a foreign body. This caused accumulation of macrophages in the healing granulation tissue [223].

After 4 days, epidermal hyperplasia and migration of the epidermis beneath necrotic tissue was observed in all histologic sections. The process of reepithelialization was in its earliest stages as the epidermis began to bridge under the denatured, desiccated, and necrotic surface tissue. The granulation tissue was limited to the wound margins. This tissue composed by fibroblasts and mononuclear cells [82]. Good tissue apposition was present in the middle layers of the dermis where a moderate amount of thermal denaturation caused tissue bonding to occur without the formation of a large zone of necrotic tissue. The wounds showed full-thickness tissue apposition, complete epithelialization, minimal inflammation, and minimal thermal injury. By day 4, a zone of thermally damaged necrotic tissue was present at the surface of the skin. At day4, sutured incisions demonstrate thicker scars while laser-welded incisions demonstrate thinner scars. For the wounds closed with sutures, the granulation tissue width was significantly thinner than that detected in the laser welds, presumably due to both the absence of thermal damage as also seen in the literature [78].

At 7 days, the incision wounds showed complete epithelialization. Newly deposited collagen could be seen within a thin layer of granulation tissue that extended full-thickness through the skin. The epidermis had formed a complete and continuous layer across the surface of the skin.

Reepithelialization was completed and the epidermal thickness had increased. As the epidermal hyperplasia decreased, some of the tissue volume was replaced with granulation tissue. There was no evidence of thermal damage in all to the tissues. No signs of thermal damage or carbonaceous substances were seen on the epidermis.

From 14 days, wound healing continued in a normal manner. The newly deposited granulation tissue filled the gap that was created after sloughing of thermally damaged tissue from the wound site, and during the recession in epidermal thickness. Significant thermal damage in the papillary dermis resulted in a large zone of granulation tissue.

Epidermis in the welded cut returned to its normal architecture by day 14, which are faster, compared to sutured cuts. The epidermis had formed a complete and continuous layer across the surface of the skin. For the laser welded wounds, the average epidermal thickness was decreased. Tissue volume was partially replaced with granulation tissue as the epidermal hyperplasia began to decrease. For the sutured wounds, some of the tissue volume was replaced with granulation tissue while the epidermal hyperplasia began to decrease. The epidermal thickness of the sutured wounds was significantly greater than the epidermal thickness of the laser group as also seen in the literature [22]. Lasered skin showed minimal scar formation. Knot openings were observed rarely in suture-group samples.

By 21 days, a full-thickness layer of granulation tissue could be seen. The epidermis continued to decrease in thickness as wound healing progressed. The epidermal thickness decreased and the epidermal thickness reached normal width.

5.3.3 Tensile Strength Analysis

In total, sixty incisions were sampled on twenty Wistar rats; incisions of ten rats exposed to CW mode of operation (100 mW, 5 s) and incisions of the other ten rats exposed to modulated mode of operation (100 mW, 200 ms ON / 200 ms OFF, for a total 'on' duration of 5 sec). Each laser dose was sampled by two rats (with twelve incisions) for first, fourth, seventh, fourteenth, and twenty-first post-operative days and then tensile strength analysis was performed. The skin samples were strained perpendicularly to the axis of the closure until breakage failure and tensile break values were recorded.

In the analysis, both weld and suture strengths continued to increase over time, indicating a normal progression of the wound healing process. At day 1, the tensile force (TF) were found as 4.78±1.54 N for CW mode of operation, and 4.67±1.75 N for modulated mode of operation. TF found at day 4 were 5.17±0.93 N and 5.21±0.66 N for CW and modulated modes of operation, respectively. At day 7, the TF were

found to be 5.57±2.85 N for CW mode of operation and 5.98±2.29 N for modulated mode of operation. At day 14, the TF were increasing significantly such that they were 11.41±2.68 N for CW mode of operation and 11.54±3.22 N for modulated mode of operation. At the last healing period day 21, TF were measured as 14.39±1.59 N for CW mode of operations and 18.66±4.84 N for modulated mode of operation (Figure 5.24). When CW and modulated modes of operation were compared, there was no statistically significant difference between CW and modulated modes for day 1 ($p=0.88$), day 4 ($p=0.93$), day 7 ($p=0.68$), day 14 ($p=0.83$), and day 21 ($p=0.10$). There was a statistically significant value between day 7 and day 14 for both CW ($p<0.01$) and modulated ($p=0.01$) modes of operation. In addition, TF was found statistically significant among day 14 and day 21 ($p<0.01$) for modulated mode of operation.

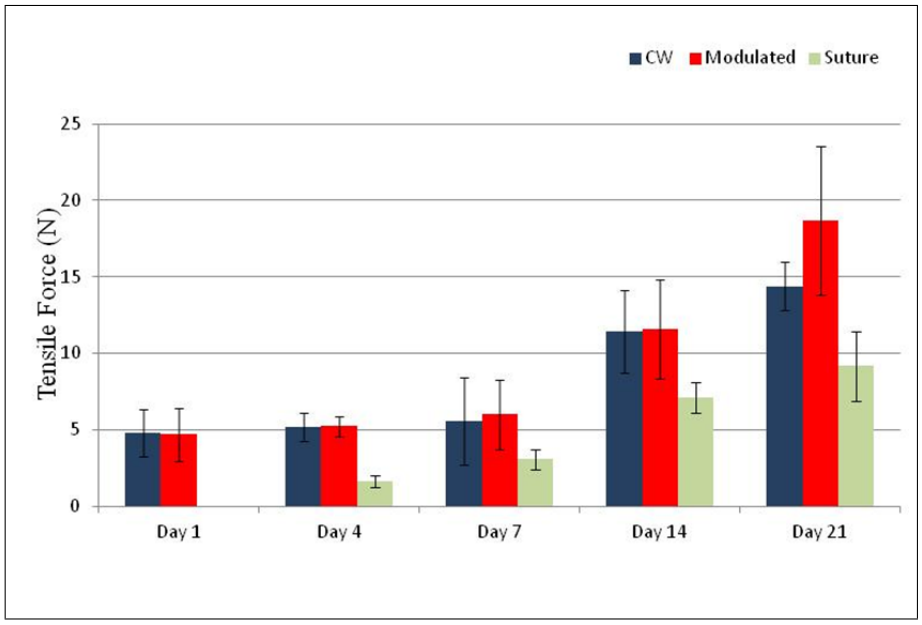

Figure 5.24 Tensile forces during 21-day healing period.

Welding creates an immediate, uniform, and fluid-tight bonding of tissue across the wound site. However, sutured tissue is initially held together only at the suture points; between suture points, the immediate tensile strength is effectively zero. TF by suture technique was found to be 0 N for day 1, 1.64±0.38 N for day 4, 3.06±0.65 N for day 7, 7.12±0.99 N for day 14, and 9.17±2.28 N for day 21. When TF values found by Tm:YAP laser welding were compared with the TF values found by suture

technique, TF found for both modulated and CW modes of operation were significantly higher ($p<0.01$) than the TF values found for conventional suture technique. Therefore, Tm:YAP laser welding possessed significantly stronger closure than conventional suture technique. This was another quantitative parameter that showed the success of laser tissue welding by Tm:YAP laser.

The collagen fibers in the extracellular matrix of the intact tissue establish the main infrastructure which is responsible for the mechanical properties of tissues, including elasticity and tensile strength. Mature collagen fibers are produced during the scar remodeling stage, by enzymatic reactions. They become elastic and strong, and provide the mature scar tissue its near-normal tissue strength. During the first days of the wound reparative process, the tensile strength increases moderately [81]. Then an acceleration of the healing process occurs, which reaches a steady state at about 8 weeks post injury [71]. It has also been reported that the thermal damage to the epithelial layer plays a role in the weaker tensile strength of the welded wounds [93].

5.4 Discussion

Determining the optimal laser parameters to minimize the thermal damage and maximize the healing effect associated with laser irradiation is the main concern for clinical application of laser tissue welding. For optimal laser parameters for successful tissue welding, uniform heating of the full thickness of the tissue is desired and the damage on tissue from excessive laser heating should be prevented. The advantages of laser tissue welding can be achieved by optimum laser wavelength, power density, pulse duration, and spot size. Therefore, an experimental study of dose determination was performed to find the optimal parameters that provide welding with highest success. The determined laser parameters were found as a power of 100 mW, an average light intensity of 34.66 W/cm^2, and exposure duration of 5 sec in both CW and modulated modes of operation. Histological and tensile sampling analysis were performed to prove the success of laser tissue welding by Tm:YAP laser.

By histological analysis of laser welded incisions, the healing process was observed in four levels: (1) thermal inflammation, (2) granulation formation, (3) tissue remodeling, and (4) extra cellular matrix. The healing process is also dependent on the effect of elevated temperature on cell survivability, the thermal stability of the biochemical elements in the acute phase of wound healing, and the endogenous growth factors [156]. Laser tissue welding mechanisms include denaturation of structural proteins, dehydration of the proteins, acceleration of natural fibrinogen polymerization, collagen-to-collagen fusion, crosslinking of proteins, formation of noncovalent bonding between collagen, and interdigitation of collagen fibers [126]. The most probable mechanism of Tm:YAP laser welding is the thermal coagulation of tissue and heat-induced collagen contracture. Tm:YAP laser offers minimal thermal damage to the dermis due to the high absorption by water.

Collagen in skin tissues plays a major role in laser tissue welding. Thermal denaturation of the collagen fibers provides tissue welding [142]. The laser heating induces the fusion of collagen fibers on both sides of the incision. After laser irradiation, the collagen fibrils are swollen, densely packed, and fused together. Cell membranes are disrupted and the proteins of the cell leak. These proteins undergo a thermal degradation of the bonds and form new molecular bonds due to cooling. There is also an effect of stimulating collagen synthesis after laser welding. When the laser is applied, the heat-labile intramolecular crosslinks of collagen are broken, and the collagen undergoes a transition from a highly organized crystalline structure to a random state, which is the denaturation process. When the laser is applied to the tissue, the collagen fibrils are thickened and shrink as a consequence of the unwinding of the triple helix [141]. As the structural basis for the laser tissue welding, the unwinding of triple helix follows interdigitation during cooling and healing period [198]. The effects of heating on collagen can be reversible or irreversible, which depends on the collagen content, the maximum temperature reached, exposure time, and the mechanical stress applied to the tissue during heating [149]. Excessive temperature increase in collagens forms a subsequent loss of fibrillar integrity.

By histology analysis, the low power levels of Tm:YAP laser at 100 mW and 5 sec duration for both CW and modulated modes of operation were found successful for tissue welding applications in Wistar rat skin with minimal thermal damage and strong welds compared to suture technique. CI values by laser welded incisions were found higher than the suture samples at day 1. Furthermore, CI values were found to be 1 at day 4, for laser welded samples whereas suture samples were not closed at day 4. On the other hand, ET was found lower for modulated application than CW mode application of Tm:YAP laser system. However, TAA was not statistically significant among CW and modulated modes of operation. The histological parameters found in this study were compared with the results found in a comparison study performed by the same methodology with 809-nm diode laser (0.5 W, 5 s) with solder (%25 bovine serum albumin), 910-nm diode laser (0.5 W, 5 s), and 1070-nm Ytterbium fiber laser (0.5 W, 5 s), where 1070-nm fiber laser yielded noticeably stronger bonds than the near infrared laser [224]. CI was significantly found higher by Tm:YAP laser (0.1 W, 5 s) than the Ytterbium fiber laser at day 4 (CI=0.24±0.29 at day 4 for 1070-nm fiber laser). TAA was not observed by Tm:YAP laser application whereas the Ytterbium fiber laser formed TAA of 0.05±0.01 mm^2. The TAA values among Tm:YAP laser and Ytterbium fiber laser were not found statistically significant at day 1. ET values were found higher by Tm:YAP laser at day 4 and they are not statistically significant after day 4.

Due to the higher water absorption near 1980 nm, lower power levels of Tm:YAP lasers (compared to lower wavelength lasers) are found sufficient for tissue welding and no solder is necessary to increase the absorption effect. This decreases the operation time and adverse effects due to the solders. The solder, acting as a biological glue, absorbs laser energy to increase the effect of denaturation and coagulation of protein components to bond tissue incisions. Three disadvantages of the solid protein solders have been reported [127]. (1) Most of the energy is generally absorbed near the upper portion of the solder. (2) The protein solder is soluble in physiological solutions. They can be mixed by blood dilution and this mechanical alteration can weaken tissue welding repair. (3) Protein solders are brittle and inflexible therefore they are not easily adapted to various tissue geometries. In addition, because of being low viscosity

materials, application of fluid solders to the repair site is difficult. Furthermore, solders may have an associated immunological risk [122].

Unlike the Er:YAG and CO_2 lasers, lasers operating at wavelengths shorter than 2.5 μm are more desirable for clinical use because their outputs can be transmitted via conventional, readily available silica fibers. Furthermore, thermal injury of surrounding tissues can be minimized by using pulsed radiation due to the cooling of the tissue between pulses [135]. When the laser pulse width is less than the tissue thermal relaxation time, thermal diffusion outside the application area is reduced and the thermal injury of the surrounding tissues is minimized [27].

Previous studies found a strong correlation between laser wavelength and the tensile strength of welded tissues. In particular, laser tissue welding at wavelengths with higher water absorption was shown to provide greater tensile strength [134]. Among varying laser wavelengths between 1220 nm and 1430 nm, the highest tensile strength was achieved at 1430 nm, whose water absorption is the highest [225]. The tensile forces found by Tm:YAP laser was significantly found higher than Ytterbium fiber laser after day 1 [224]. At day 1, the tensile forces were not found statistically significant. The greater water absorption is correlated with the higher tensile strength [134]. The strong closure by Tm:YAP laser welding was also quantitatively proved by tensile strength analysis. The tensile forces found for both CW and modulated mode of operations are significantly higher than the values found for conventional suture technique. Therefore, the Tm:YAP laser at 1980 nm has proven to possess stronger welds than the closure by suture technique.

In this part of the study, tissue welding potential of an infrared laser with high water absorption property was investigated by quantification of closure, thermal damage given and mechanical strength of welds. CW and modulated modes of operations were comparatively applied. Modulated laser delivery was expected to make less thermal damage permitting thermal relaxation of target tissue. In future, temperature changes of tissue and heat deposition as a function of laser delivery mode can be studied in order to improve the welding quality. New wavelengths of laser with well

defined energy delivery modes may provoke the enthusiasm for clinical adoption of laser welding.

In conclusion, for laser groups immediate closure at the surface layers of the incisions was observed. Full closures were observed for both modulated and CW modes of operation at day 4. The tensile forces for both modulated and CW modes of operation were found to be significantly higher than the values found by conventional suture technique. The 1980-nm Tm:YAP laser system operating in both modulated and CW modes maximizes the therapeutic effect while minimizing undesired side effects of laser tissue welding. Hence, it is a potentially important alternative tool to conventional suturing technique. Tm:YAP laser system stands as a potentially important candidate for tissue welding applications with accelerated, improved, and strong healing. Further studies are clearly worthwhile, to evaluate its full potential for clinical use.

5.5 Laser Tissue Welding in Clinics

Applications for lasers are expanding rapidly. As a new generation of smart or robotic laser systems is developed, it will be essential for the scientists and engineers to understand the various laser-tissue interactions that can take place [1]. The use of expensive lasers should be limited to procedures they can do uniquely or do more effectively than simpler, inexpensive technology. Like parallel advances in computer technology, medical doctors can expect existing lasers to become smaller, more capable, and less expensive as solid-state laser technology matures.

Laser welding provides important promise for improved tissue joining in all surgical fields. It will not replace sutures in all applications, but it will solve many existing problems with tissue repair with greater ease and speed, improved watertightness, and reduced inflammatory response and tissue injury. Over the next few years, laser welding will likely become the preferred technique for an increasing number of applications. Laser welding, in combination with other surgical technology advances, will provide the precise control over tissue effects that will be the hallmark of surgery [26].

There are three main drawbacks reported for the laser welding: (1) The immediate tensile strength, during the first few days is low; (2) There is often a noticeable thermal damage; (3) The results are frequently inconsistent [29]. Most of these obstacles were eliminated in recent years by use of new laser systems. Determining the optimal laser and surgical parameters to minimize the thermal damage associated with laser irradiation while maintaining a strong bond at the weld site is still the main concern for clinical application of this technology [101].

Laboratory investigations have demonstrated the feasibility of laser welding of tissues in aorta, urethra, ureter, bladder, vas deferens, blood vessels, skin, nerve, bone, tendon, cornea, biliary tissue, esophagus, stomach, small intestine, colon, and uterine tube. There are many other areas that have potential use for laser welding that have yet to be explored. A variety of different techniques and lasers has been used in these studies such as Argon laser, Krypton, Nd:YAG laser, diode, Ho:YAG, and CO_2 [75]. These studies clearly demonstrate the feasibility of the laser technique; however, its clinical benefit over conventional methods requires further investigation.

Although laser-based methods of wound closure have not yet gained widespread clinical acceptance, some limited clinical uses of laser tissue welding have also been studied [171, 226, 227, 228]. In the early 1980's, an Nd:YAG laser assisted extraintracranial bypass operations was performed on five patients [229]. After follow-up of 6-9 months all five patients were alive with angiographic patent anastomoses. In the late 1980, a series of 10 patients were described receiving laser assisted arteriovenous fistulas for haemodialysis [230]. Four patients needed revision operations after 4-6 months and one patient died. A various clinical experiments using a CO_2 laser was performed on arterial and venous reconstructions [231]. In 1992, the use of CO_2 laser-stay suture technique to perform 16 microvascular anastomoses in six patients. The laser repairs were characterized by greater speed and ease, equivalent patency rate, and less tissue inflammatory response compared to sutured anastomosis [232]. Laser welding already has a proven clinical safety record on in vivo bonding of dura with no damage to the underlying cerebral cortex [132].

Although the experimental techniques have been successful, the problems still retained which limit those techniques practicing in clinic. Clinical success is defined as formation of a stable, strong bond that does not deteriorate over time [24]. There were several obstacles which prevented physicians from using laser tissue welding clinically. These are collateral thermal injuries, inconsistency of the results, and a lack of understanding of the exact mechanism by which laser irradiation induces tissue bonding [84]. Most of the obstacles that prevent physicians from using laser tissue-bonding techniques are related to the low tensile strength, to the collateral thermal injury to the tissue, to technical difficulties with tissue alignment, to the ambiguity of the end point for the procedure, and poor reproducibility [91, 112, 160]. In addition, there are still major gaps in understanding of the actual laser tissue welding mechanism [26]. Improvements to tissue welding procedures and a better understanding of the mechanisms involved in the tissue welding process are required before this technique of tissue closure can be applied clinically.

For clinical trials, a more compact practical setup, probably relying on optical and thermal fibers, needs to be developed [24]. On the other hand, uniform and optimized techniques of tissue apposition are required in order to move tissue welding from the laboratory into the clinic [96]. Availability and cost are other obstacles to the widespread use of lasers in tissue welding. Most lasers are not equipped with expensive accessories. Sutures, on the contrary, are cheap, reliable and always readily available [91].

Transition from laboratory to clinical application requires the optimization of welding parameters. Despite the large number of experimental studies reported in the literature, very few of them have reached the clinical phase. The clinical use of a laser is typically based on (1) laser-tissue interaction mechanisms (wavelength, power, pulse durations), (2) the penetration depth of laser light in tissue (optical properties of the tissue at selected wavelength), (3) the availability of the laser, (4) the availability of fibers to transmit the desired wavelength [1].

In a new system design, before the clinical viability of the method can be assessed, the parameters must be carefully selected by predosimetry studies and then in vivo animal experiment. Laser welding has failed to prove itself in any clinical application to date mostly due to use of techniques which do not take advantage of such careful control. The medical laser system in this thesis for laser tissue welding has been developed and evaluated with a series of in vitro and in vivo tests. This laser system has the potential for clinical application.

Solid-state diode laser systems can be made much smaller and require much less power than other laser technologies. It may be possible with existing diode laser technology to build welding units that are completely handheld and battery powered. All of the wavelengths in diode laser technology are readily coupled to fiberoptic delivery systems, which is a very important consideration for some applications such as endoscopic surgery. Another important feature of the solid state lasers is that they interface very well with driver electronic circuitry. This allows the easy implementation of embedded microprocessor control and real-time feedback systems. The semiconductor units could also be made cheaply enough to be disposable or disposable after a certain number of uses [26]. On the other hand, they have not been found suitable for certain high power photoablative tasks. Tm:YAP laser at 1980 nm in this thesis provide successful tissue welding at 100 mW power output. Such powers around 1980 nm can be manufactured by laser diode technology, which may be handheld and battery-powered.

Laser tissue welding is a promising technique and in recent years considerable progress has been achieved. Although clinical use at present is infrequent, experimental results warrant clinical application and research in selected patients. To show a significant improvement in results, a number of patients will need to be evaluated. The future of laser tissue welding will depend on the results of large clinical trials addressing the efficacy of laser tissue welding compared to conventional suturing. Laser techniques for joining tissue, in combination with other surgical technologies, will be a hallmark of surgery in the succeeding years. Further investigation will likely reveal more applications for this valuable technology.

6. CONCLUSION

Whenever light hits tissue, it can be transmitted, scattered, reflected, or absorbed, depending on the type of tissue and the wavelength of the light. Infrared light is absorbed primarily by water, while visible and ultraviolet light are absorbed mainly by hemoglobin and melanin, respectively. Photothermal effects are governed primarily by absorption of optical energy and secondly governed by fundamental principles of heat transport. When laser light is absorbed in tissue and converted into thermal energy, different thermal effects are obtained, depending on temperature range. The detailed information about laser-tissue interactions, photothermal interactions, mathematical modeling of photothermal interactions, thermal damage and skin optics were given in the related chapters of this thesis.

The interest in lasers emitting around 2-μm is continuously increasing because they can be used for several biomedical applications. The Thulium laser is suitable for medical applications due to strong absorption in water. Therefore, it makes sense to focus on lasers that emit wavelengths absorbed by water by producing localized heating. Because having absorption band around 795 nm, Thulium lasers can easily be pumped by standard diode lasers. This will provide easy modulation of the laser by using microcontroller design.

In this thesis, a computer controlled Tm:YAP laser system with a power output up to 1 W and emission wavelength of 1980 nm were established. The Tm:YAP laser system includes a Tm:YAP laser setup, diode laser driver, water chiller for the laser setup, modulation controller unit, and an acquisition/controller software. The laser crystal temperature was fixed by using a closed-loop chiller system for stable power characteristics of the laser system. The modulation microcontroller unit provides the modulation the Tm:YAP laser output. The microcontroller unit can modulate the laser up to a frequency of 50 Hz. The user interface on the computer sets the power and the duration of the laser emission with on cycle, off cycles, and number of cycles. A pilot

beam was added to the system to simulate the invisible 1980 nm beam in applications.

Once the laser system was stabilized, its output power, spot size, and light intensity measurements were performed. The pumping current versus laser power output data was studied for fixed chilled temperatures and the stability of the laser system was performed. The laser spot size versus changing distances and average light intensities were measured.

The thermal properties of the laser system on soft tissues were investigated and dosimetry studies were performed. The target in vitro tissues were animal heart, brain, liver, and kidney samples. These experiments were performed to see the effect of the laser on biological tissues and determine the dosimetry for the future in vivo studies. In the in vitro samples, the thermally altered areas and penetration depth parameters were obtained. The laser thermal effect and damage in the tissues were macroscopically analyzed.

Mathematical models of the welding process can be a useful guide to parameter selection; however empirical trials of laser parameters must be the ultimate measure of success. The experiments should be performed for each wavelength and tissue type to be treated.

The ablation efficiency of the developed laser system was experimentally tested on brain tissue ex-vivo as a predosimetry ablation study. Optimization of the Tm:YAP laser ablation efficiency for cortical and subcortical brain tissues was performed by maximizing the therapeutic effect and minimizing unwanted side effects with different power levels of the Tm:YAP laser. Thermal changes were quantified in terms of ablation efficiency. The maximum ablation efficiency was obtained when the Tm:YAP laser was applied at the power level of 200 mW with a duration of 10 seconds (2 J). At this laser dose, the ablation efficiency was obtained as 71.4% for cortical region and 58.7% for subcortical region. The fiber-coupled Tm:YAP laser system was found to be promising for photo-ablation applications.

Furthermore, the thermal effects, coagulation and ablation zones were investigated in vivo skin samples. The success of the interactions in skin tissue samples was analyzed by histology under light microscopy during 4-day healing period. The fluence effect of the laser system for skin ablation was analyzed by histology analysis on Wistar rat skin tissues. Thermally altered length, thermally altered area, ablation area, and ablation depth parameters were measured on histology images of skin samples just after the laser operation and after four-day healing period. Continuous-wave mode of operation provided higher thermal effects on the skin samples. Lower fluence levels were found for efficient ablation effect. Diameters of lesions tended to increase with increasing power and irradiation duration for both modes of operation.

Temperature measurements were performed during the laser application on in vivo skin samples. For instant temperature detection, temperature measurement systems by thermal camera and thermocouples were investigated. The experiments were performed to see the temperature effect of Tm:YAP laser by direct temperature measurements under skin and on skin surface, to compare the temperature measurements for difference laser parameters and to compare modulated and CW mode of operation of Tm:YAP laser on skin tissue. The temperature increase was faster in CW mode and the temperature decrease was slower due to the temperature affected by surrounding tissues in CW mode of operation. The temperature increase difference between CW and modulated mode of operation on skin measured by thermal camera was higher than the temperature increase difference under skin measured by thermocouples. The effected duration for CW laser application was higher than the effected duration measured during modulated mode of operation.

Techniques for measuring the temperature of the tissues during laser welding may provide a reliable endpoint for energy application. Such methods may help optimize bond strength and make surgical results more predictable. However, accuracy, response time, and sampling errors (both spatial and temporal) are factors affecting the success of such temperature feedback systems. Unexpected higher temperatures during the operations can cause irreversible tissue damage.

The main aim of the study is to explore the welding capabilities of Thulium (Tm:YAP) laser in modulated and continuous-wave (CW) modes of operation. The laser tissue welding at 1980 nm was compared to conventional suture techniques by both histology and tensile strength measurements. Full-thickness incisions on Wistar rat skin were welded by the Tm:YAP laser system at 100 mW and 5 s in both modulated and CW modes of operation (34.66 W/cm^2). The skin samples were examined during 21-day healing period by histology and tensile tests. The results were also compared with the samples closed by conventional suture technique.

The objective of the tissue welding study in this thesis is to create rapid, strong, full-thickness welds with esthetic scar and minimize the lateral zone of thermal denaturation at the weld site while limiting thermal damage to adjacent healthy tissue by comparing the continuous-wave and modulated modes of operation of the 1.98-μm Tm:YAP laser system. In vivo experiments were conducted to optimize the laser power and energy delivered to weld site. The studies were conducted to compare sutured wounds and laser welds in both continuous-wave and modulated operation modes of the laser system. Tensile strength measurements and histological analysis were used for evaluation.

According to the histology images taken with the optical microscope, the incisions at day 1 were closed partially for both modulated and CW mode of operations. After day 4, full closure was obtained for both laser operations. On the other hand, in suture group, closure was not observed for day 1 and day 4. By histology analysis, CI values by laser welded incisions were found higher than the suture samples at day 1. Furthermore, CI values were found to be 1 at day 4, for laser welded samples whereas suture samples were not closed at day 4. On the other hand, ET was found lower for modulated application than CW mode application of Tm:YAP laser system. However, TAA was not statistically significant among CW and modulated modes of operation.

In tensile force analysis, tensile force values found by Tm:YAP laser welding were compared with the TF values found by suture technique, TF found for both modulated and CW modes of operation were significantly higher than the TF values

found for conventional suture technique. Therefore, Tm:YAP laser welding possessed significantly stronger closure than conventional suture technique.

Close apposition and alignment of wound edges is a crucial factor in achieving successful wound healing in any microsurgical procedure and has measurable effects on tensile strength and scar tissue deposition [93]. Better apposition was noticed in the laser group compared to sutured cuts. Laser welding results in full-thickness close up and full-thickness welding can also decrease the inflammation risk during healing.

In recent years, CO_2 lasers at 10.6 μm have been increasingly used in laser tissue welding. These lasers are desirable because of highest absorption band by the water. However, the transmission of CO_2 lasers by fibers is sensitive and expensive. Although they can also be used to collect the radiation from the bodies, the infrared fibers used by CO_2 lasers have high bending losses and they need much care to manipulate during the operation. On the other hand, the most widely used laser is diode lasers between 800 and 815 nm range. However, they are used with albumin protein solders.

At the wavelength of the Thulium laser, light is very strongly absorbed by water and water is the main constituent of skin. Most of the Thulium laser energy is absorbed in the outermost layers of the tissue and little of that energy penetrates to the deeper layers. Therefore, no solder is required in the laser tissue welding method. It is important to use laser alone and then it could make the closure procedure easier and faster. This decreases the operation time and adverse effects due to solders. 2-μm lasers are also considered to be in the "eye-safe" region, which makes them more suitable for clinical applications.

The rapid ablation rate and the ability to form well-defined lesions with minimal damage at boundaries have demonstrated the potential of this fiber laser to fulfill applications in the medical field. On the other hand, low-dose application of the laser system promises the successful laser tissue welding applications.

The encouraging results obtained in vivo using skin of small laboratory animals have provided the stimulus to consider introducing the technology into the clinical arena. The future studies will address the suitability of this laser system for specific medical applications in clinical area. The enhancement of healing of tissues by simple and noninvasive Thulium laser therapy have important future clinical implications and is worthy of further investigations.

REFERENCES

1. Welch, A. J., and M. J. C. van Gemert, *Optical-thermal response of laser-irradiated tissue*, Springer, 2nd ed., 2011.

2. Esterowitz, L., R. C. Stoneman, and R. Bonner, "Trivalent thulium laser at 1.95 μm for enhanced laser-tissue interactions," *Proceedings of the SPIE - The International Society for Optical Engineering*, Vol. 1202, pp. 175–178, 1990.

3. White, J. C., J. Bokor, and D. Henderson, "Optically pumped atomic thulium lasers," *IEEE Journal of Quantum Electronics*, Vol. QE-18, no. 3, pp. 320–323, 1982.

4. Elder, I. F., and M. J. P. Payne, "Yap versus yag as a diode-pumped host for thulium," *Optics Communications*, Vol. 148, no. 4, pp. 265–269, 1998.

5. Dischler, B., and W. Wettling, "Investigation of the laser materials yalo3:er and liyf4:ho," *J. Phys. D: Appl. Phys.*, Vol. 17, pp. 1115–1124, 1984.

6. Sudesh, V., and J. A. Piper, "Spectroscopy, modeling, and laser operation of thulium-doped crystals at 2.3 μm," *IEEE Journal of Quantum Electronics*, Vol. 36, no. 7, pp. 879–885, 2000.

7. Ni, H., and S. C. Rand, "Avalanche upconversion in tm:yalo3," *Optics Letters*, Vol. 16, no. 18, p. 1424, 1991.

8. Cornacchia, F., D. Parisi, C. Bernardini, A. Toncelli, and M. Tonelli, "Efficient, diode-pumped tm3+:bay2f8 vibronic laser," *Optics Letters*, Vol. 12, no. 9, pp. 1982–1989, 2004.

9. Elder, I. F., and M. J. P. Payne, "Lasing in diode-pumped tm:yap, tm, ho:yap and tm,ho:ylf," *Optics Communications*, Vol. 145, no. 1, pp. 329–339, 1998.

10. Izawa, J., H. Nakajima, H. Hara, and Y. Arimoto, "Relaxation oscillation with tm:ylf laser using a double cavity in the single-longitudinal-mode oscillation," *Optical Engineering*, Vol. 40, no. 3, pp. 466–468, 2001.

11. Stoneman, R. C., and L. Esterowitz, "Efficient 1.94-μm tm:yalo laser," *IEEE Journal of Selected Topics in Quantum Electronics*, Vol. 1, no. 1, pp. 78–82, 1995.

12. Stoneman, R. C., L. Esterowitz, and B. J. Feldman, "Diode pumped 1.94 μm tm:yalo laser," *Lasers and Electro-Optics Society Annual Meeting, 8th Annual Meeting Conference Proceedings*, Vol. 2, pp. 453–454, 1995.

13. Elder, I. F., and J. Payne, "Diode-pumped, room-temperature tm:yap laser," *Applied Optics*, Vol. 36, no. 33, pp. 8606–8610, 1998.

14. Cheong, W. F., and A. J. Welch, "A model for optical and thermal analysis of laser balloon angioplasty," *IEEE Transactions on Biomedical Engineering*, Vol. 36, no. 12, pp. 1233–1243, 1989.

15. Niemz, M. H., *Laser-tissue interactions fundamentals and applications*, Springer-Verlag, 2nd ed., 1996.

16. Ben-David, M., R. Cantor, N. Balbul, M. Yehuda, and I. Gannot, "Measuring tissue heat penetration by scattered light measurements," *Lasers in Surgery and Medicine*, Vol. 40, pp. 494–499, 2008.

17. D'Arcangelo, C., F. D. N. D. Maio, G. D. Prosperi, E. Conte, M. Baldi, and S. Caputi, "A preliminary study of healing of diode laser versus scalpel incisions in rat oral tissue: A comparison of clinical, histological, and immunohistochemical results," *Oral Surg. Oral Med. Oral Pathol. Oral Radiol. Endod.*, Vol. 103, pp. 764–773, 2007.

18. Fried, N. M., B. Choi, A. J. Welch, and J. T. Walsh, "Radiometric surface temperature measurements during dye-assisted laser skin closure: In vitro and in vivo results," *Lasers in Surgery and Medicine*, Vol. 25, pp. 291–303, 1999.

19. Fried, N. M., and J. T. Walsh, "Cryogen spray cooling during laser tissue welding," *Phys. Med. Biol.*, Vol. 45, pp. 753–763, 2000.

20. Rebecca, S. C., M. Kohlyx, M. Essenpreisk, and M. Cope, "Near-infrared optical properties of ex vivo human skin and subcutaneous tissues measured using the monte carlo inversion technique," *Phys. Med. Biol.*, Vol. 43, no. 8, pp. 2465–2470, 1998.

21. Zhou, J., J. K. Chen, and Y. Zhang, "Theoretical analysis of thermal damage in biological tissues caused by laser irradiation," *MCB*, Vol. 4, no. 1, pp. 27–39, 2007.

22. Gulsoy, M., Z. Dereli, H. O. Tabakoglu, and O. Bozkulak, "Closure of skin incisions by 980-nm diode laser welding," *Lasers Med. Sci.*, Vol. 21, pp. 5–10, 2006.

23. Pierce, M. C., S. D. Jackson, M. R. Dickinson, and T. A. King, "Laser-tissue interaction with a high-power 2-μm fiber laser: Preliminary studies with soft tissue," *Lasers in Surgery and Medicine*, Vol. 25, pp. 407–413, 1999.

24. Cilesiz, I., S. Thomsen, A. J. Welch, and E. K. Chan, "Controlled temperature tissue fusion:ho:yag laser welding of rat intestine in vivo, part two," *Lasers in Surgery and Medicine*, Vol. 21, pp. 278–286, 1997.

25. Menovsky, T., J. F. Beek, and M. J. C. van Gemert, "Effect of the co_2 milliwatt laser on tensile strength of microsutures," *Lasers in Surgery and Medicine*, Vol. 20, pp. 64–68, 1997.

26. Bass, L. S., and M. R. Treat, "Laser tissue welding: A comprehensive review of current and future clinical applications," *Lasers in Surgery and Medicine*, Vol. 17, pp. 315–349, 1995.

27. Karamzadeh, A. M., B. J. F. Wong, R. L. Crumley, and G. Ahuja, "Lasers in pediatric airway surgery: Current and future clinical applications," *Lasers in Surgery and Medicine*, Vol. 35, pp. 128–134, 2004.

28. Mohammed, Y., and J. F. Verhey, "A finite element method model to simulate laser interstitial thermo therapy in anatomical inhomogeneous regions," *BioMedical Engineering OnLine*, Vol. 4, no. 2, 2005.

29. Simhon, D., A. Ravid, M. Halpern, I. Cilesiz, T. Brosh, N. Kariv, A. Leviav, and A. Katzir, "Laser soldering of rat skin, using fiberoptic temperature controlled system," *Lasers in Surgery and Medicine*, Vol. 29, pp. 265–273, 2001.

30. Ludwig, H. C., T. Kruschat, T. Knobloch, H.-O. Teichmann, K. Rostasy, and V. Rohde, "First experiences with a 2.0-μm near infrared laser system for neuroendoscopy," *Neurosurg. Rev.*, Vol. 30, pp. 195–201, 2007.

31. Nishioka, N. S., and Y. Domankevitz, "Comparison of tissue ablation with pulsed holmium and thulium lasers," *IEEE Journal of Quantum Electronics*, Vol. 26, no. 12, pp. 2271–2275, 1990.

32. Kou, L., D. Labrie, and P. Chylek, "Refractive indices of water and ice in the 0.65-2.5 μm spectral range," *Appl. Opt.*, Vol. 32, pp. 3531–3540, 1993.

33. Wieliczka, D. M., S. Weng, and M. R. Querry, "Wedge shaped cell for highly absorbent liquids: Infrared optical constants of water," *Appl. Opt.*, Vol. 28, pp. 1714–1719, 1989.

34. Segelstein, D. J., *The complex refractive index of water*. PhD thesis, University of Missouri, Kansas City, USA, 1981.

35. Hale, G. M., and M. R. Querry, "Optical constants of waer in the 200 nm to 200 μm wavelength region," *Appl. Opt.*, Vol. 12, pp. 555–563, 1973.

36. Chan, E. K., *Laser tissue welding: Effects of solder coagulation and tissue optical properties*. PhD thesis, The University of Texas at Austin, USA, 1997.

37. Chen, B., S. L. Thomsen, R. J. Thomas, J. Oliver, and A. J. Welch, "Histological and modeling study of skin thermal injury to 2.0 μm laser irradiation," *Lasers in Surgery and Medicine*, Vol. 40, pp. 358–370, 2008.

38. Anderson, R., and J. A. Parrish, "The optics of human skin," *J Invest. Derm.*, Vol. 77, pp. 13–19, 1981.

39. Kunde, D. T., V. Daniche, M. Wendt, and R. Brinkmann, "Temperature dependence of water absorption for wavelengths at 1920 nm and 1940 nm," in *IFMBE Proceedings* (Stolen, J. V., P. Verdonek, M. Nyssen, and J. Haneisen, eds.), Vol. 22, pp. 156–166, ECIFMBE 2008, 2008.

40. Jansen, E. D., T. G. van Leeuwen, M. Motamedi, C. Borst, and A. J. Welch, "Temperature dependence of the absorption coefficient of water for midinfrared laser radiation," *Lasers Surg Med.*, Vol. 14, no. 3, pp. 258–168, 1994.

41. Lange, B. I., T. Brendel, and G. Hüttmann, "Temperature dependence of light absorption in water at holmium and thulium laser wavelengths," *Applied Optics*, Vol. 41, no. 27, pp. 5797–5803, 2002.

42. Chen, S. Y., T. L. Yeo, J. Leighton, T. Sun, K. T. V. Grattan, R. Lade, B. D. Powell, G. Foster-Turner, and M. Osborne, "Tm:ho co-doped single mode optical fibre laser pumped by a 1600 nm er fibre laser," *Optics Communications*, Vol. 281, pp. 2567–2571, 2008.

43. Khoury, J. G., R. Saluja, D. Keel, S. Detwiler, and M. P. Goldman, "Histologic evaluation of interstitial lipolysis comparing a 1064, 1320 and 2100 nm laser in an ex vivo model," *Lasers in Surgery and Medicine*, Vol. 40, pp. 402–406, 2008.

44. Abelow, S. P., "Use of lasers in orthopedic-surgery," *Current Concepts Orthopedics*, Vol. 16, no. 5, pp. 551–556, 1993.

45. Anderson, R. R., W. Farinelli, H. Haubach, and D. Manstein, "Selective photothermolysis of lipid-rich tissues: A free electron laser study," *Laser Surg Med*, Vol. 38, pp. 913–919, 2006.

46. Hayashi, K., J. A. Nieckarz, G. Thabit, J. J. Bogdanske, A. J. Cooley, and M. D. Markel, "Effect of nonablative laser energy on the joint capsule: An in vivo rabbit study using a holmium:yag laser," *Lasers in Surgery and Medicine*, Vol. 20, pp. 164–171, 1997.

47. Gordon, S., and G. Watson, "Thulium laser enucleation of the prostate," *Eur. Urol. Suppl.*, Vol. 5, no. 2, p. 310, 2006.

48. El-Sherif, A. F., and T. A. King, "Soft and hard tissue ablation with short-pulse high peak power and continuous thulium-silica fibre lasers," *Lasers Med Sci*, Vol. 18, pp. 139–147, 2003.

49. Minaev, V. P., "Laser apparatus for surgery and force theraphy based on high-power semiconductor and fibre lasers," *Quantum Electronics*, Vol. 35, no. 11, pp. 976–983, 2005.

50. Verdaasdonk, R., A. I. Rem, S. van Thoor, T. de Boorder, and J. Klaessens, "Comparison of the co_2, cw thulium and diode laser in a thermal imaging model for the optimization of various clinical applications," in *Proceedings of SPIE - Optical Interactions with Tissue and Cells XVII* (Jacques, S. L., and W. P. Roach, eds.), Vol. 6084, pp. 156–166, 2006.

51. Kincade, K., "Fiber lasers find opportunities in medical applications," *Laser Focus World*, Vol. 41, no. 9, p. 76, 2005.

52. Chen, W. R., K. E. Bartels, H. Liu, and R. E. Nordquist, "Laser-photothermal effect on skin tissue - damage and recovery," *Journal of X-Ray Science and Technology*, Vol. 14, no. 3, pp. 207–215, 2006.

53. Sawyer, P. N., "Development and application of modern devices in vascular surgery including comment on modern antithrombotic and lytic drug therapy," *Journal of Applied Biomaterials*, Vol. 1, pp. 143–151, 1990.

54. Pinto, J. F., L. Esterowitz, and R. F. Bonner, "Reduction of acoustic transients in tissue with a 2 μm thulium laser," *Proceedings of SPIE - The International Society for Optical Engineering*, Vol. 1420, pp. 242–243, 1991.

55. Charlton, A., M. R. Dickinson, P. F. Hicks, and T. A. King, "Erbium- and holmium-doped yag lasers: A comparative study," *Journal of Modern Optics*, Vol. 37, no. 4, pp. 455–462, 1990.

56. Xia, S.-J., J. Zhuo, X.-W. Sun, B.-M. Han, Y. Shao, and Y.-N. Zhang, "Thulium laser versus standard transurethral resection of the prostate: A randomized prospective trial," *European Urology*, Vol. 53, pp. 382–390, 2008.

57. Massoud, W., O. Dumonceau, N. Saheb, B. Iliescu, J. Schlosser, T. Guetta, F. Fournier, M. Fennouri, and H. Baumert, "Thulium laser enucleation of the prostate," *Eur. Urol. Suppl.*, Vol. 7, no. 3, p. 332, 2008.

58. Bach, T., H. Igelmann, T. R. W. Herrmann, R. Ganzer, and A. J. Gross, "Thulium:yag vaporesection of the prostate. experts vs. novice-functional outcome," *Eur. Urol. Suppl.*, Vol. 7, no. 3, p. 203, 2008.

59. Cruccua, G., M. J. Aminoff, G. Curioc, J. M. Guerit, R. Kakigi, F. Mauguiere, P. M. Rossini, R.-D. Treede, and L. Garcia-Larrea, "Recommendations for the clinical use of somatosensory-evoked potentials," *Clinical Neurophysiology*, Vol. 119, pp. 1705–1719, 2008.

60. Spiegel, J., C. Hansen, and R.-D. Treede, "Clinical evaluation criteria for the assessment of impaired pain sensitivity by thulium-laser evoked potentials," *Clinical Neurophysiology*, Vol. 111, pp. 725–735, 2000.

61. Warnaby, C. E., D. J. Coleman, and T. A. King, "Photothermal modelling of thulium fibre laser-tissue interactions," in *Proceedings of SPIE-OSA Biomedical Optics - Therapeutic Laser Applications and Laser-Tissue Interactions* (Steiner, R. W., ed.), Vol. 5142, pp. 68–75, 2003.

62. Edwards, L., K. Inui, C. Ring, X. Wang, and R. Kakigi, "Pain-related evoked potentials are modulated across the cardiac cycle," *Pain*, Vol. 137, pp. 488–494, 2008.

63. King, T., "Medical fiber lasers and example application to laser nerve stimulation," in *2002 IEEE/LEOS Annual Meeting Conference Proceedings*, Vol. 1, p. 307, 15th Annual Meeting of the IEEE Lasers and Electro-Optics Society, 2002.

64. Forss, N., T. T. Raij, M. Sepp, and R. Hari, "Common cortical network for first and second pain," *NeuroImage*, Vol. 24, pp. 132–142, 2005.

65. Tyvaert, L., P. Derambure, E. Laureau, J. Hurtevent, J. Hurtevent, and C. Monaca, "Thulium laser somatosensory evoked potentials in idiopathic," *Clinical Neurophysiology*, Vol. 117, pp. S121–S336, 2006.

66. Yahr, W. Z., K. J. Strully, and E. S. Hurwitt, "Non-occlusive small arterial anastomosis with a neodymium laser," *Surg Forum*, Vol. 15, pp. 224–226, 1964.

67. Yahr, W. Z., and K. J. Strully, "Blood vessel anastomosis by laser and other biomedical applications," *J Assoc Adv Med Instrumentation*, Vol. 1, pp. 28–31, 1966.

68. Çilesiz, I., "Controlled temperature photothermal tissue welding," *Journal of Biomedical Optics*, Vol. 4, no. 3, pp. 327–336, 1999.

69. Ditkoff, M., N. H. Blevins, D. Perrault, and S. M. Shapshay, "Potential use of diode laser soldering in middle ear reconstruction," *Lasers in Surgery and Medicine*, Vol. 31, no. 242–246, 2002.

70. Wadia, Y., H. Xie, and M. Kajitani, "Liver repair and hemorrhage control by using laser soldering of liquid albumin in a porcine model," *Lasers in Surgery and Medicine*, Vol. 27, pp. 319–328, 2000.

71. Brosh, T., D. Simhon, M. Halpern, A. Ravid, T. Vasilyev, N. Kariv, Z. Nevo, and A. Katzir, "Closure of skin incisions in rabbits by laser soldering ii: Tensile strength," *Lasers in Surgery and Medicine*, Vol. 35, pp. 12–17, 2004.

72. Lauto, A., L. J. R. Foster, L. Ferris, A. Avolio, N. Zwaneveld, and L. A. Poole-Warren, "Albumin-genipin solder for laser tissue repair," *Lasers in Surgery and Medicine*, Vol. 35, pp. 140–145, 2004.

73. Fried, N. M., V. C. Hung, and J. T. Walsh, "Laser tissue welding: Laser spot size and beam profile studies," *IEEE Journal of Selected Topics in Quantum Electronics*, Vol. 5, no. 4, pp. 1004–1012, 1999.

74. Zilker, Z., B. I. Nageris, R. Feinmesser, E. Fridman, A. Ravid, N. Kariv, and A. Katzir, "Carbon dioxide laser and silver halide infrared transmitting fibers for tympanoplasty: An experimental animal model," *Otolaryngology-Head and Neck Surgery*, Vol. 125, no. 3, pp. 157–160, 2001.

75. Savage, H. E., R. K. Halder, U. Kartazayeu, R. B. Rosen, T. Gayen, S. A. McCormick, N. S. Patel, A. Katz, H. D. Perry, M. Paul, and R. R. Alfano, "Nir laser tissue welding of in vitro porcine cornea and sclera tissue," *Lasers in Surgery and Medicine*, Vol. 35, pp. 293–303, 2004.

76. Bleustein, C. B., C. N. Walker, D. Felsen, and D. P. Poppas, "Semi-solid albumin solder improved mechanical properties for laser tissue welding," *Lasers in Surgery and Medicine*, Vol. 27, pp. 140–146, 2000.

77. Kamegaya, Y., W. A. Farinelli, A. V. V. Echague, H. Akita, J. Gallagher, T. J. Flotte, R. R. Anderson, R. W. Redmond, and I. E. Kochevar, "Evaluation of photochemical tissue bonding for closure of skin incisions and excisions," *Lasers in Surgery and Medicine*, Vol. 37, pp. 264–270, 2005.

78. Fried, N. M., and J. T. Walsh, "Laser skin welding: In vivo tensile strength and wound healing results," *Lasers in Surgery and Medicine*, Vol. 27, pp. 55–65, 2000.

79. Lobik, L., A. Ravid, I. Nissenkorn, N. Kariv, J. Bernheim, and A. Katzir, "Bladder welding in rats using controlled temperature co_2 laser system," *J Urol*, Vol. 161, pp. 1662–1665, 1999.

80. Abergel, R. P., R. Lyons, R. Dwyer, R. R. White, and J. Uitto, "Use of lasers for closure of cutaneous wounds: experience with nd:yag, argon and co_2 lasers," *J Dermatol Surg Oncol*, Vol. 12, pp. 1181–1185, 1986.

81. Gobin, A. M., D. P. O'Neal, D. M. Watkins, N. J. Halas, R. A. Drezek, and J. L. West, "Near infrared laser-tissue welding using nanoshells as an exogenous absorber," *Lasers in Surgery and Medicine*, Vol. 37, pp. 123–129, 2005.

82. Capon, A., E. Souil, B. Gauthier, C. Sumian, M. Bachelet, B. Buys, B. S. Polla, and S. Mordon, "Laser assisted skin closure (lasc) by using a 815-nm diode-laser system accelerates and improves wound healing," *Lasers in Surgery and Medicine*, Vol. 28, pp. 168–175, 2001.

83. Bleustein, C. B., D. Felsen, and D. P. Poppas, "Welding characteristics of different albumin species with and without fatty acids," *Lasers in Surgery and Medicine*, Vol. 27, pp. 82–86, 2000.

84. Sorg, B. S., K. M. McNally, and A. J. Welch, "Biodegradable polymer film reinforcement of an indocyanine green-doped liquid albumin solder for laser-assisted incision closure," *Lasers in Surgery and Medicine*, Vol. 27, pp. 73–81, 2000.

85. Xie, H., B. S. Shaffer, S. A. Prahl, and K. W. Gregory, "Laser ureteral anastomosis using intraluminal albumin stent in a porcine model," *Lasers in Surgery and Medicine*, Vol. 32, pp. 294–298, 2003.

86. Bleustein, C. B., B. Cuomo, G. C. Mingin, M. Ohebshalom, A. Lauto, S. J. Shin, R. B. Stewart, D. Felsen, R. A. Soslow, M. Sennett, and D. P. Poppas, "Laser-assisted demucosalized gastrocystoplasty with autoaugmentation in a canine model," *Urology*, Vol. 55, no. 3, pp. 437–442, 2000.

87. Lauto, A., A. H. Hamawy, A. B. M. Phillips, P. B. Petratos, J. Raman, D. Felsen, W. Ko, and D. P. Poppas, "Carotid artery anastomosis with albumin solder and near infrared lasers: A comparative study," *Lasers in Surgery and Medicine*, Vol. 28, no. 50–55, 2001.

88. Xie, H., B. S. Shaffer, S. A. Prahl, and K. W. Gregory, "Intraluminal albumin stent assisted laser welding for ureteral anastomosis," *Lasers in Surgery and Medicine*, Vol. 31, pp. 225–229, 2002.

89. Jain, K. K., "Current status of laser applications in neurosurgery," *IEEE Journal of Quantum Electronics*, Vol. QE-20, no. 12, pp. 1401–1406, 1984.

90. Menovsky, T., and J. F. Beek, "Carbon dioxide laser-assisted nerve repair: Effect of solder and suture material on nerve regeneration in rat sciatic nerve," *Microsurgery*, Vol. 23, pp. 109–116, 2003.

91. McNally, K. M., B. S. Sorg, A. J. Welch, J. M. Dawes, and E. R. Owenk, "Photothermal effects of laser tissue soldering," *Phys. Med. Biol.*, Vol. 44, no. 983–1002, 1999.

92. Self, S. B., D. A. Coe, and J. M. Seeger, "Limited thrombogenicity of low temperature, laser-welded vascular anastomoses," *Lasers in Surgery and Medicine*, Vol. 18, pp. 241–247, 1996.

93. Suh, D. D., I. P. Schwartz, D. A. Canning, H. M. Snyder, S. A. Zderic, and A. J. Kirsch, "Comparison of dermal and epithelial approaches to laser tissue soldering for skin flap closure," *Lasers in Surgery and Medicine*, Vol. 22, pp. 268–274, 1998.

94. Lauto, A., D. P. Poppas, and G. A. C. Murrell, "Solubility study of albumin solders for laser tissue-welding," *Lasers in Surgery and Medicine*, Vol. 23, pp. 258–262, 1998.

95. Lauto, A., R. Trickett, R. Malik, J. M. Dawes, and E. R. Owen, "Laser-activated solid protein bands for peripheral nerve repair: An in vivo study," *Lasers in Surgery and Medicine*, Vol. 21, pp. 134–141, 1997.

96. Sorg, B. S., and A. J. Welch, "Preliminary biocompatibility experiment of polymer films for laser-assisted tissue welding," *Lasers in Surgery and Medicine*, Vol. 32, pp. 215–223, 2003.

97. Kirsch, A. J., J. W. Duckett, H. M. Snyder, D. A. Canning, D. W. Harshaw, P. Howard, E. J. Macarak, and S. A. Zderic, "Skin flap closure by dermal laser soldering: A wound healing model for sutureless hypospadias repair," *Urology*, Vol. 50, no. 2, pp. 263–272, 1997.

98. Ott, B., M. A. Constantinescu, D. Erni, A. Banic, T. Schaffner, and M. Frenz, "Intraluminal laser light source and external solder: In vivo evaluation of a new technique for microvascular anastomosis," *Lasers in Surgery and Medicine*, Vol. 35, pp. 312–316, 2004.

99. Ott, B., B. J. Züger, D. Erni, A. Banic, T. Schaffner, H. P. Weber, and M. Frenz, "Comparative in vitro study of tissue welding using a 808 nm diode laser and a ho:yag laser," *Lasers Med. Sci.*, Vol. 16, pp. 260–266, 2001.

100. Jonge, I. C. D. Y. M. W., J. F. Beek, and R. Balm, "25 years of laser assisted vascular anastomosis (lava): What have we learned?," *European Journal of Vasc. Endovasc. Surgery*, Vol. 27, pp. 466–476, 2004.

101. Wright, B., M. Vicaretti, N. Schwaiger, J. Wu, R. Trickett, L. Morrissey, R. Rohanizadeh, J. Fletcher, P. Maitz, and M. Harris, "Laser-assisted end-to-end bioweld anastomosis in an ovine model," *Lasers in Surgery and Medicine*, Vol. 39, pp. 667–673, 2007.

102. Kim, K., and Z. Guo, "Ultrafast radiation heat transfer in laser tissue welding and soldering," *Numerical Heat Transfer - Part A*, Vol. 46, pp. 23–40, 2004.

103. Steinstraesser, L., M. Wehner, G. Trust, M. Sorkin, D. Bao, T. Hirsch, H. Sudhoff, A. Daigeler, I. Stricker, H.-U. Steinau, and F. Jacobsen, "Laser-mediated fixation of collagen-based scaffolds to dermal wounds," *Lasers in Surgery and Medicine*, Vol. 42, pp. 141–149, 2010.

104. Chivers, R. A., "In vitro tissue welding using albumin solder: Bond strengths and bonding temperatures," *International Journal of Adhesion and Adhesives*, Vol. 20, pp. 179–187, 2000.

105. Nageris, B. I., Z. Zilker, M. Zilker, N. Kariv, R. Feinmesser, and A. Katzir, "Esophageal incisions repair by co_2 laser soldering," *Otolaryngology-Head and Neck Surgery*, Vol. 131, no. 6, pp. 856–859, 2004.

106. Xie, H., S. C. Bendre, A. P. Burke, K. W. Gregory, and A. P. Furnary, "Laser-assisted vascular end to end anastomosis of elastin heterograft to carotid artery with an albumin stent: A preliminary in vivo study," *Lasers in Surgery and Medicine*, Vol. 35, pp. 201–205, 2004.

107. Sorg, B. S., and A. J. Welch, "Laser-tissue soldering with biodegradable polymer films in vitro: Film surface morphology and hydration effects,"

108. Matteini, P., F. Rossi, L. Menabuoni, and R. Pini, "Microscopic characterization of collagen modifications induced by low-temperature diode-laser welding of corneal tissue," *Lasers in Surgery and Medicine*, Vol. 39, pp. 597–604, 2007.

109. Bleustein, C. B., M. Sennett, R. T. V. Kung, D. Felsen, D. P. Poppas, and R. B. Stewart, "Differential scanning calorimetry of albumin solders: Interspecies differences and fatty acid binding effects on protein denaturation," *Lasers in Surgery and Medicine*, Vol. 27, pp. 465–470, 2000.

110. Rivera, A., C. N. Walker, C. Bleustein, B. Choi, D. P. Poppas, and D. Felsen, "Enhanced adenoviral-vector mediated gene transfer using human albumin solder," *Lasers in Surgery and Medicine*, Vol. 30, pp. 313–319, 2002.

111. Stewart, R. B., L. S. Bass, J. K. Thompson, N. D. Nikoi, G. Becker, and R. T. V. Kung, "Improved microvessel repair: Laser welding with an anti-thrombotic solder," *Lasers in Surgery and Medicine*, Vol. 31, pp. 36–40, 2002.

112. McNally, K. M., B. S. Sorg, E. K. Chan, A. J. Welch, J. M. Dawes, and E. R. Owen, "Optimal parameters for laser tissue soldering: Ii. premixed versus separate dye-solder techniques," *Lasers in Surgery and Medicine*, Vol. 26, pp. 346–356, 2000.

113. Lauto, A., I. Kerman, M. Ohebshalon, D. Felsen, and D. P. Poppas, "Two-layer film as a laser soldering biomaterial," *Lasers in Surgery and Medicine*, Vol. 25, 1999.

114. Birch, J. F., D. J. Mandley, S. L. Williams, D. R. Worrall, P. J. Trotter, F. Wilkinson, and P. R. Bell, "Methylene blue based protein solder for vascular anastomoses: An in vitro burst pressure study," *Lasers in Surgery and Medicine*, Vol. 26, pp. 323–329, 2000.

115. Mendoza, G. A., E. Acuna, M. Allen, J. Arroyo, and R. A. Quintero, "In vitro laser welding of amniotic membranes," *Lasers in Surgery and Medicine*, Vol. 24, pp. 315–318, 1999.

116. Petratos, P. B., R. N. Baergen, C. B. Bleustein, D. Felsen, and D. P. Poppas, "Ex vivo evaluation of human fetal membrane closure," *Lasers in Surgery and Medicine*, Vol. 30, pp. 48–53, 2002.

117. Lauto, A., J. Hook, M. Doran, F. Camacho, L. A. Poole-Warren, A. Avolio, and L. J. R. Foster, "Chitosan adhesive for laser tissue repair: In vitro characterization," *Lasers in Surgery and Medicine*, Vol. 36, no. 193–201, 2005.

118. Lauto, A., M. Stoodley, H. Marcel, A. Avolio, M. Sarris, G. McKenzie, D. D. Sampson, and L. J. R. Foster, "In vitro and in vivo tissue repair with laser-activated chitosan adhesive," *Lasers in Surgery and Medicine*, Vol. 39, pp. 19–27, 2007.

119. Fung, L. C., G. C. Mingin, M. Massicotte, D. Felsen, and D. P. Poppas, "Effects of temperature on tissue thermal injury and wound strength after photothermal wound closure," *Lasers in Surgery and Medicine*, Vol. 25, pp. 285–290, 1999.

120. Massicotte, J. M., R. B. Stewart, and D. P. Poppas, "Effects of endogenous absorption in human albumin solder for acute laser wound closure," *Lasers in Surgery and Medicine*, Vol. 23, pp. 18–24, 1998.

121. Lauto, A., J. M. Dawes, J. A. Piper, and E. R. Owen, "Laser nerve repair by solid protein band technique. ii: Assessment of long-term nerve regeneration," *Microsurgery*, Vol. 18, pp. 60–64, 1998.

122. Stewart, R. B., C. B. Bleustein, P. B. Petratos, K. C. Chin, D. P. Poppas, and R. T. V. Kung, "Concentrated autologous plasma protein: A biochemically neutral solder for tissue welding," *Lasers in Surgery and Medicine*, Vol. 29, pp. 336–342, 2001.

123. Cooper, C. S., I. P. Schwartz, D. Suh, and A. J. Kirsch, "Optimal solder and power density for diode laser tissue soldering (lts)," *Lasers in Surgery and Medicine*, Vol. 29, pp. 53–61, 2001.

124. Fujita, M., Y. Morimoto, S. Ohmori, N. Usami, T. Arai, T. Maehara, and M. Kikuchi, "Preliminary study of laser welding for aortic dissection in a porcine model using a diode laser with indocyanine green," *Lasers in Surgery and Medicine*, Vol. 32, pp. 341–345, 2003.

125. Chan, E. K., Q. Lu, B. Bell, M. Motamedi, C. Frederickson, D. T. Brown, I. S. Kovach, and A. J. Welch, "Laser assisted soldering: Microdroplet accumulation with a microjet device," *Lasers in Surgery and Medicine*, Vol. 23, pp. 213–220, 1998.

126. Menovsky, T., J. F. Beek, and M. J. C. van Gemert, "Laser tissue welding of dura mater and peripheral nerves: A scanning electron microscopy study," *Lasers in Surgery and Medicine*, Vol. 19, no. 152–158, p. 8, 1996.

127. McNally, K. M., B. S. Sorg, and A. J. Welch, "Novel solid protein solder designs for laser-assisted tissue repair," *Lasers in Surgery and Medicine*, Vol. 27, pp. 147–157, 2000.

128. Sorg, B. S., and A. J. Welch, "Tissue welding with biodegradable polymer films-demonstration of acute strength reinforcement in vivo," *Lasers in Surgery and Medicine*, Vol. 31, pp. 339–342, 2002.

129. Berguer, R., R. L. Staerkel, E. E. Moore, F. A. Moore, W. B. Galloway, and M. B. Mockus, "Warning: fatal reaction to the use of fibrin glue in deep hepatic wounds," *J Trauma*, Vol. 31, pp. 408–411, 1991.

130. Oransky, I., "Soldering tissue," *Scientist*, Vol. 33, p. 6, 2003.

131. Lanzafame, R. J., P. Brondon, I. Stadler, D. P. DeVore, R. Soltz, and B. A. Soltz, "Histologic assessment of mesh fixation following laser-assisted tissue soldering in a lapine model," *Lasers in Surgery and Medicine*, Vol. 37, pp. 130–137, 2005.

132. Foyt, D., W. H. Slattery, and M. J. Carfrae, "Underlay tympanoplasty with laser tissue welding," *ENT-Ear, Nose and Throat Journal*, Vol. 85, no. 4, pp. 247–258, 2006.

133. Constantinescu, M. A., A. Alfieri, G. Mihalache, F. Stuker, A. Ducray, R. W. Seiler, M. Frenz, and M. Reinert, "Effect of laser soldering irradiation on covalent bonds of pure collagen," *Lasers Med. Sci.*, Vol. 22, pp. 10–14, 2007.

134. Tang, J., J. M. Evans, V. Petricevic, P. Ho, and R. R. Alfano, "Tissue welding using near-infrared forsterite and cunyite tunable lasers," *IEEE Journal of Selected Topics in Quantum Electronics*, Vol. 5, no. 4, pp. 1103–1106, 1999.

135. McDonald, A. V., N. M. Claffey, G. J. Pearson, W. Blau, and D. J. Setchell, "Effect of nd:yag radiation at millisecond pulse duration on dentine crater depth," *Lasers in Surgery and Medicine*, Vol. 27, no. 3, pp. 213–223, 2000.

136. Geldi, C., O. Bozkulak, H. O. Tabakoglu, S. Isci, A. Kurt, and M. Gulsoy, "Development of a surgical diode-laser system: Controlling the mode of operation," *Photomedicine and Laser Surgery*, Vol. 24, no. 6, pp. 723–729, 2006.

137. Ding, Y., H. Ying, and S. Shao, "A time-varying fuzzy on-off control system with application to the control of tissue temperature during laser heating," *The Ninth IEEE International Conference on Fuzzy Systems*, Vol. 1, pp. 528–533, 2000.

138. Tang, J., D. O'Callaghan, S. Rouy, and G. Godlewski, "Quantitative changes in collagen levels following 830-nm diode laser welding," *Lasers in Surgery and Medicine*, Vol. 22, pp. 207–211, 1998.

139. Hasegawa, M., T. Sakurai, M. Matsushita, N. Nishikimi, Y. Nimura, and M. Kobayashi, "Comparison of argon-laser welded and sutured repair of inferior vena cava in a canine model," *Lasers in Surgery and Medicine*, Vol. 29, pp. 62–69, 2001.

140. Cheong, W. F., S. A. Prahl, and A. J. Welch, "A review of the optical properties of biological tissue," *IEEE J. Quantum Electron.*, Vol. 26, no. 12, pp. 2166–2185, 1990.

141. Allain, J. C., M. LeLous, L. Cohen-Solal, S. Bazin, and P. Maroteaus, "Isometric tensions developed during the hydrothermal swelling of rat skin," *Connect Tissue Res*, Vol. 7, no. 3, pp. 127–133, 1980.

142. Abela, G. S., E. E. Hage-Korban, T. Tomaru, G. R. Barbeau, O. G. Abela, and S. E. Fried, "Vascular procedures that thermo-coagulate collagen reduce local platelet deposition and thrombus formation: Laser and laser-thermal versus balloon angioplasty," *Lasers in Surgery and Medicine*, Vol. 29, pp. 455–463, 2001.

143. Cooley, B. C., "Heat-induced tissue fusion for microvascular anastomosis," *Microsurgery*, Vol. 17, pp. 198–208, 1996.

144. Theodossiou, T., G. S. Rapti, V. Hovhannisyan, E. Georgiou, K. Politopoulos, and D. Yova, "Thermally induced irreversible conformational changes in collagen probed by optical second harmonic generation and laser-induced fluorescence," *Lasers Med. Sci.*, Vol. 17, pp. 34–41, 2002.

145. Tang, J., G. Zhang, F. Zeng, P. P. Ho, and R. R. Alfano, "Near-infrared photo-excited emission from tissues treated at different temperature levels," *Lasers in Surgery and Medicine*, Vol. 29, pp. 18–22, 2001.

146. Chen, B., S. L. Thomsen, R. J. Thomas, and A. J. Welch, "Modelling thermal damage in skin from 2000-nm laser irradiation," *Journal of Biomedical Optics*, Vol. 11, no. 6, p. 064028, 2006.

147. Tang, J., G. Godlewski, S. Rouy, and G. Delacretaz, "Morphologic changes in collagen fibers after 830 nm diode laser welding," *Lasers in Surgery and Medicine*, 1997.

148. Stratigos, A. J., and J. S. Dover, "Overview of laser and their properties," *Dermatologic Theraphy*, Vol. 13, pp. 2–16, 2000.

149. Xu, F., T. J. Lu, and K. A. Seffen, "Biothermomechanical behavior of skin tissue," *Acta. Mech. Sin.*, Vol. 24, pp. 1–23, 2008.

150. Maitland, D. J., and J. T. Walsh, "Quantitative measurements of linear birefringence during heating of native collagen," *Lasers in Surgery and Medicine*, Vol. 20, pp. 310–318, 1997.

151. Wenzel, G. I., B. Pikkula, C.-H. Choi, B. Anvari, and J. S. Oghalai, "Laser irradiation of the guinea pig basilar membrane," *Lasers in Surgery and Medicine*, Vol. 35, pp. 174–180, 2004.

152. Franz, M. G., M. A. Kuhn, T. E. Wright, T. L. Wachtel, and M. C. Robson, "Use of the wound healing trajectory as an outcome determinant for acute wound healing," *Wound Repair Regen*, Vol. 8, pp. 511–516, 2000.

153. Robson, M. C., "Wound infection. a failure of wound healing caused by an imbalance of bacteria," *Surg Clin North Am*, Vol. 77, pp. 637–650, 1997.

154. Robson, M. C., D. P. Hill, M. E. Woodske, and D. L. Steed, "Wound healing trajectories as predictors of effectiveness of therapeutic agents," *Arch. Surg.*, Vol. 135, pp. 773–777, 2000.

155. Tanenbaum, M., "Skin and tissue techniques," *Oculoplastic Surgery - 3rd ed.*, Vol. 3-4, 1995.

156. Lawrence, W. T., "Physiology of the acute wound," *Clin. Plast. Surg.*, Vol. 25, pp. 321–340, 1998.

157. Glat, P. M., and M. T. Longaker, "Wound healing," *Grabb and Smith's Plastic Surgery - Chap 1*, 1997.

158. Hawkins, D., and H. Abrahamse, "Influence of broad-spectrum and infrared light in combination with laser irradiation on the proliferation of wounded skin fibroblasts," *Photomed Laser Surg.*, Vol. 25, no. 3, pp. 159–169, 2007.

159. Domankevitz, Y., K. McMillan, and N. S. Nishioka, "Characterization of tissue ablation with a continuous wave holmium laser," *Lasers Surg Med.*, Vol. 19, no. 1, pp. 97–102, 1996.

160. Tabakoglu, H. O., N. Topaloglu, and M. Gulsoy, "The effect of irradiance level in 980-nm diode laser skin welding," *Photomedicine and Laser Surgery*, Vol. 28, no. 4, pp. 453–458, 2010.

161. Ashworth, E. M., M. C. Dalsing, J. F. Olson, W. P. Hoagland, S. Baughman, and J. L. Glover, "Large-artery welding with a milliwatt carbon dioxide laser," *Arch Surg*, Vol. 122, pp. 673–677, 1987.

162. Oz, M. C., M. R. Williams, R. Moscarelli, M. Kaynar, C. I. Fras, S. K. Libutti, H. Smith, A. J. Setton, M. R. Treat, and R. Nowygrod, "Laser-assisted solder closure of bronchial stumps," *Proc SPIE*, Vol. 16431, pp. 191–194, 1992.

163. Bass, L. S., M. C. Oz, J. S. Auteri, M. R. Williams, J. Rosen, S. K. Libutti, A. M. Eaton, J. Lontz, R. Nowygrod, and M. D. Treat, "Laparoscopic application of laser-activated tissue glues," *Proc SPIE*, Vol. 1421, pp. 164–168, 1991.

164. Bass L. S., S. K. Libutti, M. C. O. J. R. M. R. W. R. N., and M. R. Treat, "Canine choledochotomy closure with diode laser-activated fibrinogen solder," *Surgery*, Vol. 115, no. 3, pp. 398–401, 1994.

165. Fayez, J. A., V. W. Jobson, S. S. Lentz, D. G. Payne, D. F. Westra, and D. K. Martin, "Tuba1 microsurgery with the carbon dioxide laser," *Am J Obstet Gynecol*, Vol. 146, no. 4, pp. 371–373, 1982.

166. Fischer, D. W., J. L. Beggs, D. L. Kenshalo, and A. G. Shetter, "Comparative study of microepineural anastomoses with the use of co_2 laser and suture techniques in rat sciatic nerve: Part 1: Surgical technique, nerve action potentials, and morphological studies," *Neurosurgery*, Vol. 17, pp. 300–308, 1985.

167. Henrick, A., R. N. Gaster, and P. J. Silverstone, "Organic tissue glue in the closure of cataract incisions," *J Cat Ref Surg*, Vol. 13, pp. 551–553, 1987.

168. Mourant, J. R., G. D. Anderson, I. J. Biglio, and T. M. Johnson, "Laser welding of bone: Successful in vitro experiments," *Proc. SPIE*, Vol. 2128, pp. 484–488, 1994.

169. Frazier, O. H., A. Painvin, J. R. Morris, T. Sharon, and C. R. Neblett, "Laser-assisted microvascular anastomoses: angiographic and anatomopathologic studies on growing microvascular anastomoses: Preliminary report," *Surgery*, Vol. 97, no. 3, pp. 585–589, 1985.

170. Gilbert, P. T. O., and R. Beckert, "Laser-assisted vasovasostomy," *Lasers Surg Med*, Vol. 9, pp. 42–44, 1989.

171. Jain, K. K., and W. Gorisch, "Repair of small blood vessels with the neodymium-yag laser: A preliminary report," *Surgery*, Vol. 85, pp. 684–688, 1979.

172. Oskoui, P., I. Stadler, and R. J. Lanzafame, "A preliminary study of laser tissue soldering as arterial wall reinforcement in an acute experimental aneurysm model," *Lasers in Surgery and Medicine*, Vol. 32, no. 346–348, 2003.

173. Trauner, K., N. Nishioka, and D. Patel, "Pulsed holmium:yttriumaluminum-garnet (ho:yag) laser ablation of fibrocartilage and articular cartilage," *Am J Sports Med*, Vol. 18, no. 3, pp. 316–320, 1990.

174. Zueger, B. J., B. Ott, P. Mainil-Varlet, T. Schaffner, J.-F. Cleamence, H. Weber, and M. Frenz, "Laser solder welding of articular cartilage: Tensile strength and chondrocyte viability," *Lasers in Surgery and Medicine*, Vol. 28, pp. 427–434, 2001.

175. Forer, B., T. Vasilyev, T. Brosh, N. Kariv, Z. Gil, D. M. Fliss, and A. Katzir, "Repair of pig dura in vivo using temperature controlled co_2 laser soldering," *Lasers in Surgery and Medicine*, Vol. 37, no. 4, pp. 286–292, 2005.

176. Satoa, S., H. Kamoi, Y. Wasakia, and K. Kamoi, "Application of a carbon dioxide laser for early closure of gingival flaps," *International Congress Series*, Vol. 1248, pp. 333–337, 2003.

177. Pini, R., F. Rossi, L. Menabuoni, I. Lenzetti, S. Yoo, and J.-M. Parel, "A new technique for the closure of the lens capsule by laser welding," *Ophthalmic Surgery, Lasers and Imaging*, Vol. 39, no. 3, pp. 260–261, 2008.

178. Overton, G., "Microscopy shows corneal laser welding speeds healing," *Laser Focus World*, Vol. 42, no. 3, p. 22, 2006.

179. Oz, M. C., M. R. Treat, S. K. Libutti, H. W. Popp, L. S. Bass, and S. Popilskis, "Preliminary report: laser welding and fibrinogen soldering are superior to sutured cholecyctostomy closure in a canine model," *Proceedings of SPIE - The International Society for Optical Engineering*, Vol. 1200, pp. 55–59, 1990.

180. Stewart, R. B., G. M. LaMuraglia, and R. T. V. Kung, "Controlled heating of vascular tissue with a 1.9 micron laser," *Lasers Surg Med Supplement*, Vol. 6, no. 55, 1994.

181. Stewart, R. B., A. Benbrahim, G. M. LaMuraglia, M. Rosenberg, G. J. L'ltalien, W. M. Abbott, and R. T. V. Kung, "Laser assisted vascular welding with real time temperature control," *Lasers in Surgery and Medicine*, Vol. 19, pp. 9–16, 1996.

182. Oz, M. C., L. S. Bass, H. W. Popp, R. S. Chuck, J. P. Johnson, S. L. Trokel, and M. R. Treat, "In vitro comparison of thulium-holmium-chromium:yag and argon ion lasers for welding of biliary tissue," *Lasers in Surgery and Medicine*, Vol. 9, no. 3, pp. 248–253, 2005.

183. Popp, H. W., M. C. Oz, L. S. Bass, R. S. Chuck, S. L. Trokel, and M. R. Treat, "Welding of gallbladder tissue with a pulsed 2.15 μm thulium-holmium-chromium:yag laser," *Lasers in Surgery and Medicine*, Vol. 9, no. 2, pp. 155–159, 2005.

184. Ngo, A. K., U. Sharma, J. U. Kang, and N. M. Fried, "Laser welding of urinary tissues, ex vivo, using a tunable thulium fiber laser," in *Proceedings of SPIE* (Kollias, N., H. Zeng, B. Choi, R. S. Malek, B. J. Wong, J. F. R. Ilgner, E. A. Trowers, W. T. de Riese, H. Hirschberg, S. J. Madsen, M. D. Lucroy, L. P. Tate, K. W. Gregory, and G. J. Tearney, eds.), Vol. 6078 of *Photonic Therapeutics and Diagnostics II*, 2006.

185. Phillips, A. B. M., B. Y. Ginsburg, S. J. Shin, R. Soslow, W. Ko, and D. Poppas, "Laser welding for vascular anastomosis using albumin solder: An approach for mid-cab," *Lasers in Surgery and Medicine*, Vol. 24, pp. 264–268, 1999.

186. Bass, L. S., M. R. Treat, and C. Dzakonski, "Sutureless microvascular anastomosis using the thc:yag laser: A preliminary report," *Microsurgery*, Vol. 10, pp. 189–193, 1989.

187. Kung, R. T. V., R. B. Stewart, D. T. Zelt, G. J. L'Italien, and G. M. LaMuraglia, "Absorption characteristics at 1.9 micron: Effect on vascular welding," *Lasers Surg Med*, Vol. 13, pp. 12–17, 1993.

188. Trabucchi, G., P. G. Gobbi, R. Brancato, F. Carones, A. G. Resti, A. Jansen, and R. Pini, "Laser welding of corneal tissue: preliminary experiences using 810 nm and 1950 nm diode lasers," *Proceedings of SPIE*, Vol. 2623, pp. 380–387, 1996.

189. Foltz, M. S., M. L. Denton, K. J. Schuster, L. E. Estlack, and S. S. Kumru, "An in vitro corneal model with a laser damage threshold at 2 μm that is similar to that in the rabbit," in *Proceedings of SPIE* (Jacques, S. L., W. P. Roach, and R. J. Thomas, eds.), Vol. 6854 of *Optical Interactions with Tissue and Cells XIX*, 2008.

190. Desmettre, T., S. R. Mordon, and V. A. Mitchell, "Tissue welding for corneal wound suture with a cw 1.9-μm diode laser: an in-vivo preliminary study," *Proceedings of SPIE*, Vol. 2623, pp. 372–379, 1996.

191. Seiler, T., M. Matallana, and T. Bende, "Laser thermalkeratoplasty by means of a pulsed ho1mium:yag laser for hyperopic correction," *Refract. Corneal Surg.*, Vol. 6, p. 611416, 1990.

192. McCally, R. L., R. A. Farrell, and C. B. Bargeron, "Cornea epithelial damage thresholds in rabbits exposed to tm:yag laser radiation at 2.02 microns," *Lasers Surg Med*, Vol. 12, no. 6, pp. 598–603, 1992.

193. Rasier, R., M. Ozeren, O. Artunay, H. Bahcecioglu, I. Seckin, H. Kalaycıoğlu, A. Kurt, A. Sennaroğlu, and M. Gülsoy, "Corneal tissue welding with infrared laser irradiation after clear corneal incision," *Cornea*, Vol. 29, no. 9, pp. 985–990, 2010.

194. Yufeng, L., B. Yao, Y. Wang, Y. Ju, G. Zhao, Y. Zong, and J. Xu, "High efficient diode-pumped tm:yap laser at room temperature," *Chin. Opt. Lett.*, Vol. 5, pp. 286–287, 2007.

195. Yao, B. Q., Y. Cai, X. M. Duan, L. L. Zheng, Y. L. Ju, Y. Z. Wang, G. J. Zhao, Y. H. Zong, and J. Xu, "Diode-pumped q-switched tm:yap laser with a pump recycling scheme," *Laser Physics*, Vol. 18, no. 10, pp. 1128–1130, 2008.

196. Kalaycioglu, H., A. Sennaroglu, and A. Kurt, "Influence of doping concentration on the power performance of diode-pumped continuous-wave tm^{3+}:$yalo_3$ lasers," *IEEE J of Sel Top. Quan Electronics*, Vol. 11, pp. 667–673, 2005.

197. Kalaycioglu, H., and A. Sennaroglu, "Low-threshold continuous-wave tm^{3+}:$yalo_3$ laser," *Optics Communications*, Vol. 281, pp. 4071–4074, 2008.

198. Schober, R., F. Ulrich, T. Sander, H. Dürselen, and S. Hessel, "Laser-induced alteration of collagen substructure allows microsurgical tissue welding," *Science, New Series*, Vol. 232, no. 4756, pp. 1421–1422, 1986.

199. Zhang, J. Z., Y. G. Shen, and X. X. Zhang, "A dynamic photo-thermal model of carbon dioxide laser tissue ablation," *Lasers in Medical Science*, Vol. 24, no. 3, pp. 329–338, 2008.

200. Bozkulak, O., H. O. Tabakoglu, A. Aksoy, O. Kurtkaya, A. Sav, R. Canbeyli, and M. Gulsoy, "980-nm diode laser for brain surgery: Histopathology and recovery period," *Lasers Med. Sci.*, Vol. 19, pp. 41–47, 2004.

201. Gulsoy, M., T. A. Celikel, A. Kurt, R. Canbeyli, and I. Çilesiz, "Er:yag laser ablation on cerebellar and cerebral tissue," *Lasers Med. Sci.*, Vol. 16, pp. 40–43, 2001.

202. Baranoski, G. V. G., and A. Krishnaswamy, "An introduction to light interaction with human skin," *RITA*, Vol. 11, no. 1, pp. 33–62, 2004.

203. Xu, F., K. A. Seffen, and T. J. Lu, "Non-fourier analysis of skin biothermomechanics," *International Journal of Heat and Mass Transfer*, Vol. 51, pp. 2237–2259, 2008.

204. Chen, Y.-J., J.-H. Jeng, C.-C. J. Yao, M.-H. Chen, L.-T. Hou, and W.-H. Lan, "Long-term effect of pulsed nd:yag laser irradiation on cultured human periodontal fibroblasts," *Lasers in Surgery and Medicine*, Vol. 36, pp. 225–233, 2005.

205. Thomsen, S., J. A. Pearce, and W.-F. Cheong, "Changes in birefringence as markers of thermal damage in tissues," *IEEE Transactions on Biomedical Engineering*, Vol. 36, no. 12, pp. 1174–1179, 1989.

206. Fitzpatrick, R. E., E. F. Rostan, and N. Marchell, "Collagen tightening induced by carbon dioxide laser versus erbium:yag laser," *Lasers in Surgery and Medicine*, Vol. 27, pp. 395–403, 2000.

207. Barbeau, G. R., G. S. Abela, J. M. Seeger, S. E. Fried, T. Tomaru, and P. P. Giacomino, "Temperature monitoring during peripheral thermo-optical laser recanalization in humans," *Clin Cardiol.*, Vol. 13, pp. 690–697, 1990.

208. Bown, S. G., "Phototherapy of tumors," *World J Surg*, Vol. 7, pp. 700–709, 1983.

209. Prudhomme, M., J. Tang, S. Rouy, G. Delacretaz, R. P. Salathe, and G. Godlewski, "Interstitial diode laser hyperthermia in the treatment of subcutaneous tumor," *Lasers Surg Med*, Vol. 19, pp. 445–450, 1996.

210. Dinerman, J. L., R. D. Berger, and H. Calkins, "Temperature monitoring during radiofrequency ablation," *J Cardiovasc Electrophysiol*, Vol. 7, pp. 163–173, 1996.

211. Choi, J. Y., B. S. Tanenbaum, T. E. Milner, X. V. Dao, J. S. Nelson, E. N. Sobol, and B. J. F. Wong, "Thermal, mechanical, optical, and morphologic changes in bovine nucleus pulposus induced by nd:yag ($\lambda = 1.32$ μm) laser irradiation," *Lasers in Surgery and Medicine*, Vol. 28, pp. 248–254, 2001.

212. Svaasand, L. O., L. L. Randeberg, G. Aguilar, B. Majaron, S. Kimel, E. J. Lavernia, and J. S. Nelson, "Cooling efficiency of cryogen spray during laser therapy of skin," *Lasers in Surgery and Medicine*, Vol. 32, pp. 137–142, 2003.

213. Constantinescu, M. A., A. Alfieri, G. Mihalache, F. Stuker, A. Ducray, R. W. Seiler, M. Frenz, and M. Reinert, "Effect of laser soldering irradiation on covalent bonds of pure collagen," *Lasers Med. Sci.*, Vol. 22, no. 10–14, 2007.

214. Lauto, A., R. Stewart, M. Ohebshalom, N. D. Nikkoi, D. Felsen, and D. P. Poppas, "Impact of solubility on laser tissue-welding with albumin solid solders," *Lasers in Surgery and Medicine*, Vol. 28, pp. 44–49, 2001.

215. Cohen, M., A. Ravid, V. Scharf, D. Hauben, and A. Katzir, "Temperature controlled burn generation system based on a co_2 laser and a silver halide fiber optic radiometer," *Lasers in Surgery and Medicine*, Vol. 32, pp. 413–416, 2003.

216. Manns, F., P. J. Milne, X. Gonzalez-Cirre, D. B. Denham, J.-M. Parel, and D. S. Robinson, "In situ temperature measurements with thermocouple probes during laser interstitial thermotherapy (litt): Quantification and correction of a measurement artifact," *Lasers in Surgery and Medicine*, Vol. 23, pp. 94–103, 1998.

217. Harrington, J. A., "A review of ir transmitting, hollow waveguides," *Fiber and Integrated Optics*, Vol. 19, pp. 211–217, 2000.

218. Harrington, J. A., C. Rabii, and D. Gibson, "Transmission properties of hollow glass waveguides for delivery of co_2 surgical laser power," *IEEE Journal of Selected Topics in Quantum Electronics*, Vol. 5, no. 4, pp. 948–953, 1999.

219. Lobel, B., O. Eyal, N. Kariv, and A. Katzir, "Temperature controlled co_2 laser welding of soft tissues: Urinary bladder welding in different animal models (rats, rabbits, and cats)," *Lasers in Surgery and Medicine*, Vol. 26, pp. 4–12, 2000.

220. Lauto, A., "Repair strength dependence on solder protein concentration: A study in laser tissue-welding," *Lasers Surg Med*, Vol. 22, no. 120–125, 1998.

221. Ho, D. D. M., R. London, G. B. Zimmerman, and D. A. Young, "Laser-tattoo removal-a study of the mechanism and the optimal treatment strategy via computer simulations," *Lasers Surg Med*, Vol. 30, pp. 389–397, 2002.

222. Fenner, J., H. Moseley, W. Martin, and D. Wheatley, "Strength of tissue bond as a function of surface apposition," *Lasers Med Sci*, Vol. 7, pp. 375–379, 1992.

223. D.Simhon, T. Brosh, M. Halpern, A. Ravid, T. Vasilyev, N. Kariv, A. Katzir, and Z. Nevo, "Closure of skin incisions in rabbits by laser soldering: I: Wound healing pattern," *Lasers in Surgery and Medicine*, Vol. 35, pp. 1–11, 2004.

224. Tabakoglu, H. O., and M. Gulsoy, "In vivo comparison of near infrared lasers for skin welding," *Lasers Med Sci.*, Vol. 25, no. 3, pp. 411–421, 2010.

225. Tang, J., F. Zeng, J. M. Evans, B. Xu, H. Savage, P. P. Ho, and R. R. Alfano, "Comparison of cunyite and fosterite nir tunable laser tissue welding using native collagen fluorescence imaging," *Journal of Clinical Laser Medicine and Surgery*, Vol. 18, no. 3, pp. 117–123, 2000.

226. White, R. A., G. H. White, R. M. Fujitani, J. W. Vlasak, C. E. Donayre, G. E. Kopchok, and S.-K. Peng, "Initial human evaluation of argon laser-assisted vascular anastomoses," *J Vasc Surg*, Vol. 9, pp. 542–547, 1989.

227. Rebeiz, E. E., Z. Wang, D. J. Annino, J. A. McGilligan, and S. M. Shapshay, "Preliminary clinical results of window partial laryngectomy: A combined endoscopic and open technique," *Ann Otol Rhinol Laryngol*, Vol. 109, pp. 123–127, 2000.

228. Kirsch, A. J., C. S. Cooper, J. Gatti, H. C. Scherz, D. A. Canning, S. A. Zderic, and H. M. Snyder, "Iii. laser tissue soldering for hypospadias repair: Results of a controlled prospective clinical trial," *J Urol*, Vol. 165, pp. 574–577, 2001.

229. Jain, K. K., "Sutureless extra-intracranial anastomosis by laser," *Lancet*, Vol. 8406, pp. 816–817, 1984.

230. White, R. A., G. H. White, R. M. Fujitani, J. W. Vlasak, C. E. Donayre, G. E. Kopchok, and S. K. Peng, "Initial human evaluation of argon laserassisted vascular anastomoses," *J Vasc Surg*, Vol. 4, no. 542–547, 1989.

231. Okada, M., K. Shimizu, H. Ikuta, H. Horii, and K. Nakamura, "An alternative method of vascular anastomosis by laser: experimental and clinical study," *Lasers Surg Med*, Vol. 3, pp. 240–248, 1987.

232. Kiyoshige, Y., H. Tsuchida, M. Hamasaki, M. Takayanagi, and Y. Watanabe, "Co_2 laser-assisted microvascular anastoanastomosis. biomechanical studies and clinical applications," *J Reconstr Microsurg*, Vol. 7, no. 3, pp. 225–230, 1991.